AD-A199 759 AGARD (ADVISORY GROUP FOR AEROSPACE RESEARCH & DEVELOPMENT) ENGINE DISC C..(U) ADVISORY GROUP FOR AEROSPACE RESEARCH AND DEVELOPMENT NEUILLY.. 1/1

UNCLASSIFIED A J MOM ET AL. AUG 88 AGARD-R-766 F/G 11/6.1 NL

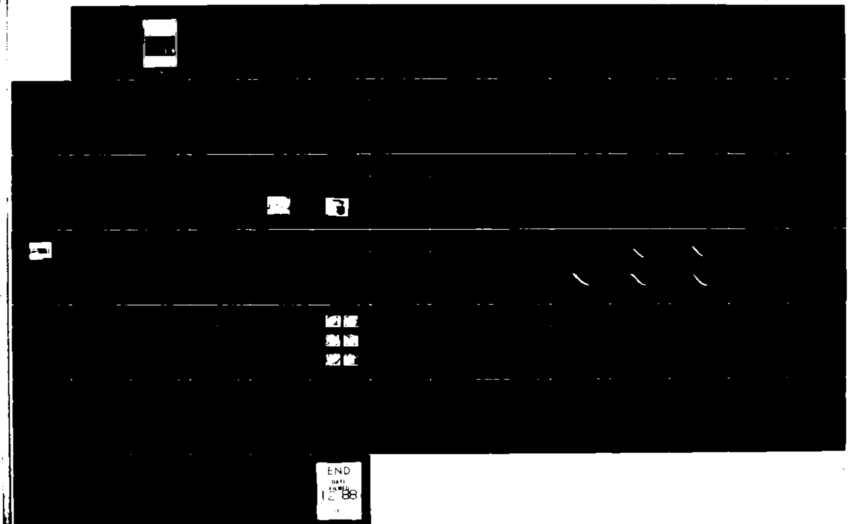

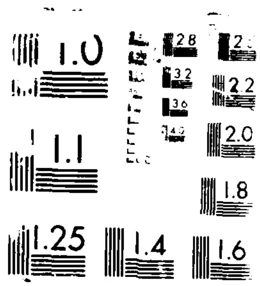
1.0
2.8
3.2
3.6
2.2
2.0
1.1
1.8
1.25
1.4
1.6

(1)

AGARD-R-766

AGARD-R-766

AGARD

ADVISORY GROUP FOR AEROSPACE RESEARCH & DEVELOPMENT

AGARD REPORT No.766

AGARD Engine Disc Cooperative Test Programme

NORTH ATLANTIC TREATY ORGANIZATION

DISTRIBUTION AND AVAILABILITY
ON BACK COVER

AGARD-R-766

NORTH ATLANTIC TREATY ORGANIZATION

ADVISORY GROUP FOR AEROSPACE RESEARCH AND DEVELOPMENT

(ORGANISATION DU TRAITE DE L'ATLANTIQUE NORD)

AGARD Report No.766

AGARD ENGINE DISC COOPERATIVE TEST PROGRAMME

by

A.J.A.Mom
National Aerospace Laboratory NLR
P.O. Box 90502
1006 BM Amsterdam
The Netherlands

and

M.D.Raizenne
National Aeronautical Establishment
National Research Council
Montreal Road
Ottawa, Ontario K1A 0R6
Canada

This publication was sponsored by the Structures and Materials Panel of AGARD.

THE MISSION OF AGARD

According to its Charter, the mission of AGARD is to bring together the leading personalities of the NATO nations in the fields of science and technology relating to aerospace for the following purposes:

- Recommending effective ways for the member nations to use their research and development capabilities for the common benefit of the NATO community;
- Providing scientific and technical advice and assistance to the Military Committee in the field of aerospace research and development (with particular regard to its military application);
- Continuously stimulating advances in the aerospace sciences relevant to strengthening the common defence posture;
- Improving the co-operation among member nations in aerospace research and development;
- Exchange of scientific and technical information;
- Providing assistance to member nations for the purpose of increasing their scientific and technical potential;
- Rendering scientific and technical assistance, as requested, to other NATO bodies and to member nations in connection with research and development problems in the aerospace field.

The highest authority within AGARD is the National Delegates Board consisting of officially appointed senior representatives from each member nation. The mission of AGARD is carried out through the Panels which are composed of experts appointed by the National Delegates, the Consultant and Exchange Programme and the Aerospace Applications Studies Programme. The results of AGARD work are reported to the member nations and the NATO Authorities through the AGARD series of publications of which this is one.

Participation in AGARD activities is by invitation only and is normally limited to citizens of the NATO nations.

The content of this publication has been reproduced directly from material supplied by AGARD or the authors.

Published August 1988

ISBN 92-835-0475-5

Printed by Specialised Printing Services Limited
40 Chigwell Lane, Loughton, Essex IG10 3TZ

PREFACE

The Structures and Materials Panel has been involved in studies of fatigue and fracture of critical jet engine components for many years. In 1982 a Sub-committee on "Damage Tolerance Concepts for Critical Engine Components" was formed to study the overall philosophy and the implications of introducing damage tolerance concepts (DTC) into the design and use of critical engine components.

The damage tolerance philosophy offers potential cost savings of considerable magnitude when compared with a "safe-life" approach provided such a concept can be implemented with an assurance that current safety standards will not be prejudiced. As an example of possible cost savings, it has been estimated that over 80% of engine discs have ten or more low cycle fatigue lives remaining when discarded under "safe-life" rules, and it is the useful remaining life that DTC aims to exploit in service. Apart from economic advantages, the DTC approach offers a practical method for using modern high-strength disc materials that could be rejected by the application of "safe-life" conditions of usage.

In 1983 the Sub-committee on Damage Tolerance Concepts for Critical Engine Components, under the chairmanship of D.A.Fanner (UK), organized a Cooperative Test Programme on Damage Tolerance in Titanium Alloy Engine Disc Materials. A separate Sub-committe on Engine Discs Cooperative Tests (TX-114) was formed to direct this activity. Over the years the following Panel members participated in the sub-committee:

A.Ankara (TU)
H.M.Burte (US)
H.J.G.Carvalhinhos (PO)
M.N.Clark (CA), Chairman 1983–85
D.Coutsouradis (BE)
J.J.De Luccia (US)
G.L.Denman (US)
A.Deruyttere (BE)
M.Doruk (TU)
W.Elber (US)
D.A.Fanner (UK)
J.J.Kacprzynski (CA) Chairman 1986–
R.Labourdette (FR)
J.S.L.Leach (UK)
A.Salvetti (IT)
R.Schmidt (US)
H.P.van Leeuwen (NL)
W.Wallace (CA)
H.Zocher (GE)

The cooperative tests were performed by twelve laboratories represented by

J.Foth, IABG, GE
A.Frediani, Univ. of Pisa, IT
C.Gostelow, RAE UK
C.Harmsworth, AFML, US
C.Howland, RR, UK
R.H.Jeal, RR, UK
E.U.Lee, NADC, US
A.Liberge, CEAT, FR
N.McLeod, RR, UK
A.J.A.Mom, NLR, NL
T.Pardessus, CEAT, FR
M.D.Raizenne, NAE, CA
W.Schütz, IABG, GE
P.Sooley, Univ. of Toronto, CA
J.Telesman, NASA, US
M.Yanishevsky, QETE, CA
C.Wilkinson, RR, UK

The coordinators of the programme were:

for Europe — A.J.A.Mom
for North America — M.D.Raizenne

As a result of the very large size of the test programme, it appeared to be convenient from an administrative point of view to divide it into a Core Programme followed by Supplemental Programmes. In the Core Programme all the laboratories performed identical fatigue and fracture tests for one material at constant amplitude and at room temperature. A summary of these tests is included in the present report, and all the test data are stored at the National Aeronautical Establishment of the National Research Council of Canada and are available on request. In the Supplementary Programme, now in progress, three

materials are tested at room temperature and with load patterns represented by TURBISTAN. High temperature tests of fatigue and crack growth will be performed in a separate programme.

The part of the Cooperative Engine Disc Test Programme completed to date produced very valuable results and represents a significant progress in implementation of damage tolerance concepts to life evaluation of engine critical components. Many thanks to all who contributed to this very difficult activity and particularly to the participants and the coordinators. Special thanks are due to R.H.Jeal, who, in spite of his busy professional life at Rolls Royce, was a catalyst and strong supporter of the programme.

Many thanks to participating laboratories and particularly to:

NLR — for producing programme reports, bookkeeping, fractography tests and analysis of test data.
Rolls Royce — for supplying engine discs and producing test specimens.
NAE — for data collection, statistical analysis, presentation and storing.
QETE — for fractography tests on selected specimens.

During the execution of this test programme, close cooperation has been developed with participants of other panels' activities and particularly with the Short Cracks Test Cooperative Programme. Not only did the chairman of that sub-committee, H.Zocher, participate as an Engine Discs Sub-committee member, but also both coordinators, Dr P.R.Edwards and Dr J.C.Newman volunteered to participate actively. Their contribution is greatly appreciated. As a result of the cooperation of these two Sub-committees an additional joint test programme has been formulated. It is now in progress and the results will be included in future reports.

The objectives of the Engine Discs Cooperative Test Programme have been achieved. Even more than was planned has been achieved. This is demonstrated by the fact that each of the participating laboratories independently produced results as good as the others. This may diminish the reluctance to use other's data for life determination of critical components.

The second unplanned achievement was the development of close friendships between the participants. As a result of this, a person performing a difficult and risky life evaluation of a critical engine component can consult his friends in other NATO countries. This may help in finding better solutions to our common problems.

The development of close cooperation of professionals of NATO countries was a dream of Theodore von Karman and it is a pleasure to see that it has been achieved.

J.J.Kacprzynski
Chairman 1986—
Sub-Committee on
Engine Disc Cooperative Test Programme

STRUCTURES AND MATERIALS PANEL

Chairman: Prof[illegible] Paolo Santini
Dipartimento Aerospaziale
Universita degli Studi di Roma
"La Sapienza"
Via Eudossiana, 16
00185 Roma — Italy

Deputy Chairman: Prof. Dr-Ing Hans Försching
Direktor der DFVLR Institut fur
Aeroelastik
Bunsenstrasse 10
D-3400 Gottingen — Germany

SUB-COMMITTEE MEMBERS

Chairman: Dr J.J.Kacprzynski
Structures and Materials Laboratory
National Aeronautical Establishment
Ottawa, Ont K1A 0R6 — Canada

SMP MEMBERS

Dr H.J.G.Carvalhinhos — PO
Mr D.Coutsouradis — BE
Dr J.J.De Luccia — US
Dr G.L.Denman — US
Prof. A.Deruyttere — BE
Prof. M.Doruk — TU
Dr W.Elber — US
Mr R.Labourdette — FR
Prof. L.S.L.Leach — UK
Dr-Ir H.P.van Leeuwen — NL
Prof. A.Salvetti — IT
Dr W.Wallace — CA
Mr H.Zocher — GE

TECHNICAL COORDINATORS

Ir A.J.A.Mom — NL
Mr M.D.Raizenne — CA

PANEL EXECUTIVE

Mr Murray C.McConnell — UK

AGARD-OTAN
7, rue Ancelle
92200 Neuilly sur Seine
France
Tel: (Paris) (1) 47.38.57.90 Telex: 610176

From USA & Canada
AGARD-NATO
Attn: SMP Executive
APO New York 09777

ABSTRACT

This report describes the initial results of an AGARD test programme on fatigue behaviour of engine disc materials. The first phase of this programme, the Core Programme, was aimed at test procedure and specimen standardisation and calibration of the various laboratories. A detailed working document has been prepared and is included in this report. It describes the testing fundamentals and procedures and includes the analysis procedures used for handling the test data.

Fatigue crack initiation and propagation testing was performed on Ti-6Al-4V material under room temperature and constant amplitude loading conditions using four different specimen designs. All results were statistically analysed for possible significant differences in material behaviour due to disc processing variables, specimen location in the disc or testing laboratory. [illegible]

* * *

Ce rapport presente les premiers resultats d'un programme de tests de l'AGARD sur le comportement en fatigue des matériaux constitutifs des disques de moteur. La premiere phase de ce programme, appele le programme Core, a pour objectif de normaliser les procédures d'essai et les echantillons et de procéder a l'etalonnage des appareils de mesure detenus par les différents laboratoires. Un document de travail detaille a ete prepare. Il est joint a ce rapport. Il fournit une description des principes des tests et des procedures utilisees, y compris les procedures d'analyse mises en oeuvre pour le dépouillement des données de test.

Des tests sur le début et la progression des fissurations de fatigue ont ete executes sur du materiel Ti-6Al-4V a température ambiante, avec chargement à amplitude constante, en utilisant quatre echantillons differents, composes du même matériau. L'Ensemble des resultats a été analyse statistiquement afin de noter d'éventuels ecarts significatifs dans le comportement des matériaux, en fonction de l'endroit du prelèvement sur le disque, dûs aux paramètres de fabrication et aux techniques employées par les différents laboratoires.

AGARD ENGINE DISC COOPERATIVE TEST PROGRAMME

by
A.J.A. Mom[1] and M.D. Raizenne[2]
[1] National Aerospace Laboratory NLR
P.O. Box 90502, 1006 BM Amsterdam,
The Netherlands

[2] National Aeronautical Establishment
National Research Council
Montreal Road, Ottawa, Ontario K1A 0R6,
Canada

SUMMARY

This report describes the initial results of an AGARD test programme on fatigue behaviour of engine disc materials. The first phase of this programme, the CORE programme, was aimed at test procedure and specimen standardization and calibration of the various laboratories. A detailed working document has been prepared and is included in this report. It describes the testing fundamentels and procedures and includes the analysis procedures used for handling the test data.

Fatigue crack initiation and propagation testing were performed on Ti-6Al-4V material under room temperature and constant amplitude loading conditions using four different specimen designs. All results were statistically analysed for possible significant differences in material behaviour due to disc processing variables, specimen location in the disc or testing laboratory.

1. PREFACE

The results in this report are a collaborative effort of the following participants and their representatives (in parenthesis the code name of each participant used throughout the text is indicated):

Air Force Materials Laboratory (AFML), WPAFB, Dayton, Ohio, USA; C. Harmsworth	(code: AF)
Centre d'Essais Aéronautique de Toulouse (CEAT), Toulouse, France; A. Liberge, T. Pardessus	(code: CE)
Industrie-Anlagen Betriebsgesellschaft (IABG), Ottobrunn, Germany; W. Schütz, J. Foth	(code: IA)
Naval Air Development Center (NADC), Warminster, Pennsylvania, USA; E.U. Lee	(code: ND)
National Aeronautics and Space Administration (NASA), Cleveland, Ohio, USA; J. Telesman	(code: NS)
National Aerospace Laboratory NLR, Amsterdam, The Netherlands; A.J.A. Mom	(code: NL)
National Research Council, National Aeronautical Establishment (NAE), Ottawa, Canada; M.D. Raizenne	(code: NR)
Quality Engineering Test Establishment (QETE), Ottawa, Canada; M. Yanishevsky	(code: QE)
Royal Aircraft Establishment (RAE), Farnborough, United Kingdom; C. Wilkinson, C. Gostelow	(code: RA)
Rolls Royce (RR), Derby, United Kingdom; R.H. Jeal, N. McLeod, C. Howland	(code: RR)
University of Pisa, Pisa, Italy; A. Frediani	(code: PI)
University of Toronto, Toronto, Canada; P. Sooley	(code: UT)

2. INTRODUCTION

The AGARD engine disc cooperative test programme is a joint international effort to address the problem of fatigue crack growth and fracture of disc materials under operational loading conditions. Knowledge of fatigue and fracture characteristics is a major requirement before a damage tolerance disc lifing approach can be successfully implemented. These aspects are discussed in Reference [1] of which details are given below.

For airframe structures, the damage tolerance design approach was introduced by the USAF in 1970, and it has been effectively applied since then on a number of civil and military aircraft (MIL-STD-1530 and MIL-A-83444). However, for engine components, damage tolerant design has been a recent development. Application of this design approach, with respect to disc lifing, is currently under consideration and occasionally applied. A specification on engine damage tolerance requirements, listed as MIL-STD-1783, has recently been developed.
Nevertheless, most discs are currently designed based upon the so-called safe-life philosophy. Both design approaches are concisely reviewed below.

Safe life design

Currently safe life design is still the most widely used approach in the lifing of engine discs. In this respect, "safe life" means that parts are designed for a finite service life during which no significant damage will occur. No critical defects are assumed to be present in the new structure and no inspections are required during the design life. After reaching the safe life limit, the part is retired from service.
With respect to aircraft engine discs, the safe life is defined as the number of cycles at which, statistically, one of every 1000 components will develop a crack of 0.8 mm (1/32 in) surface length. This crack size has been chosen because:

(1) at this size, high cycle fatigue (HCF) crack growth under vibratory conditions would not yet occur,
(2) this crack size was, for existing materials, significantly smaller than the critical crack size for rupture, and
(3) a 0.8 mm crack was considered to be the smallest crack detectable.

The safe life design of discs implies that 999 out of 1000 components are rejected based on the statistical probability of a crack forming without actually requiring the presence of a detectable crack. From economic considerations this is not very attractive. It has been shown [2-4] that owing to a large scatter in the time to initiate and grow a crack to a detectable size, most of these retired components still have considerable service life left. If components could be withdrawn from service based on the presence of an actual crack, then a much better usage of this inherent available life would become possible. This latter approach is in essence the basis of the damage tolerance design philosophy.

Damage tolerance design

In damage tolerance design, the possibility of a crack or defect present in a new structure is accounted for. Assuming that crack growth can be predicted in critical locations under operational loading conditions, safe inspection intervals can be established. Regular inspections will then screen out those components which have insufficient life to be returned to service, as indicated in Figure 1. As can be seen from this figure, the inspection interval is based on the maximum allowable crack size in service, a_m, the minimum reliably detectable crack size by means of non destructive inspection (NDI) or other techniques, a_d, and the availability of crack growth data.

From the foregoing it is clear that several key design parameters are required before the damage tolerance lifing approach can be successfully implemented:
- the operational load history of discs,
- material crack growth data for the appropriate loading conditions, and
- the suitability of NDI or other techniques for the reliable detection of very small cracks.

In recent years considerable progress has been made in inspection capability. It has been claimed [5] that under proper inspection conditions, working with well motivated people and very special equipment, cracks of 0.375 mm surface length and 0.125 mm depth can be detected at the 90 % probability/95 % confidence level. At present, however, it seems more realistic to assume a crack detection capability for cracks of at least 0.750 x 0.375 mm [6].

With respect to monitoring of operational load parameters, several systems are presently in use, e.g. the AID (Aircraft Integrated Data) and EUM (Engine Usage Monitoring) Systems. Proper analysis of the recorded signal to enable accurate determination of life consumation or crack growth prediction is, however, still in an exploratory stage. A considerable amount of work in this area is being performed by the Turbistan working group, with the goal of developing a standard or reference load sequence for gas turbine discs [7].

The third basic requirement, essential for application of the damage tolerance philosophy, is knowledge about material crack growth and fracture behaviour under operational conditions. This is the area which the current AGARD cooperative test programme addresses. An extensive amount of data and a basic understanding of material fatigue crack growth behaviour is needed before damage tolerance lifing procedures can be implemented. By adopting the common effort of a number of laboratories, a broad data base and an improved knowledge and understanding of the testing techniques could be realised. This was achieved by the first phase of this collaborative programme.

3. TEST PROGRAMME OBJECTIVES

The major objectives of this AGARD coordinated programme are:
- the determination of material behaviour, crack initiation and propagation characteristics under realistic engine conditions, and
- the examination of the ability of fracture mechanics to predict crack growth behaviour in discs under service conditions.

The first phase, the CORE programme, was aimed at test and specimen standardisation and familiarisation, and calibration of the different laboratories. The second phase, the SUPPLEMENTARY programme, will specifically address parameters representative of real service operation-like mission loading, sequence and dwell effects, temperature, fatigue thresholds, etc. In addition, life prediction methods, their applicability and limitations, will be addressed in this phase.

The major objectives of the CORE programme are:
- familiarisation of various laboratories in North America and Europe with new test techniques, such as the potential drop technique for crack length measurement and automated data acquisition,
- standardization of test specimens and test techniques for engine disc materials,
- calibration of the various laboratories via a round robin test programme in order to gain confidence in each other's results, and
- material data collection, using Ti-6Al-4V, for verification of life prediction techniques used in damage tolerance design of engine discs,
- identification and documentation of data analysis techniques.

The set-up of the CORE programme, the test procedures and the results are presented in the following sections.

4 CORE PROGRAMME

4.1 CORE Programme Set-Up

The CORE programme test matrix is shown in Table 1. Each laboratory performed all the tests in the matrix for comparison and calibration purposes. The test matrix consisted of a series of fatigue life tests (unnotched and notched specimens) and a series of crack propagation tests (compact tension and corner crack specimens). With these data, both the safe life and the damage tolerance approach could be addressed.

All testing was performed under load control, constant amplitude and room temperature conditions. The fatigue load levels were chosen to achieve realistic lifetimes to failure and/or crack propagation rates. For valid comparison of the individual laboratory test results, a working document detailing the procedures for instrumentation, measurement, testing and data acquisition was developed and is included in this report as Appendix A. Coordinators, one from Europe and one from North-America, were selected to oversee the programme and to collate and analyse the data.

4.2 Specimens

4.2.1 Specimen types/background

For standardisation purposes four specimens were selected for fatigue life and crack propagation testing. One of the goals of the programme was to establish specimens as standards and thus encourage other laboratories to use them. In this way a broad data base using these specimen geometries would be created. The selected specimens are shown in Figure 2. The specimen shown in Figure 2a is a smooth

cylindrical specimen (designated as LCF-specimen) used for fatigue life testing. The flat double edge notched specimen with a $K_t = 2.2$ (designated as K_t 2.2 specimen), Figure 2b, is also used for fatigue life testing. However, apart from the life to failure the life to crack initiation (or better: life to a certain crack size) can also be determined. The well known ASTM compact type, also called compact tension specimen (designated CT-specimen) with a through thickness notch is shown in Figure 2c. This specimen is used for crack propagation testing in the so-called long crack regime, where the crack geometry is normally two-dimensional and the initial crack length is much larger than the grain size of the material. The total da/dN-ΔK curve including the fatigue threshold, ΔK_{th}, can be determined using this specimen. The fourth specimen, shown in Figure 2d, is the corner crack specimen (designated CC-specimen).This specimen was designed specifically for crack propagation testing of disc materials to simulate the same three-dimensional stress fields as those encountered in critical locations such as bolt holes. In this respect, it is necessary to refer to Pickard et al (8) who have shown that the crack propagation curve obtained with CC-specimens clearly falls below the curve generated with CT-specimens. As a result, when comparing specimen crack growth data with crack growth in an actual disc, the latter will be well predicted with CC-specimen data, whereas the use of CT-data could result in an underestimation of life by a factor of two. Bearing this in mind it was considered essential that both types of crack propagation specimens be used in the programme. As well, the CC-specimen was considered ideal for determining short crack effects for coarse grained materials.

4.2.2 Specimen machining and location

All specimens for the CORE programme were machined by Rolls-Royce. The specimens were extracted from two nominally identical fan disc forgings supplied to Rolls-Royce by two different forging vendors. The forgings were made from Ti-6Al-4V in the solution treated and aged (STA) condition. The disc cut-up drawing indicating the location of each individual specimen is shown in Figure 3. The orientation of the specimen crack planes in relation to the forging directions was specified so it would be the same as encountered in service. The distribution of specimens was arranged such that three North-American and three European laboratories obtained complete sets of specimens from one disc, and the remaining laboratories obtained complete sets of specimens from the other disc, as seen in Figure 3c. This would allow possible differences in material behaviour between the two discs to be identified and to facilitate the exchange of material from the two discs for metallurgical examination.

4.2.3 Basic material properties

Basic material properties for these discs were determined by Rolls-Royce. These are given in Table 1, and are compared with the "Material Specification minimum value" (i.e. the lowest acceptable property values expected from such forgings). In general, the measured properties were equal to or better than the specified minima. The sole exception to this was the 150 °C ductility (% RA) which was slightly low. However, this anomaly was ameliorated by the elongation measured from the same specimen.

It was concluded that the two discs supplied formed a good basis for this cooperative programme.

4.2.4 Microstructure

The microstructure of the Ti-6Al-4V disc material, which was in the STA (solution treated and aged) condition, consisted of equiaxed α-phase in a transformed β-matrix containing coarse acicular α (Figure 4). Occasional α-alignments were observed as seen in Figure 5.

The amount of α-phase, determined with quantitative metallography, was about 40%. Cross-sections were prepared in three perpendicular directions: in the plane of the disc, perpendicular to the disc plane in the radial direction and perpendicular to the disc plane in the circumferential direction. No obvious differences in microstructure in these three directions were observed.

Texture differences between selected specimens were determined by the RAE. For this purpose slices were prepared from tested specimens, see Figure 6. Note that the surface on which the texture measurement was performed was a radial plane perpendicular to the disc plane. Slices for the texture determination were prepared from specimens CC 14, 16, 18, 20 and 22 from both discs. Specimens CC 14, 16 and 18 were selected to indicate texture variation in the axial direction of the disc, whereas specimens CC 16, 20 and 22 were selected to indicate radial texture variation.

An indication of texture in a material can be obtained by the use of pole figures. In the following a short explanation of the construction and purpose of pole figures is given.

Crystallographic planes, axes and angles can be represented on a sphere, known as the reference or polar sphere, when a crystal is assumed to be small compared to the sphere and to be located at its centre. One way to represent the crystal planes on the sphere is to erect perpendiculars to the planes. These plane normals are made to pass through the sphere centre and to intersect the spherical surface at points known as the poles of the planes. The array of poles on the sphere form a pole figure, which represents the orientation of the crystal planes. In practice it is more convenient to use a map of the sphere known as the stereographic projection. This enables a two-dimensional representation of the pole figure. Such representations are commonly used to compare textures, which are preferred orientations of crystal planes within a polycrystalline sample. To do this the stereographic projection is aligned to the overall geometrical features of the specimen and the number of grains in various ranges of orientation are then indicated in it by a series of contour lines. The experimental information is usually obtained from the relative intensities of X-ray reflections from the polycrystal at various angular settings.

The pole figures of the selected specimens are shown in Figure 7 for disc LWMD 7200 and in Figure 8 for disc WGWMD 1113. Each set of figures (a) through (f) shows the {0002} pole figures, whereas the figures (g) through (l) show the {110} pole figures (equivalent to {11$\bar{2}$0} in 4-axis notation) for various positions in the discs. (Note that the specimens CC 20 and CC 22 of disc WGWMD 1113 where processed in a slightly different way. Instead of the {110} (equivalent to {11$\bar{2}$0}) pole figures the {10$\bar{1}$0} pole figures were determined, see Figures 8(k) and 8(l). However, this does not alter the conclusions.) The figures (a), (b) and (c) give an indication of the texture itself and the texture variation in the axial direction (specimens CC 14, CC 16 and CC 18 respectively, see also Figure 3 for their detailed position) and figures (d), (e) and (f) give an indication of texture variation in the radial direction (specimen nrs CC 16, CC 20 and CC 22 respectively). The figures show that the textural differences between the discs are relatively small. If a strong texture would exist then much higher figures for the contour levels would have been encountered. As mentioned before, these contour levels indicate relative densities of crystallographic orientations in specific directions. Disc WGWMD 1113 (Figure 8) showed slightly more texture and a

greater variation in texture in the axial direction than disc IWMP 7200 (Figure 7). In the radial direction the variation was less than that displayed in the axial case. In fact, very little difference was observed between specimen positions CC 20 and CC 27. Discussions with RAE indicated that the observed texture and texture differences were not very marked, even between the two discs, and that these differences would not be expected to result in appreciable changes in material properties.

5. TEST PROCEDURES

5.1 General

All testing was done according to the "Working document for the AGARD cooperative test programme on titanium alloy engine disc material" (9). During the actual test phase of the programme, as a result of data generation and testing experience, this document was modified and amended and is included as Appendix A.

5.2 Potential drop crack measurement technique

An interesting aspect of the test programme was that crack initiation and growth was monitored by means of the potential drop (PD) technique. This technique requires that a constant current be passed through the specimen and the electrical potential over the crack plane be measured by two probes located on opposite sides of the crack. If the relationship between crack length and voltage is known, as seen in Figures A6 and A13 of Appendix A for the CT and CC specimen respectively, an accurate determination of crack length can be achieved.

The advantage of the PD method is that crack length detection is also possible in a closed furnace and that automated data collection is easily attained. Additionally, the average crack length is determined instead of the surface crack length as in the case of optical measurements. Changes in crack front curvature are thus accounted for.

A typical set-up for fatigue testing and crack length measurement is shown in Figure [illegible]. Note that apart from the notch voltage, a reference voltage is measured to account for temperature effects and current variations. Thermoelectric effects and drift of the system are eliminated by taking the difference of two measurements, one with current-on, one with current-off.

5.3 Example description of crack length measurement using the PD technique

To illustrate how the actual procedure for crack growth measurement was performed, the following example using a CC specimen is given. An instrumented corner crack specimen is shown in Figure [illegible] (note that for reasons of simplicity both the notch probe wires and the reference wires were welded on the same edge). In the actual test programme, to prevent the occurrence of a reference potential change due to crack growth the reference probes were welded at a location at which the potential field was not affected by crack growth, i.e. at the opposite corner.

The result of a preliminary test on the dummy specimen shown in Figure 10 is presented in Figure [illegible]. The figure illustrates the importance of the location of the reference probes, clearly showing the decrease in reference potential as a result of being located in the vicinity of the growing crack.

The actual crack growth curve (average crack length versus cycles) was constructed after calibration of the notch voltage versus crack length. For this purpose the average crack size at the end of the test was determined first. The specimen was deliberately broken open and the mean of five fracture surface crack length readings were taken; two at the side surfaces, i.e. the surface crack lengths, the other three at angles of 22.5°, 45° and 67.5°. This averaging method resulted in only a very minor difference from the real average crack length obtained by fracture area measurement. The calibration curve is now obtained by drawing a straight line through this final data point and the origin (Figure [illegible]). This straight line assumption is justified if the distance between the notch probes is small with respect to the specimen width (see Appendix A, Figure A13; for this particular specimen [illegible]).

Figure 12 also shows the relation between the notch voltage and crack size measured optically at the specimen surface during the test. This curve indicates that the optical measurement underestimates the average crack length as defined by the calibration curve. The cause of this effect is the crack front curvature at the specimen surface, as seen in Figure 14. This example clearly illustrates the advantage of the PD method for crack length determination over the optical method. In addition, the PD method sensitivity is very good. The system shown in Figure 9 allows changes in crack length to be detected with better than 5µm sensitivity.

In Figure 13 another feature can also be seen. In the early [illegible] of the test, testing was interrupted for heat tinting in order to have an additional data point for calibration. This data point, also plotted in Figure 12, lies exactly on the calibration curve, giving additional confidence in the adopted method.

The calibration procedure described above for the CC specimen is similar to that used for the CT specimen with the exception that the calibration curve for this specimen is a third order polynomial function. However, measurement of the final average crack size from the fracture surface as was done for the CC specimen, is sufficient to fix the position of the calibration curve.

5.4 Test procedure variations

Although the procedures for testing are described in detail, there were still variations between laboratories in the actual testing techniques. This was due to: hardware limitations; differences in programmes for computer controlled fatigue testing; and differences in the way the potential drop method was applied. Some of the more important variations in test procedures are documented below.

The major variations in test procedures concern the potential drop measurement technique. In particular, the CC specimen PD-data was not always obtained or could not be easily analysed because of slight differences in probe wire attachment. In one case of a CT specimen, both the Rumul foil PD method and the optical crack length measurement techniques were employed. (The RUMUL foil is an electrically conductive tape which is adhesively bonded to the specimen so that surface crack growth, which extends into the foil, can be measured). The Rumul foil was attached to one side of the CT-specimen, giving PD crack length data

only for that particular surface.

The PD-measurement technique itself was performed in different ways. The recommended procedure is sh[illegible]n in Figure A5 of Appendix A. In the procedure both current-on and current-off measurements are done at [illegible]ximum load within the timeframe of one second. However, because of hardware limitations, the time needed for two successive measurements of notch and reference voltages was sometimes in excess of one second. Thus, these voltage readings at times could not be measured simultaneously. This problem was accentuated with the K_t 2.2 specimen, where two notch voltages and one reference voltage had to be measured simultaneously. In addition, the current should be stabilized between current-on and current-off measurements.

The above problem was overcome either by lengthening the time at load for these particular measurement cycles or by doing notch and reference measurements in successive cycles. If the first method was applied the maximum time at load had in one case to be increased from 1 to 1.3 seconds; in another case from 1 to 4 seconds. Other laboratories adopted the second method: the execution of PD measurements in successive cycles.

Both methods might have an effect on the test results. An increased time at maximum load (for the measurement cycles) could enhance the dwell effect although this effect is probably very minor. PD measurements in successive cycles might give, at very high crack growth rates, a minor shift in crack growth data but this can be simply overcome by counting the cycles during the actual notch measurement (the current-off and reference voltage will change only slowly).

6. RESULTS

The test results for the four specimens tested are discussed individually in the following subsections.

6.1 Smooth cylindrical LCF specimens

6.1.1 General introduction

All test results are presented in Table 3 and are shown graphically in Figure 14. Note that, unlike engineering convention, the stress range as the independent variable is plotted on the horizontal axis and the cycles to failure on the vertical axis for commonality with the statistical analyses of the results (next sections). The results appear to indicate that the LWMD 7200 disc data are slightly above the WGWMD 1113 disc data. This agrees with the data in Table 2. A statistical analysis of the results was performed to detect possible differences in material behaviour for the two discs, or for particular locations in the discs, or to indicate deviating trends in the results of individual laboratories. The analysis involved the establishment of linear relationships between stress and life based on a log-normal distribution, the establishment of confidence intervals for these curves, and tests on the validity of the application of the linear model.

The linear expression used in the statistical analysis was:

$$Y = A + BX \qquad \text{in which } \begin{aligned} Y &= \log N \\ X &= \Delta\sigma \\ N &= \text{number of cycles to failure} \\ \Delta\sigma &= \text{stress range} \end{aligned}$$

The statistical analysis was performed according to the procedures described in ASTM standard Practice E 739-80 [10]. A short summary is given in Appendix B.

6.1.2 Statistical handling of the smooth cylindrical LCF specimen data

An initial statistical analysis was performed on all the data, except the one run-out, CEAT LCF 38 which failed in the thread after 16,262 cycles. The results, see Figure 15, show that data obtained at very high stress levels (stress range ~ 875 MPa) exhibited large scatter causing a major shift in the position of the mean curve for all the results. The high stress range of 875 MPa corresponded to a maximum stress of 972 MPa which is near or above the minimum specified tensile strength for the material as seen in Table 2. For this reason these test data were omitted from the statistical analysis. The results obtained in the lower stress ranges of 700 to 830 MPa had more appropriate lives to failure of 2000 to 50,000 cycles with less scatter.

The data were reanalysed and the resultant mean curve and the 95 % confidence interval are shown in Figure 16. The meaning of the confidence interval is that, based on the analysis of a series of independent data sets, we may expect that 95 % of the computed intervals will include the mean curve. Or, in other words, the statement "the mean curve (of the total distribution) lies within the computed interval" has a 95 % probability of being correct (see Reference [10]). Figure 16 also shows the computed statistical parameters $\hat{A}$ and $\hat{B}$ (which are the maximum likehood estimators of A and B, the line-coefficients) and their intervals for a 90 and 95 % confidence level. In addition, the variance and the parameters indicating the correctness of the linearity hypothesis are indicated. These parameters are described in more detail in Appendix B.

As can be seen from the computed statistical data (see Fig. 16) the linearity hypothesis, for all results, was invalid. However, the rejection of the linearity hypothesis is caused by a single data point ($\Delta\sigma$ = 828 MPa, N = 437 cycles, disc WGWMD 1113). When the statistical data handling was repeated with the omittance of this particular test point, the linearity hypothesis was shown to be valid. For reasons of simplicity, the assumption of linearity in the range of 2000 - 50,000 cycles to failure was therefore considered to be appropriate. The linear model was also used in all subsequent analysis. (Note: the particular data point was not removed in the analysis).

6.1.3 Statistical comparison of individual laboratories, discs and disc locations

Figures 17 through 28 show the outcome of the subsequent statistical analyses in which various comparisons were made as follows:

1. individual disc results with respect to the overall data,
2. individual laboratory results with regard to the respective disc data (and corresponding confidence intervals) and with regard to the overall data, and
3. various disc locations with regard to the respective disc data.

Figures 17 and 18 show the test results and associated median curves and confidence intervals for discs WGWMD 1113 and LWMD 7200 respectively. The statistical parameters are also given. The results show that the assumption of a linear relationship is valid for the LWMD 7200 disc data but that this assumption is incorrect for the WGWMD 1113 disc data. This was caused by the single data point discussed in Section 6.1.2 resulting in a steep line coefficient B (i.e. slope) for disc WGWMD 1113.

A comparison between the individual median curves for the two discs, as constructed in the Figures 17 and 18, with the overall median curve for all results, Figure 16, is shown in Figure 19. In this figure, the test data for disc WGWMD 1113 tend to fall slightly below the disc LWMD 7200 data as mentioned in Section 6.1.1. for the somewhat higher stress ranges. At these highest stress ranges ($\Delta\sigma \sim 820$ MPa) the maximum difference in fatigue life is about a factor of 1.5.

Figure 20 shows the overall median curve and the median curve for disc WGWMD 1113. The individual fitted curves of the six laboratories which tested this disc are also plotted. Most of the individual curves fall within the 95 % confidence interval for the overall curve. However, some data fall outside this interval. This behaviour may be expected since the number of specimens tested per laboratory was small.

In Figure 21 a similar comparison is made. However, the overall median curve and associated confidence interval have been omitted and the indicated 95 % confidence interval now relates to disc WGWMD 1113 only. In this case the individual laboratory curves fall within the wider 95 % confidence interval. Although there is a clear difference in line coefficients for the various laboratories and a slight shift in the line position, there is no major indication that the results from an individual laboratory clearly fall outside the scatter band.

Figures 22 and 23 are equivalent to Figures 20 and 21 but now refer to disc LWMD 7200. Most of the individual laboratory curves for this disc run almost parallel to the overall median curve and the disc median curve with one exception, which shows a more steep relationship. Figure 23 also shows that all individual curves fall within the 95 % confidence interval for the disc median curve. Thus there is no indication of clearly deviating results for individual laboratories.

During disc design and production the intention was to obtain homogeneous properties throughout the disc. The test results enabled us to check whether this objective was met. To this end different locations in the disc were identified (see Figure 24) which could provide an indication about radial and axial variations in material behaviour. Figures 25 and 26 show, for the respective discs, a comparison of the fitted relationships for various radial locations with respect to the median disc curve. Figures 27 and 28 show similar comparisons for different axial locations.

The results indicate that differences do occur due to location. However, these differences appear to be insignificant. In Figure 25, disc WGWMD 1113, the RIM area tends to be superior with respect to the MID and BORE locations at the higher stress range, but it is inferior at lower stress ranges. This behaviour is not very logical. If the RIM area would indeed have superior fatigue properties than one would expect that this superiority would manifest itself over the entire life regime, especially because it is not expected that the failure mode would change significantly in this particular regime, and thus that it would result in an upward shift of the fatigue life curve. The observed line-crossings of the RIM, MID and BORE life lines are therefore most probably the result of normal scatter in the test data and the relatively small batches used for this location analysis. Another important point supporting the above conclusion is that one would expect that a certain trend in material behaviour for various locations would be similar for both discs. However, in comparing Figures 25 and 26 such a trend could not be observed. Figure 26 for example, disc LWMD 7200, shows that the RIM, MID and BORE locations are essentially similar in fatigue behaviour.

A comparison with respect to axial locations for both discs was made in Figures 27 and 28. Line-crossings were also observed in Figure 27, disc WGWMD 1113, MID and AFT locations. In addition, the two discs do not show similar behaviour for the various locations, which would have been expected if there was a trend in material properties for a certain location. In Figure 28 the fitted curves, per location, are grouped closer together although the MID results tend to be somewhat lower.

In reviewing the above obtained location relationships all results seem to suggest that there is no apparent material inhomogeneity in relation to LCF fatigue properties for the various locations studied in this analysis.

6.2 Flat double edge notched K_t 2.2 specimens

6.2.1 Introduction

For the K_t 2.2 specimens both the life to crack initiation and the life to failure were determined. Life to crack initiation was defined as the number of cycles at which a 1 % increase in potential drop value was obtained. The actual crack size for a 1 % PD increment was estimated by breaking open one of the (dummy) specimens at the 1 % PD increase level, as seen in Figure 29. The crack shape was semi-elliptical and had a maximum crack depth of about 0.6 mm, with a surface length of 1.6 mm.

All test data are presented in Table 4. The life to failure results for both discs are shown in Figure 30. Again, unlike engineering convention but for commonality with the statistical analyses, the stress range as the independent variable is plotted on the horizontal axis whereas the cycles to failure are plotted on the vertical axis. Figure 31 shows the life to initiation and the life to failure for disc LWMD 7200 only. Figure 30 shows that the spread in results for the K_t 2.2 specimens is smaller than for the LCF specimens. This effect is especially evident for the high stress levels. Another finding (see Table 4) is that life to initiation and life to failure are closely related. Furthermore the life to initiation, as defined, accounts for the greatest part (~ 85-95 %) of the total life of the specimen. This occurs because of the fairly large crack size associated with an initiation level of 1 % PD increment.

Almost no difference in notched fatigue behaviour between the two discs was observed. However, in order to detect possible trends in material behaviour between the two discs, and between individual laboratories and disc locations, similar statistical analyses were performed as on the LCF data.

6.2.2 Statistical handling of the K_t 2.2 data

An initial statistical analysis was performed on all data, excluding the run-outs (in total three), shown in Figure 32. The single data point at the highest stress range ($\Delta\sigma$ = 1091 MPa, N_f = 38 cycles) affects the position ($\hat{A}$) and the line coefficient ($\hat{B}$) (i.e. slope) of the median curve in the area of interest, the life regime between 1000 and 100,000 cycles. Following the procedure adopted for the LCF specimens, this data point was omitted from all subsequent statistical analysis. The remaining data were

again statistically analysed and the results are shown in Figure 33, together with the 95 % confidence interval for the median curve. As can be seen the linearity hypothesis for the median curve was determined to be correct in this life regime.

6.2.3 Statistical comparison of individual laboratories, discs and disc locations

Figures 34 through 45 show the outcome of the statistical analyses in which the following comparisons were made:

1. individual disc results with respect to the overall data,
2. individual laboratory results with regard to the respective disc data (and corresponding confidence intervals) and with regard to the overall data, and
3. various disc locations with regard to the respective disc data.

Figures 34 and 35 show the test data and fitted relationships including the 95 % confidence intervals, for discs WGWMD 1113 and LWMD 7200 respectively. The assumption of linearity for the median curve was justified, as can be seen from the statistical parameters. A comparison between the median curves of the two individual discs with the overall median curve for all results (Fig. 33) is shown in Figure 36. The individual median curves lie close to the overall median curve and, in addition, line-crossing was observed. Both facts suggest that there is no apparent difference in the notched fatigue behaviour of the two discs.

In Figure 37 the overall median curve and the median curve for disc WGWMD 1113 are shown and, in addition, the fitted curves for the six individual laboratories which tested this disc have been plotted. All individual curves fall within the 95 % confidence interval of the overall median curve. In Figure 38 a similar comparison is made. However, the overall curve and its associated confidence interval have been omitted and the 95 % confidence interval now relates to disc WGWMD 1113 only. Although some difference in line positions and coefficients can be observed there is no indication that the results of individual laboratories clearly fall outside the scatter band.

The individual laboratory curves for disc LWMD 7200 are shown in Figures 39 and 40. These curves have a wider spread than in the case of disc WGWMD 1113. Figure 39 shows that not all individual curves fall completely within the 95 % confidence interval for the overall median curve. However, Figure 40 shows that these curves fall within the 95 % confidence interval of the disc median curve. Because of the small size of the individual batches no firm conclusions can be drawn about the significance of the variation in individual laboratory test results.

A comparison in notched fatigue behaviour between different locations in the discs was also made. Figure 41 shows the identification of the various radial and axial locations used in the subsequent analysis. Figures 42 and 43 show for both discs the comparison in fatigue behaviour of the radial locations with the median disc curves. Similar comparisons with respect to the various axial locations are shown in Figures 44 and 45. The results indicate that the variations between different disc locations are very small; there is no apparent material inhomogeneity with respect to the notched fatigue properties for both discs.

6.3 Corner Crack (CC) and Compact Tension Type (CT) Specimens

6.3.1 Data Analysis

Fatigue crack growth data from 33 corner crack and 35 compact tension type specimens were collected and analysed. Typically for each specimen data set, 50 pairs of crack length and cycle count data were provided for the analysis. The data were provided in the as recorded condition in order to facilitate the use of a common smoothing technique.

Four smoothing techniques were considered for the da/dN analysis procedure: the secant method, the modified difference method, the seven point incremental polynomial method and the total polynomial method. The seven point incremental polynomial technique was ultimately chosen because there were sufficient numbers of data points available in each data set, the technique is recommended in the current ASTM standard for fatigue crack growth rate testing, Reference [11], and it possessed sufficient smoothing capability to identify possible trends in the data.

The seven point incremental polynomial method for computing da/dN as a function of ΔK is described in detail in Reference [11]. Briefly the technique involves fitting a second-order polynomial (parabola) to sets of seven successive values of observed crack length. The form of the equation for the local fit of crack length is:

$$a_i = b0 + b1 \left(\frac{N_i - C_1}{C_2} \right) + b2 \left(\frac{N_i - C_1}{C_2} \right)^2$$

where $C_1 = \frac{1}{2} \left(N_{i-3} + N_{i+3} \right)$

$$C_2 = \frac{1}{2} \left(N_{i+3} - N_{i-3} \right)$$

and b0, b1 and b2 are regression parameters.

The rate of crack growth, da/dN, is obtained by taking the first derivative of the above equation with respect to N:

$$da_i/dN_i = \frac{b_1}{C_2} + 2b_2 \left(N_i - C_1 \right) / C_2^2$$

The value of a_i is used for the calculation of the corresponding ΔK_i. The stress intensity solutions for the CT and CC specimens are described in Sections 3.3.3 and 3.4.4 of Appendix A respectively.

6.3.2 Fatigue Crack Growth Rate Description

In order to utilize the data generated in this analysis for design and life prediction efforts, a curve fitting model is usually applied to the data. A number of curve fitting models have been proposed to describe the sigmoidal shape of the crack growth rate curve. Miller and Gallagher [12] describe an ASTM round robin programme where ten different models were used. One of the most successful models and one of two models selected for this analysis is the table lookup procedure. In this technique tabulated values of da/dN and ΔK values are obtained at regular log da/dN intervals. To build the table, the data for each specimen geometry were combined and sorted by da/dN. At selected intervals of da/dN, the data were averaged and a mean da/dN and ΔK were calculated. Because of the large number of data points available for each specimen geometry, an accurate estimation of the mean performance of the data was thus obtained. The mean crack growth curves are described by 36 pairs of data for the corner crack specimen geometry and by 32 pairs of data for the compact tension specimen geometry. The mean data are presented in Figure 47 and are listed in Tables 5 and 6. Standard deviation data for da/dN are also presented in Tables 5 and 6.

A second model utilized to describe the crack growth behaviour is the power law or Paris model [13]. This model assumes that the crack propagation behaviour over discrete ranges of da/dN is linear and can thus be described by the equation:

$$da/dN = C\Delta K^{n}$$

To obtain the coefficients C and n, the crack propagation data in the assumed upper linear portion of the data were selected by specimen geometry and a least-squares regression line was fitted. The results are shown in Table 7 and in Figure 47. The fitted lines in Figure 47 show an excellent correlation with the mean data obtained using the table lookup model described above.

6.3.3 Test results

The data sets of da/dN versus ΔK are presented in Figures 46 through 63:

Figure 46	The data for each laboratory are identified as a common group for interlaboratory comparisons,
Figure 47	Mean data and power law lines are presented for the two specimen geometries,
Figure 48	The CC data for the two discs are compared,
Figure 49	The CT data for the two discs are compared,
Figures 50 and 51	The data for the two discs, LWMD 7200 and WGWMD 1113, are compared, and
Figures 52 through 63	The data sets for each laboratory are compared to the combined mean data for the two specimen geometries, CC and CT.

In figures 46 to 51, one trend in the data appears consistently. As evident in the mean data in Figure 47, the CT specimen produces a higher crack growth rate than the CC specimen, especially in the higher ΔK ranges. The compact tension data are the more conservative of the two specimen geometries. At ΔK = 16 MPa√m the difference is a factor of 1.42 and at ΔK = 40 MPa√m the factor increases to 1.75. This effect was also noted for Ti-6Al-4V in Reference [8] using the same compact tension and corner crack specimen geometries.

7. FRACTOGRAPHY

Fractographic investigations were carried out by QETE [14] and NLR on both CT and CC specimens. Striation spacings on the fracture surface determined by means of scanning electron microscopy have been compared with the macroscopically observed crack growth rates, determined by the PD method or by optical means. The results of the comparison are shown in Figure 64 for both a CT and a CC specimen. In Table 8 a detailed comparison is given for the CT-specimen.

The results indicate that in general, at the lower ΔK values, the measured striation spacings are larger than the macroscopically determined cyclic crack growth by a factor of approximately 1.7. This situation is reversed at high ΔK values. This behaviour may be explained by the following considerations. At lower ΔK values striations are difficult to observe. Only the larger ones tend to be found, resulting in an overestimation of crack growth rate. At higher ΔK values non-cyclic crack growth, e.g. microvoid coalescence, can contribute such that striation spacing does not reflect the overall (higher) crack growth rate.

In figure 65 an illustration is given of the fractographic appearance of specimen CC 8 at various locations [14]. From these photographs it is clear that microscopic crack growth directions at the lower ΔK values can deviate considerably from the macroscopic growth direction, indicating a strong micro-structural effect. At higher ΔK values, microscopic crack growth aligns itself more with the overall crack growth direction.

8. DISCUSSION

The major objectives of the CORE programme were:

- familiarisation of the participating laboratories with new test techniques, e.g. the potential drop technique and automated data collection;
- standardization of test specimens and test techniques for engine disc materials;
- calibration of the participating laboratories to gain confidence in each other's results; and
- material data collection, using Ti-6Al-4V, for verification of life prediction techniques used in damage tolerance design of engine discs.

The programme succeeded almost completely in the realization of the above objectives. Standard test specimens were selected and test techniques were developed and standardized. The participants, and in addition other laboratories, adopted the new test procedures for their own research programmes and even require that testing under contract be carried out according to the standardized procedures.

As all laboratories applied the same test procedures, their results could easily be compared. A detailed statistical analysis was performed to indicate possible deviating trends in individual laboratory test results. However, the analysis did not confirm any such behaviour. Individual laboratory results fall within expected scatterbands and there was no obvious trend indicating a particular test outcome for

certain laboratories. This is an important result because the participants have now been mutually calibrated, which will give confidence in each other's future test results without the need of continuous duplication.

In the current programme a large amount of data was generated, both in the LCF life area as well as in the crack propagation area. The data will be used as baseline data for the SUPPLEMENTARY programme in which the effect of subcycles, spectrum loading (simple and complex sequences) and different materials (with different grain size) will be investigated. At that stage the baseline test data will be used for comparing material behaviour and will serve as input for the various life prediction models to be applied. In the SUPPLEMENTARY programme the applicability and limitations of these models will be addressed.

The applied testing procedures, making use of PD measurement techniques and automated data collection, proved to be very effective. The accuracy of the system can be brought to a high level if good quality equipment is used, together with a careful PD-instrumentation of the specimens. Ultimately a better than 5 μm crack length sensitivity could be obtained for CC-specimens and about a 10 μm sensitivity for CT-specimens. It should be realized that this accuracy is based on the real average crack length. Even if the same accuracy could be realized with optical measurements the PD-method would still be in favour because the optical method only provides a surface crack length. The difference in crack sizes obtained can be quite large; with the CT-specimens differences of about 1 mm in crack length between the surface and the average value were measured.

9. CONCLUSIONS

1. Standardization of test specimens and testing procedures allowed comparison and calibration of participating laboratories.
2. The statistical analysis of all test results indicated no deviating test outcome for individual laboratories. All laboratories fall within expected scatterbands.
3. The CORE programme collaborative effort generated a large amount of data in both the LCF area and the crack propagation area. The data will be used as baseline data for the SUPPLEMENTARY programme and serve as input for the life prediction models to be applied at that stage.
4. The two specimen types, CT and CC, provided fatigue crack growth information for through thickness and surface/corner crack flaw geometries.
5. The fatigue crack growth data results indicated that the CC crack growth rate data were between 30 to 50 percent slower than the CT data for given values of ΔK between 15 and 35 $MPa\sqrt{m}$.
6. Two numerical techniques, the table lookup procedure and the Paris law technique, proved suitable as curve fitting models.
7. The PD technique is extremely accurate in measuring small flaw sizes in the CC-specimen geometry. A crack length measurement sensitivity down to 5 μm [illegible] be realised.

10. REFERENCES

[1] A.J.A. Mom and M.D. Raizenne; AGARD cooperative test programme on titanium alloy engine disc material, in: Damage tolerance concepts for critical components, AGARD CP 393, 9/1-9, 1985.

[2] S.A. Tatter and J.T. Hill; Design of jet engine rotors for long life, paper 750619 presented at SAE Air Transportation Meeting, Hartford 1975.

[3] C.G. Annis et al; Gas turbine engine disk retirement for cause: an application of fracture mechanics and NDE, ASME-80-GT-127.

[4] E.J. Reed, D.T. Hunter and R.J. Hill; LCC evaluation of advanced engine damage tolerance goals for a hot section disk, AIAA-83-1407.

[5] T.D. Cooper and D.M. Forney; Increased inspection requirements for critical air force engine components; paper presented at the Air Transport Association Non-destructive Testing Forum, Phoenix, September 1982.

[6] C.H. Cook, H.E. Johnson and C.E. Spaeth; Damage tolerant design for cold section turbine engine disks, AFWAL-TR-81-2045.

[7] A.J.A. Mom, W.J. Evans and A.A. ten Have; Turbistan, a standard load sequence for aircraft engine discs, presented at the AGARD Specialists Meeting on Damage Tolerance Concepts for Critical Engine Components, San Antonio, Texas, April 1985; AGARD CP 393, pp 20/1-11.

[8] A.C. Pickard, C.W. Brown and M.A. Hicks; The development of advanced specimen testing and analysis techniques applied to fracture mechanics lifing of gas turbine components, in: ASME International Conference on Advances in Life Prediction Methods; Ed. by D.A. Woodford and J.R. Whitehead, published by ASME, New York, 1983.

[9] A.J.A. Mom; Working document for the AGARD cooperative test programme on titanium alloy engine disc material, NLR TR 84022 L, 1984.

[10] ASTM E 739-80 "Standard practice for statistical analysis of linear and linearized stress-life (S-N) and strain-life (ε-N) fatigue data".

[11] ASTM Standard Test Method E647-83 "Constant-Load-Amplitude Fatigue Crack Growth Rates above 10E-08 M/Cycle", 1983.

[12] M.S. Miller and J.P. Gallagher; An analysis of several fatigue crack growth rate (FCGR) descriptions", ASTM STP 738, 1981.

[13] P. Paris and F. Erdogan; A critical analysis of crack propagation laws, Trans. Am. Soc. Mech. Engrs, J. Bas. Engng, Vol. 85, Series D, No. 4, December 1963, pp. 528-534.

[14] M. Yanishevsky; NATO/AGARD Ti-6Al-4V engine disc material cooperative test programme, QETE report A048383, April 1987.

TABLE 1
CORE Programme test matrix

Type of test		LCF life / crack formation		Crack propagation	
Test specimen		Smooth cylindrical	flat notched $K_t = 2.2$	corner crack	ASTM CT
Number of specimens		6	6	[illegible]	3
CRACK DETECTION TECHNIQUES	potential drop		+	+	+
	optical			+	
goal		total life	total life + initial crack formation	"short" crack range	total da/dN - ΔK curve

Note: All tests conducted at room temperature

TABLE 2
Minimum specified and measured material properties for the two discs tested

	Material specification minimum value	Minimum measured values	
		disc WGWMD 1113	disc LWMD 7200
Room temperature			
tensile strength, MPa	900	949	969
0.2% yield strength, MPa	830	856	865
% elongation	10	11.0	11
% reduction in area	25	29.9	26
150 °C tensile strength, MPa	770	799	819
0.2% yield strength, MPa	650	672	692
% elongation	14	15	14
% reduction in area	35	34.4	41
rotating bend fatigue test			
10^7 cycles, MPa	440*	460	440
LCF fatigue test, R = 0			
10^4 cycles, MPa			
bore	772	890	870
web	772	835	860
rim	772	772	890
fracture toughness, $MN/m^{3/2}$	49.5	53.7	52.3

* minimum value not specified; target minimum is 440 MPa.

TABLE 3
Fatigue life test results on LCF specimens (R=0.1)

DISC WGWMD 1113

laboratory	specimen no.	stress amplitude $\Delta\sigma$ MPa	cycles to failure N_f	laboratory	specimen no.	stress amplitude $\Delta\sigma$ MPa	cycles to failure N_f
UT	LCF 2	800	2850	RR	LCF 33	878	3
	LCF 6	800	2340		LCF 35	828	437
	LCF 4	775	4790		LCF 36	788	5067
	LCF 5	775	5150		LCF 34	788	5687
	LCF 1	750	13540		LCF 38	742	21217
	LCF 3	-	-		LCF 37	742	14515
QE	LCF 19	800	3509	NL	LCF 23	875	<1
	LCF 16	775	5665		LCF 21	800	3151
	LCF 18	775	7050		LCF 25	775	8605
	LCF 17	750	8851		LCF 22	775	7264
	LCF 14	750	12484		LCF 20	750	9457
	LCF 15	700	40341		LCF 24	750	19426
NR	LCF 12	800	1800	RA	LCF 31	880	<1
	LCF 7	800	1900		LCF 27	790	5982
	LCF 9	750	12100		LCF 28	750	8545
	LCF 8	750	8800		LCF 32	750	13284
	LCF 10	725	18500		LCF 29	720	22474
	LCF 11	700	42000		LCF 30	720	15209

DISC LWMD 7200

AF	LCF 19	800	3928	CE	LCF 33	878	40
	LCF 18	775	4672		LCF 35	832	3136
	LCF 16	775	5632		LCF 36	788	8508
	LCF 14	750	16142		LCF 34	788	5440
	LCF 17	750	25933		LCF 38	742	>16262
	LCF 15	-	-		LCF 37	742	23076
ND	LCF 5	825	3831	IA	LCF 27	878	1158
	LCF 2	800	6235		LCF 29	878	348
	LCF 3	775	8174		LCF 30	810	3298
	LCF 6	750	21709		LCF 32	810	4466
	LCF 4	725	41222		LCF 28	742	12805
	LCF 1	-	-		LCF 31	742	14656
NS	LCF 9	809	2679	PI	LCF 22	800	3071
	LCF 8	809	2350		LCF 23	800	2472
	LCF 7	779	5510		LCF 24	775	6874
	LCF 12	766	11016		PCF 25	775	4724
	LCF 10	751	8156		LCF 20	750	9964
	LCF 11	747	11327		LCF 21	750	7540

TABLE 4

Fatigue life test results on K_t 2.2 specimens (R=0.1)

DISC WGWMD 1113

laboratory	specimen no.	stress amplitude $\Delta\sigma$ MPa	cycles to "1% crack initiation" N_i	cycles to failure N_f	laboratory	specimen no.	stress amplitude $\Delta\sigma$ MPa	cycles to "1% crack initiation" N_i	cycles to failure N_f
UT	K_t 5	775	3420	3476	RR	K_t 36	700	5950	6700
	K_t 1	775	4202	4247		K_t 40	562	6700	7900
	K_t 4	625	8484	8920		K_t 35	562	13000	14200
	K_t 2	625	10630	10999		K_t 39	562	17500	19500
	K_t 6	475	22764	23856		K_t 37	486	20500	23500
	K_t 3	475	31717	33026		K_t 38	486	34000	36500
OE	K_t 17	775	3501	3701	NL	K_t 25	775	3026	3557
	K_t 14	775	3301	3726		K_t 26	775	3301	3714
	K_t 15	625	-	10952		K_t 23	625	16941	18584
	K_t 13	625	7701	8826		K_t 24	625	10207	11436
	K_t 18	475	41680	43730		K_t 27	475	27101	29352
	K_t 16	475	36601	38826		K_t 28	475	21501	24118
NR	K_t 10	775	2707	2771	RA	K_t 31	775	2832	3288
	K_t 9	775	2750	2841		K_t 32	775	3023	3810
	K_t 11	625	10090	11191		K_t 29	625	11357	12342
	K_t 8	625	8875	8921		K_t 33	625	11349	12176
	K_t 7	475	29500	30061		K_t 30	475	48748	51337
	K_t 12	475	38500	39551		K_t 34	475	>56511	>56511

DISC LWMD 7200

AF	K_t 14	775	2037	2334	CE	K_t 38	698	4691	5230
	K_t 13	775	2704	3039		K_t 35	562	19832	20599
	K_t 17	625	8131	9254		K_t 37	562	13811	14953
	K_t 16	625	9043	9768		K_t 39	428	201594	211330
	K_t 18	475	21775	23053		K_t 40	428	36500	40190
	K_t 15	475	59499	61568		K_t 36	-	-	-
ND	K_t 1	775	2150	2765	IA	K_t 32	780	2040	2466
	K_t 5	625	5850	6038		K_t 33	776	2510	3039
	K_t 4	625	9200	10258		K_t 34	627	6550	7317
	K_t 6	475	46950	48995		K_t 31	626	7340	9040
	K_t 2	475	27300	29800		K_t 30	528	12300	13180
	K_t 3	-	-	-		K_t 29	475	>63750	>63750
NS	K_t 9	775	4050	4340	PI	K_t 26	1091	28	38
	K_t 12	775	2575	2890		K_t 23	775	3010	3182
	K_t 7	625	9200	9660		K_t 27	625	5964	6800
	K_t 8	625	8950	9810		K_t 28	625	7888	8855
	K_t 11	500	27000	29350		K_t 24	550	17024	17933
	K_t 10	500	25100	27120		K_t 25	475	>55197	>55197

TABLE 5
Mean fatigue crack growth rate data for CC specimens
1247 Data Sets

da/dN m/cycle	Std.dev. m/cycle	ΔK MPa√m	Data Sets	da/dN m/cycle	Std.dev. m/cycle	ΔK MPa√m	Data Sets
5.92E-09	1.41E-09	12.50	11	4.91E-07	1.40E-08	28.00	40
1.08E-08	1.42E-09	12.89	40	5.47E-07	1.94E-08	29.04	40
1.51E-08	1.01E-09	13.43	40	6.11E-07	1.77E-08	30.21	40
1.99E-08	1.85E-09	13.78	40	6.64E-07	1.44E-08	31.03	40
2.95E-08	4.19E-09	14.22	40	7.28E-07	1.97E-08	32.58	40
4.33E-08	4.11E-09	15.06	40	7.98E-07	1.96E-08	33.65	40
6.49E-08	6.58E-09	16.07	40	8.65E-07	1.82E-08	34.72	40
9.10E-08	7.81E-09	17.33	40	9.44E-07	2.99E-08	35.93	40
1.15E-07	8.78E-09	18.31	40	1.05E-06	3.17E-08	36.78	40
1.47E-07	9.10E-09	19.46	40	1.17E-06	3.55E-08	37.77	40
1.75E-07	7.94E-09	20.19	40	1.31E-06	4.80E-08	39.32	40
2.04E-07	1.04E-08	21.66	40	1.47E-06	5.29E-08	40.83	40
2.46E-07	1.15E-08	22.48	40	1.67E-06	6.79E-08	42.12	40
2.79E-07	9.83E-09	23.07	40	1.88E-06	7.01E-08	43.83	40
3.12E-07	9.31E-09	24.48	40	2.12E-06	7.97E-08	45.13	40
3.55E-07	1.45E-08	25.06	40	2.44E-06	1.09E-07	46.41	40
4.02E-07	1.22F-08	26.19	40	2.89E-06	1.69E-07	48.42	40
4.47E-07	1.32E-08	27.66	40	4.10E-06	6.49E-07	51.16	40

TABLE 6
Mean fatigue crack growth rate data for CT specimens
1385 Data Sets

da/dN m/cycle	Std.dev. m/cycle	ΔK MPa√m	Data Sets	da/dN m/cycle	Std.dev. m/cycle	ΔK MPa√m	Data Sets
6.50E-09	1.19E-09	10.98	39	2.68E-07	6.95E-09	20.90	40
1.22E-08	2.45E-09	12.30	40	2.93E-07	8.35E-09	21.31	40
2.15E-08	3.04E-09	12.42	40	3.25E-07	9.70E-09	22.14	40
3.64E-08	5.21E-09	13.70	40	3.58E-07	1.01E-08	22.94	40
5.39E-08	4.86E-09	14.84	40	4.01E-07	1.19E-08	23.61	40
7.40E-08	6.64E-09	15.15	40	4.49E-07	1.56E-08	24.65	40
9.39E-08	4.90E-09	16.16	40	5.04E-07	1.65E-08	25.87	40
1.08E-07	3.57E-09	16.18	40	5.58E-07	1.88E-08	26.65	40
1.19E-07	3.87E-09	16.98	40	6.34E-07	2.68E-08	27.66	40
1.33E-07	3.91E-09	17.21	40	7.53E-07	3.61E-08	29.07	40
1.45E-07	5.00E-09	17.64	40	9.08E-07	5.54E-08	30.77	40
1.64E-07	6.08E-09	18.30	40	1.12E-06	6.64E-08	32.29	40
1.80E-07	3.95E-09	18.48	40	1.29E-06	7.07E-08	33.28	40
1.98E-07	6.32E-09	19.06	40	1.75E-06	1.73E-07	35.97	40
2.19E-07	8.78E-09	19.90	40	2.84E-06	6.75E-07	38.62	40
2.47E-07	7.26E-09	20.27	40	5.24E-06	1.55E-06	42.14	8

TABLE 7
Power law FCGR data

Specimen geometry	Applicable da/dN range (m/cycle)	C	n
CT	8.26E-08 to 1.20E-06	8.3979E-12	3.395
CC	1.80E-07 to 1.96E-06	2.5987E-11	2.951

TABLE 8
Comparison between measured striation spacing and calculated macroscopic growth rate based on PD-data for specimen CT 12 (disc WGWMD 1113)

Distance from notch (mm)	ΔK $MPa\sqrt{m}$	Striation spacing (μm) measured from fracture surface at:				Macroscopic crack growth rate (μm/cycle) based on PD-data	Relation between macroscopic growth rates and measured striation spacing
		¼ W	½ W	¾ W	mean value		
1	15.0	0.084		0.094	0.089	.046	0.52
1.5	15.8	0.103		0.087	0.095	.065	0.68
2.0	16.6	0.150	0.177	0.090	0.139	.085	0.61
2.5	17.5	0.164	0.168	0.155	0.162	.112	0.69
3.0	18.3	0.152	0.198	0.217	0.189	.141	0.75
3.5	19.3	0.178	0.277	0.277	0.244	.161	0.66
4.0	20.3	0.284	0.291	0.221	0.265	.187	0.71
4.5	21.3	0.235	0.325	0.335	0.298	.215	0.72
5.0	22.5	0.245	0.398	0.504	0.382	.251	0.66
5.5	23.7	0.297	0.342	0.322	0.320	.281	0.88
6.0	25.0	0.417	0.355	0.414	0.395	.315	0.80
6.5	26.5	0.291	0.462	0.493	0.415	.418	1.01
7.0	28.2	0.459	0.455	0.568	0.494	.512	1.04
7.5	30.0	0.453	0.660	0.723	0.612	.577	0.94
8.0	32.1	0.612	0.881	0.726	0.740	.682	0.92
8.5	34.4	0.657	0.702	0.918	0.759	.807	1.06
9.0	36.8	0.902	0.781	1.10	0.929	.986	1.06
9.5	39.7	1.77	1.06	1.45	1.43	1.29	0.90
10.0	43.0	1.12	1.12	0.974	1.08	1.70	1.57
10.5	46.8	1.21	1.70	1.33	1.41	2.4	1.70
11.0	51.4	2.27		2.05	2.16	3.7	1.71

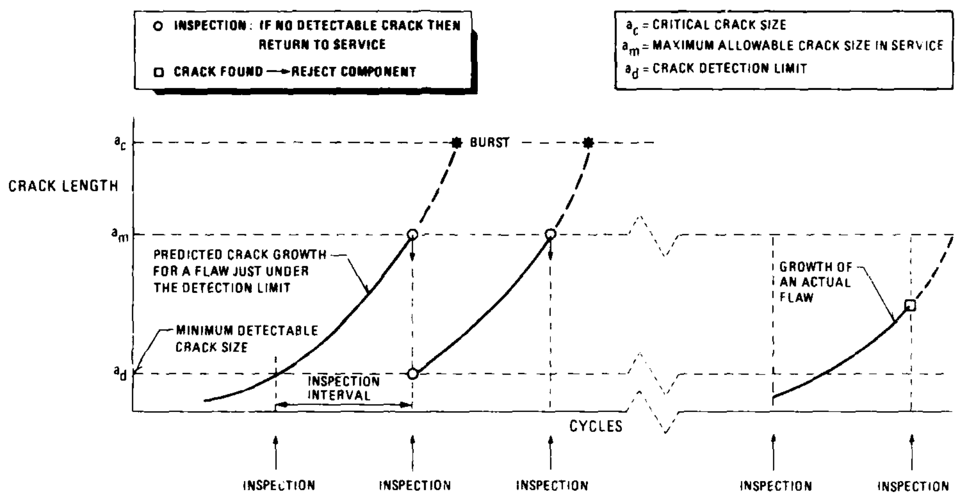

Fig. 1 Schematic of damage tolerance lifing approach

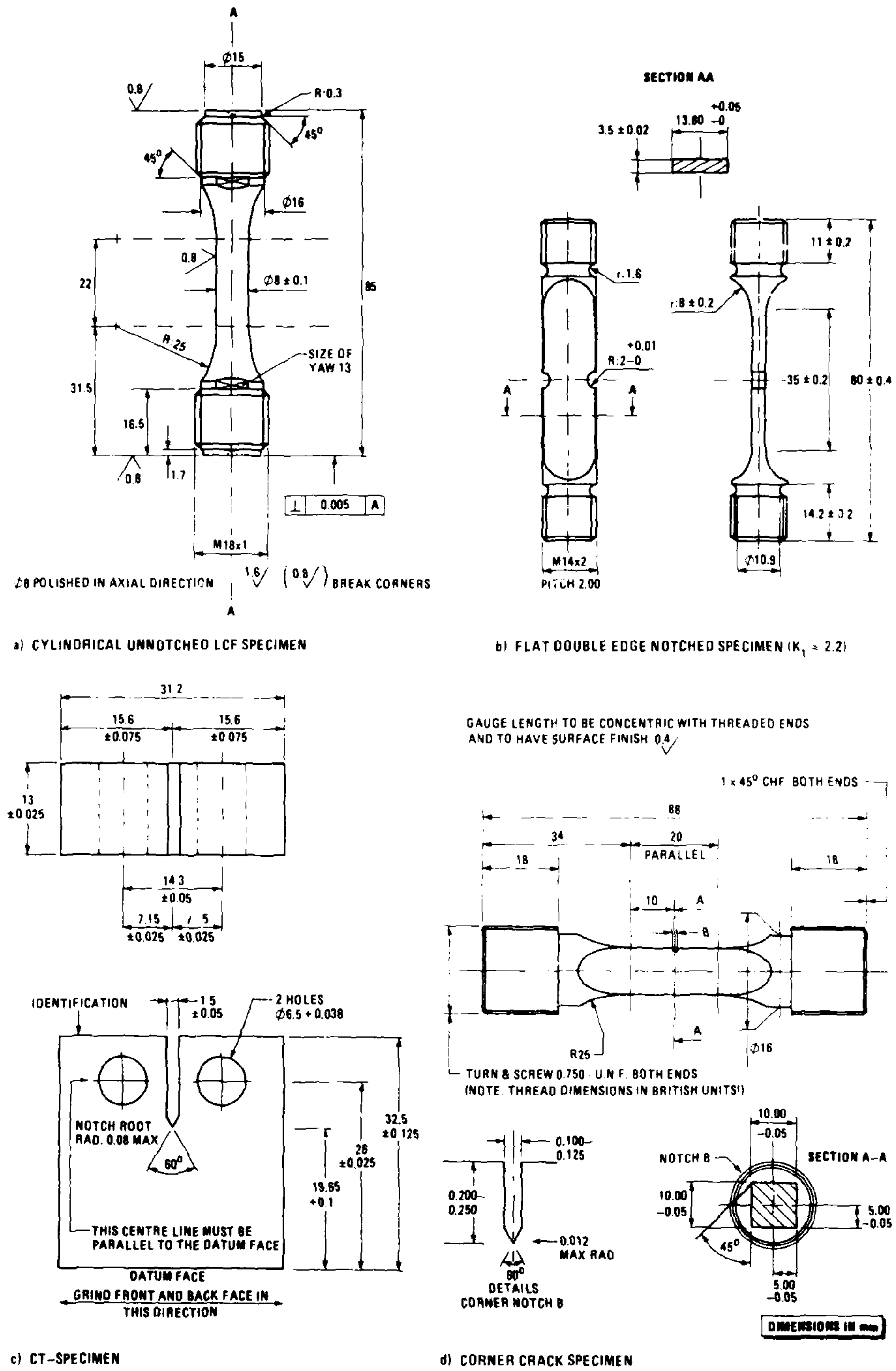

Fig. 2 Specimens used in the programme

IMPORTANT

RETAIN NOTCH FACE &
SPECIMEN POSITION IDENTITY ON ALL SEGMENTS

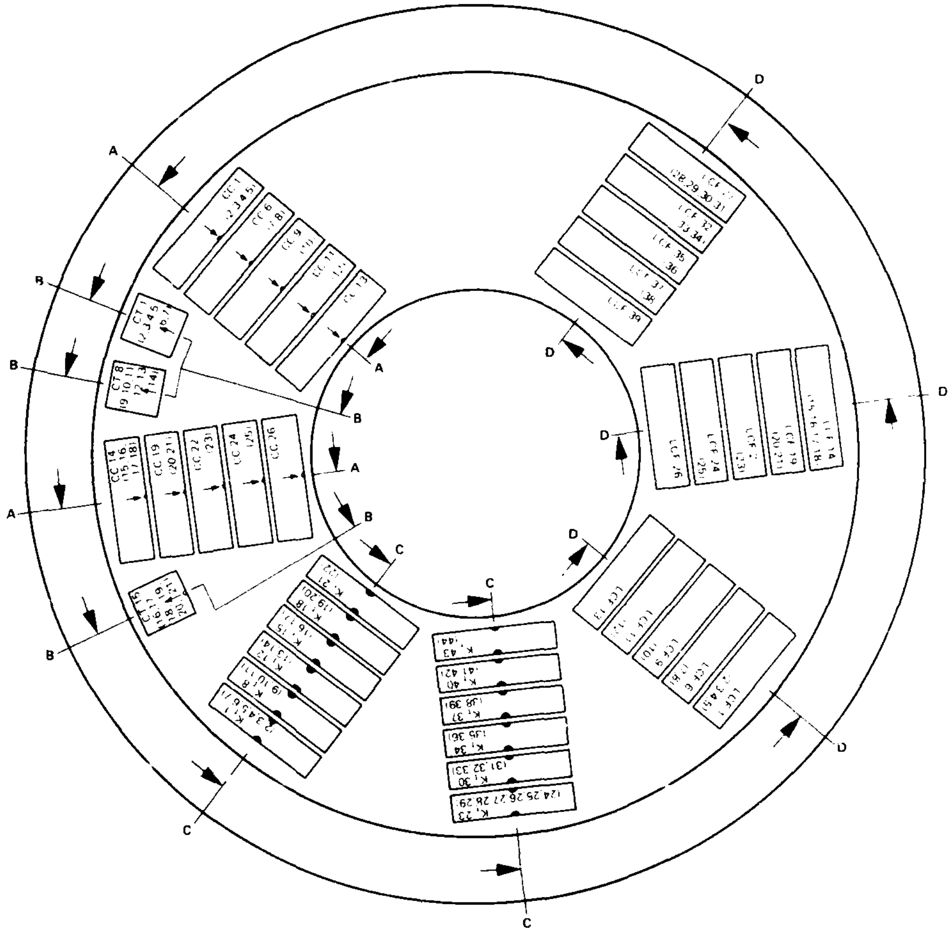

Fig. 3 Disc cut-up drawing indicating location of each specimen for the AGARD engine disc programme.
3a Overview of specimen positions

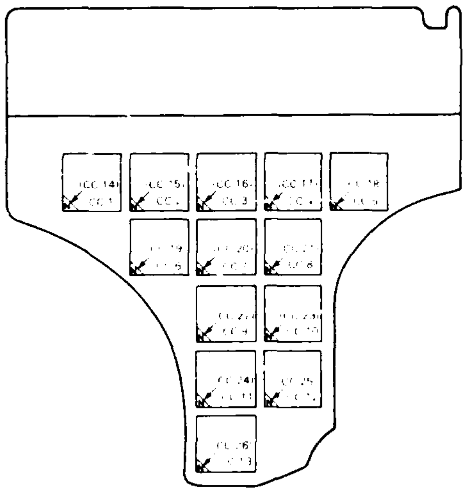

AA

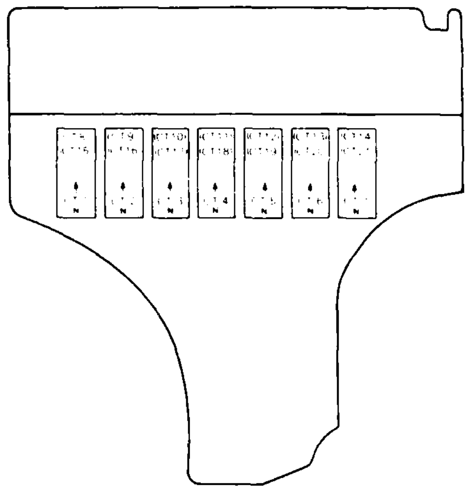

BB

SPECIMEN TYPE		BLANK SIZE	QUANTITY	POS-NOS	SECTIONS
SMOOTH CYLINDRICAL	LCF	90 × 23 SQ mm	39	1 – 39	DD
DOUBLE EDGE NOTCHED	K_t 2.2	85 × 18 SQ mm	44	1 – 44	CC
ASTM COMPACT TYPE	CT	36 × 34 × 15 mm	21	1 – 21	BB
CORNER CRACK	CC	93 × 23 SQ mm	26	1 – 26	AA

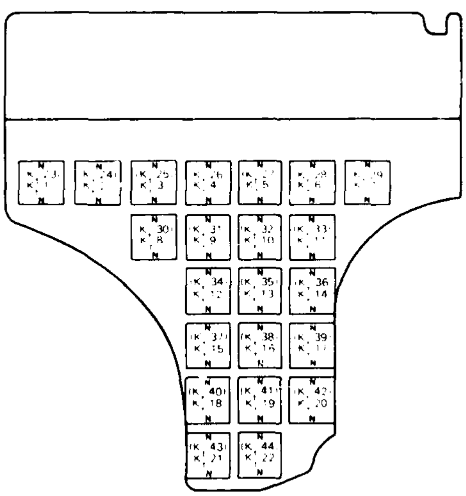

CC

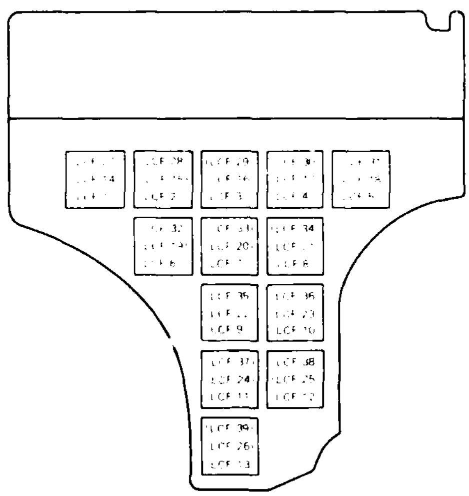

DD

Fig. 3 Continued.
3b Cross-sections showing individual specimen positions

DISC WGWMD 1113				DISC LWMD 7200			
SET No	LABORATORY	TYPE	POSITION	SET No	LABORATORY	TYPE	POSITION
1	UT	LCF	1 6	7	ND	LCF	2 6, 13
		K_t 2 2	1–6			K_t 2 2	1 6
		CT	1 3			CT	1–3
		CC	4 6			CC	1–3
2	NR	LCF	7–12	8	NS	LCF	7 12
		K_t 2 2	7–12			K_t 2 2	7 12
		CT	4–6			CT	4–6
		CC	1–3			CC	4–6
3	QI	LCF	14–19	9	AF	LCF	14 19
		K_t 2 2	13 18			K_t 2 2	13 18
		CT	7 9			CT	7 9
		CC	7 9			CC	7 9
4	NL	LCF	20 25	10	PI	LCF	20 25
		K_t 2 2	23 28			K_t 2 2	23–28
		CT	10 12			CT	10–12
		CC	14–16			CC	14–16
5	RA	LCF	27 32	11	IA	LCF	27–32
		K_t 2 2	29 34			K_t 2 2	29–34
		CT	13 15			CT	13–15
		CC	17 19			CC	17–19
6	RR	LCF	33 38	12	CE	LCF	33 38
		K_t 2 2	35–40			K_t 2 2	35–40
		CT	16 18			CT	16 18
		CC	20 22			CC	20 22

Fig. 3 Continued.
3c Distribution of specimens to participants

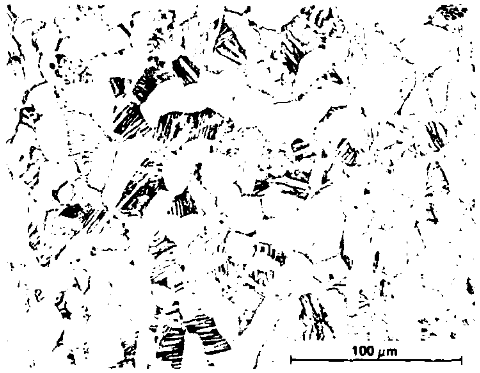

Fig. 4 Microstructure of Ti-6Al-4V disc material, showing equiaxed α (white phase) in a transformed β matrix (dark phase) containing coarse, acicular α

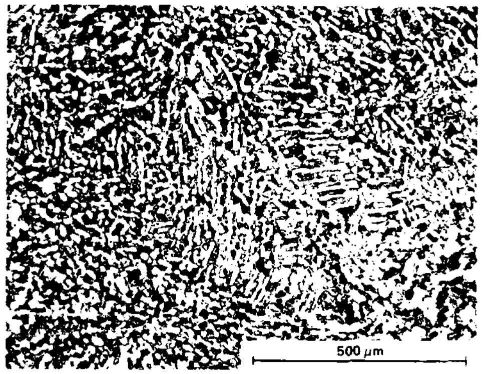

Fig. 5 Microstructure of Ti-6Al-4V disc material showing occasional α-alignments

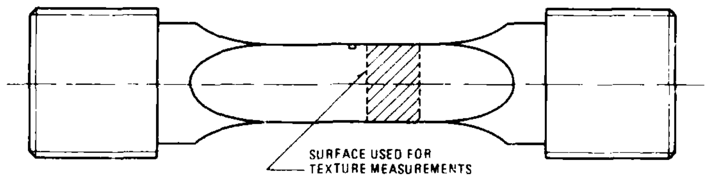

Fig. 6 Preparation of slices from CC specimens for texture measurements

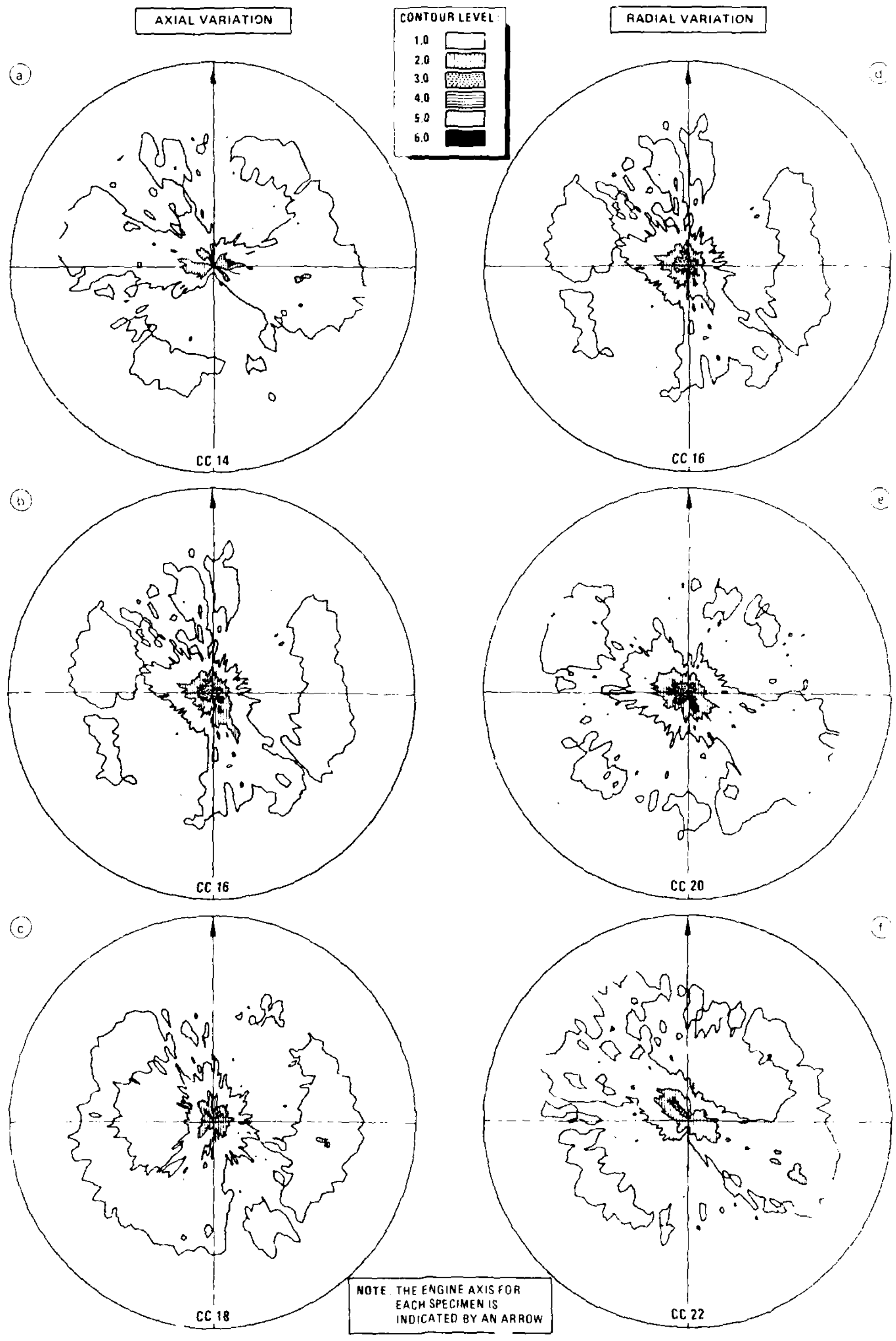

Fig 7 0002 Pole figures indicating texture variation in the disc, disc LWMD 7200

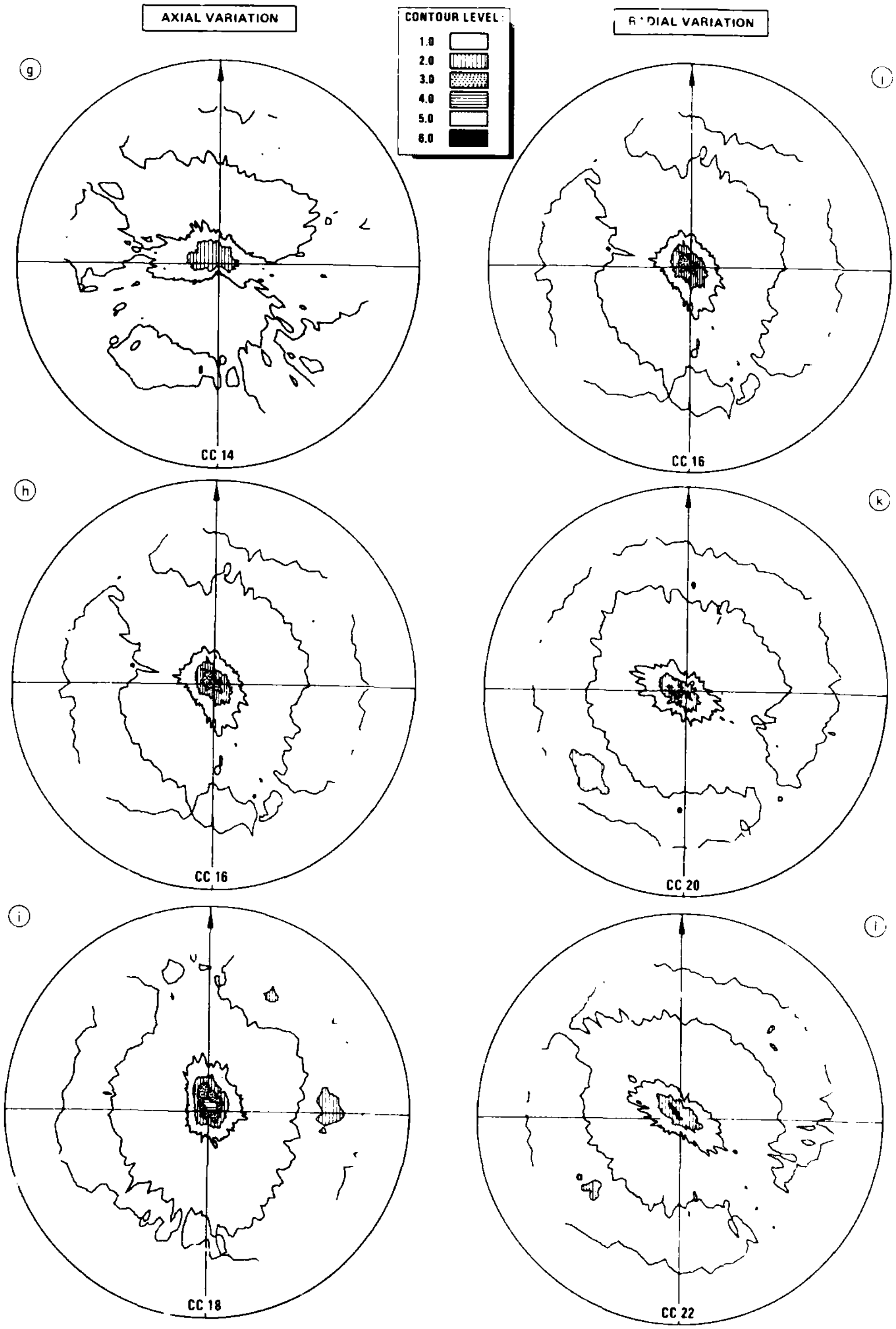

Fig. 7 (cont.) {110} Pole figures indicating texture variation in the disc; disc LWMD 7200

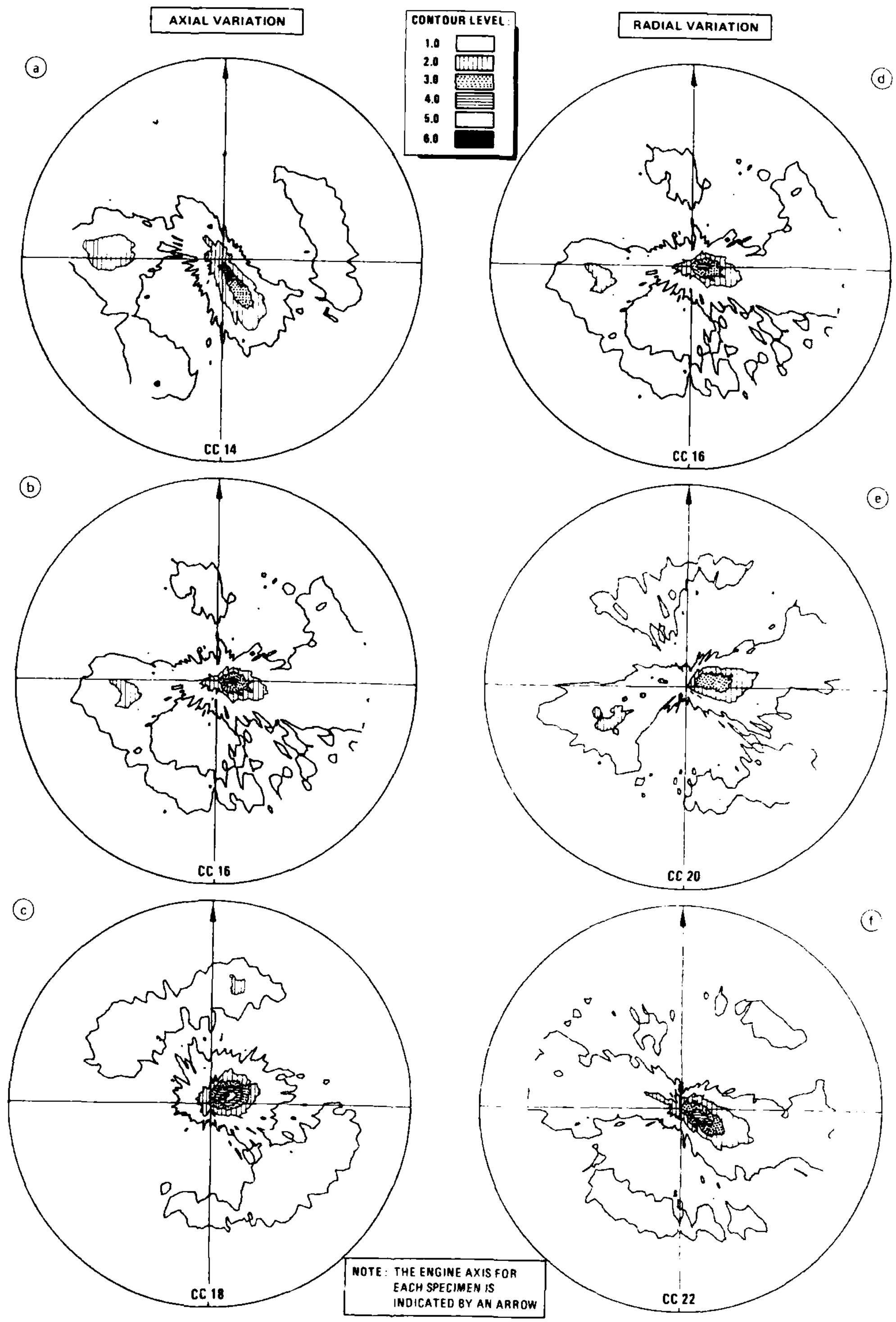

Fig. 8 (0002) Pole figures indicating texture variation in the disc; disc WGWMD 1113

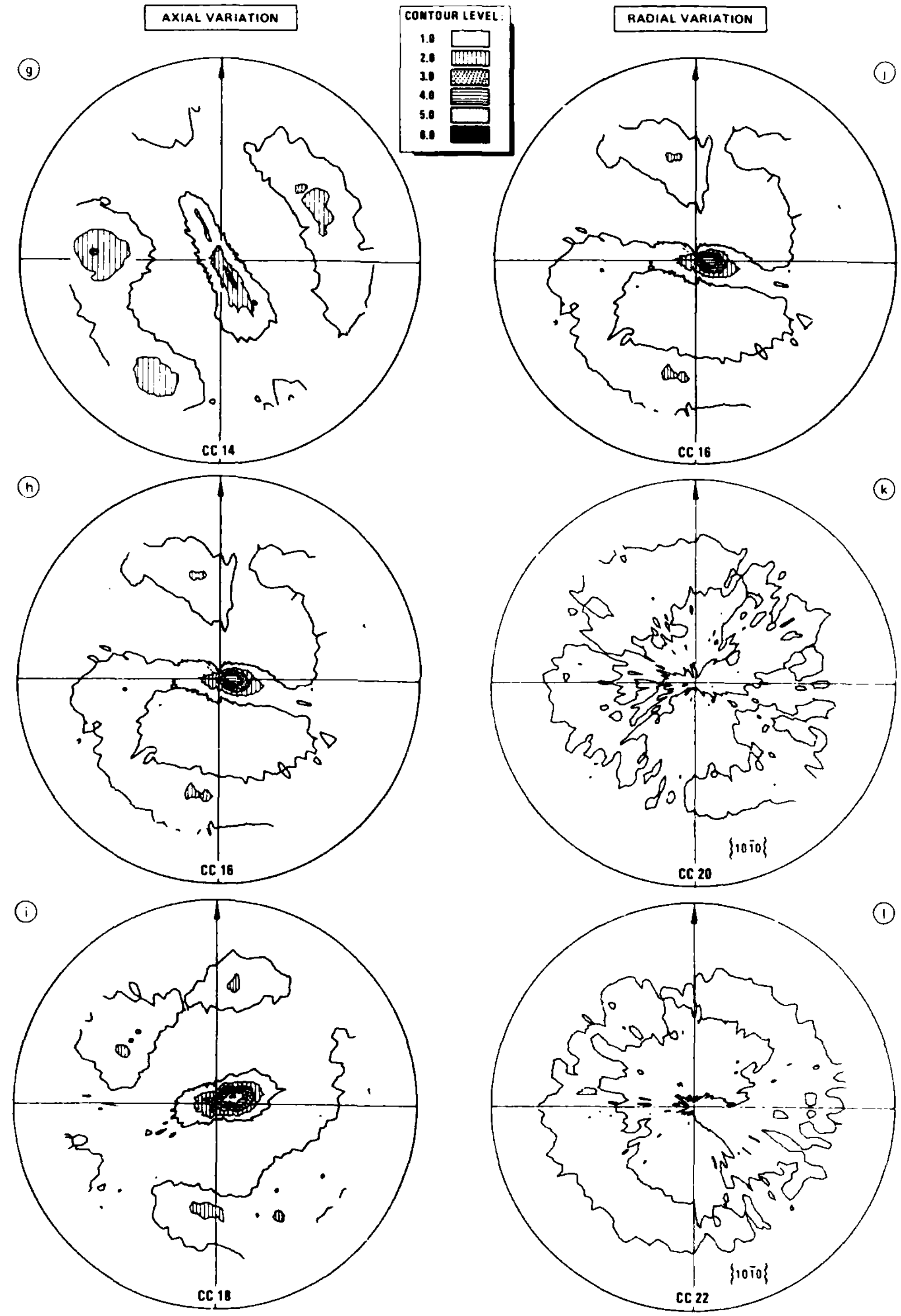

Fig. 8 (cont.) {110} Pole figures indicating texture variation in the disc; disc WGWMD 1113

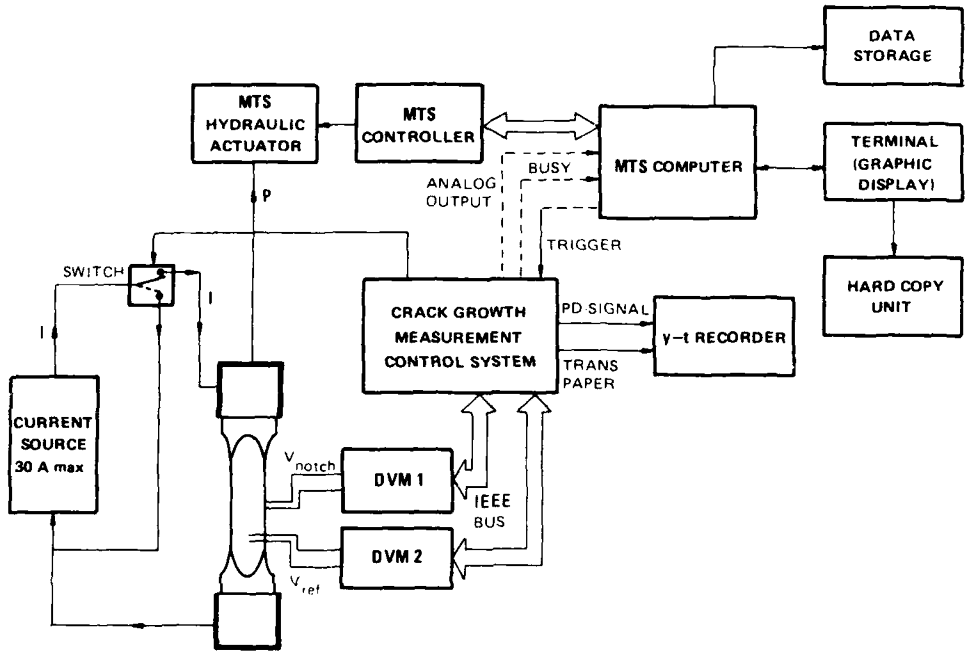

Fig. 9 Instrumentation for fatigue testing and crack growth measurement

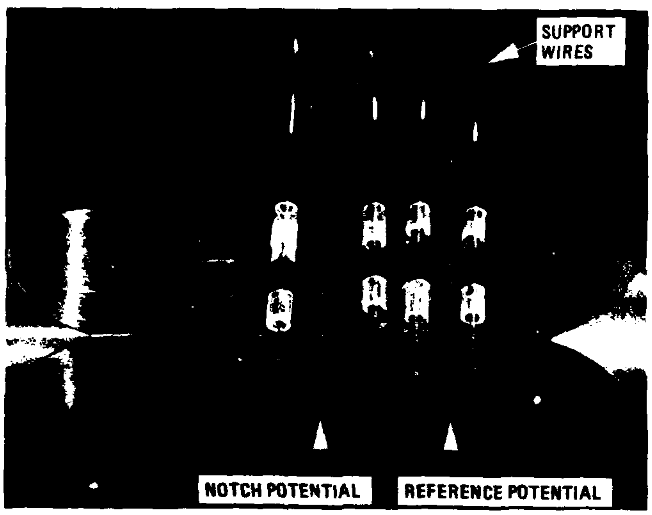

Fig. 10 Potential drop instrumentation of dummy corner crack specimen. The 50 μm diameter notch probe wires are located on both sides of a 100 μm deep starter notch (not visible).
N.B. For actual test specimens the reference probes should not be welded on the same edge (see text)

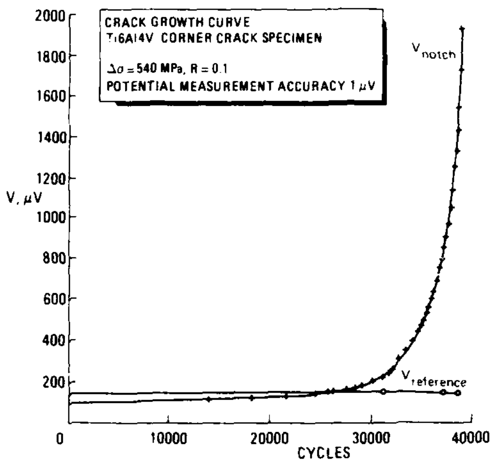

Fig. 11 Potential drop versus number of cycles during fatigue testing of the corner crack specimen shown in Figure 10

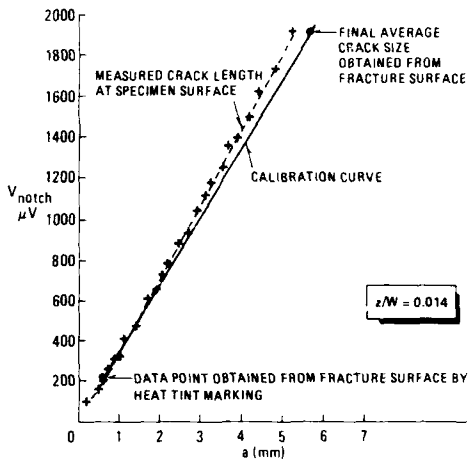

Fig. 12 Notch voltage versus crack length for corner crack specimen

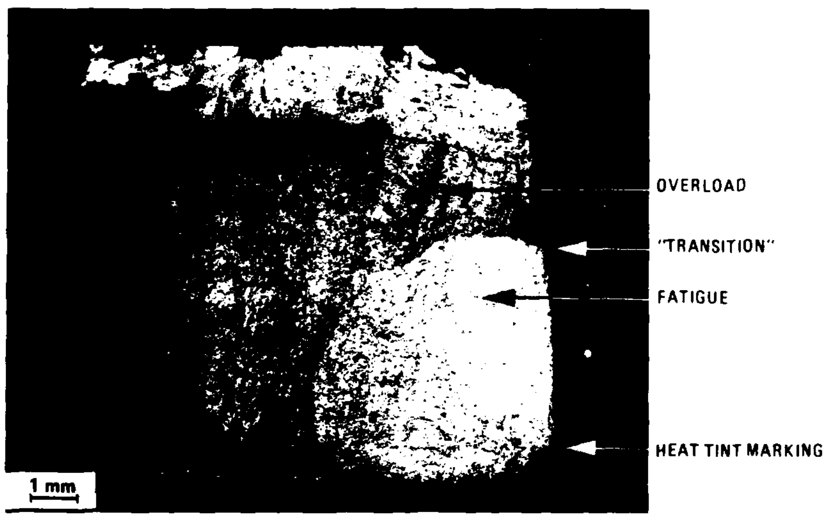

Fig. 13 Markings on fracture surface of corner crack specimen

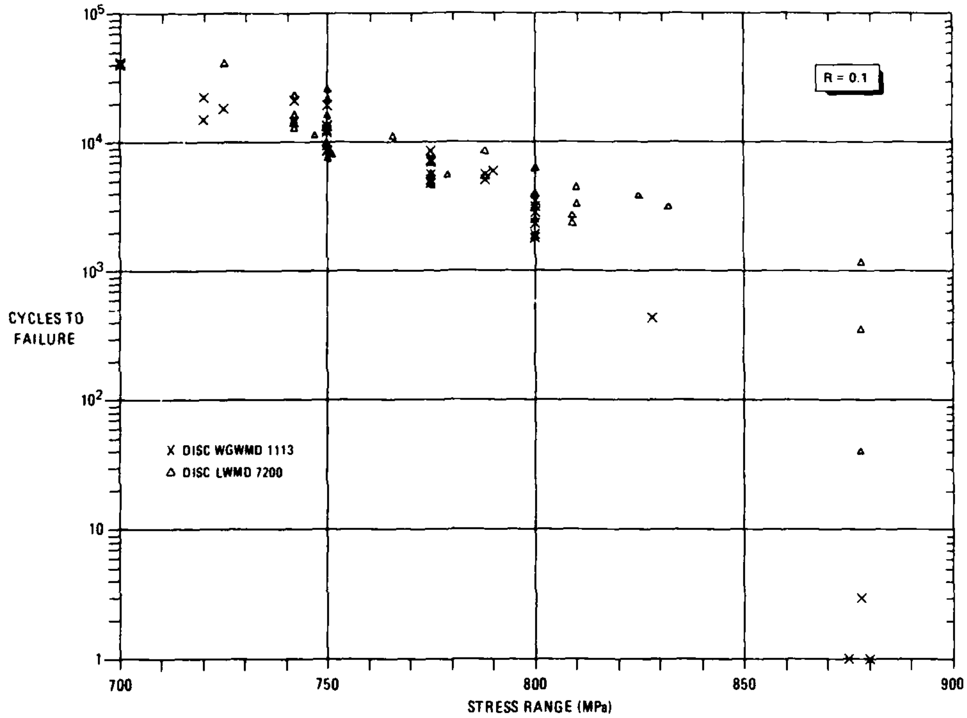

Fig. 14 Fatigue life test results for LCF specimens

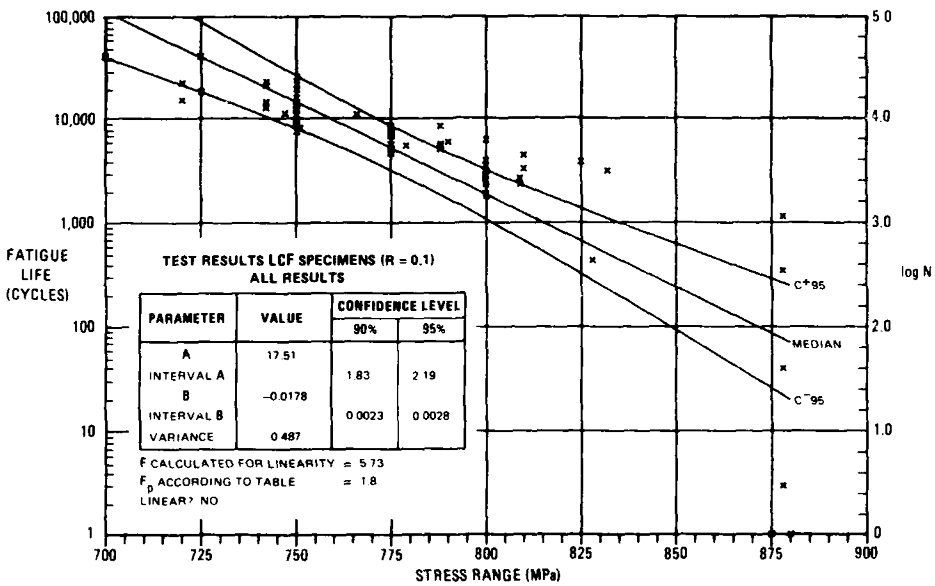

PARAMETER	VALUE	CONFIDENCE LEVEL 90%	CONFIDENCE LEVEL 95%
A	17.51		
INTERVAL A		1.83	2 19
B	–0.0178		
INTERVAL B		0 0023	0 0028
VARIANCE	0 487		

F CALCULATED FOR LINEARITY = 5 73
F_p ACCORDING TO TABLE = 1.8
LINEAR? NO

Fig. 15 Fitted relationship between fatigue life and stress range for all LCF data on both discs; 95% confidence interval for the entire median curve is also indicated

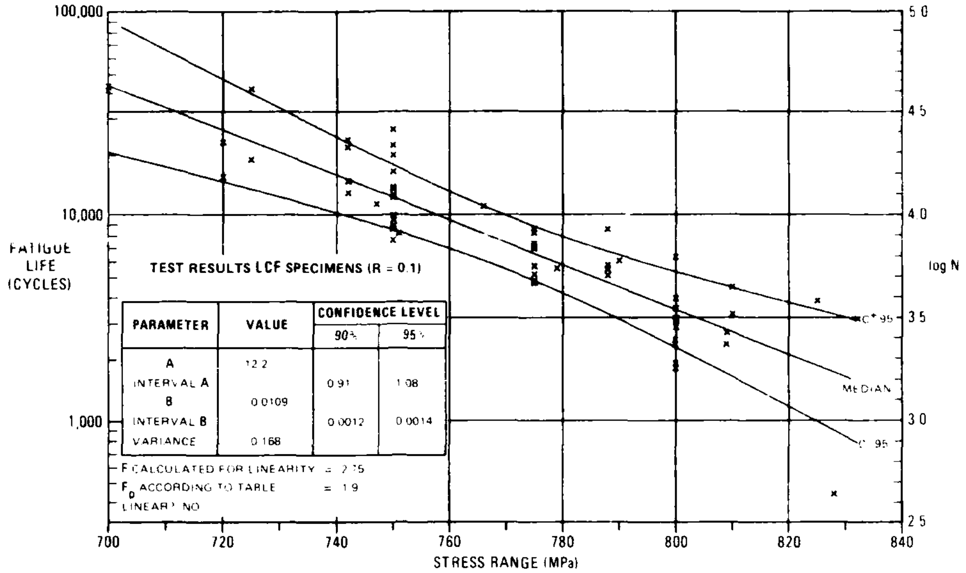

Fig. 16 Fitted relationship between fatigue life and stress range for all LCF data in the appropriate stress range/life regime (see section 6.1.2)

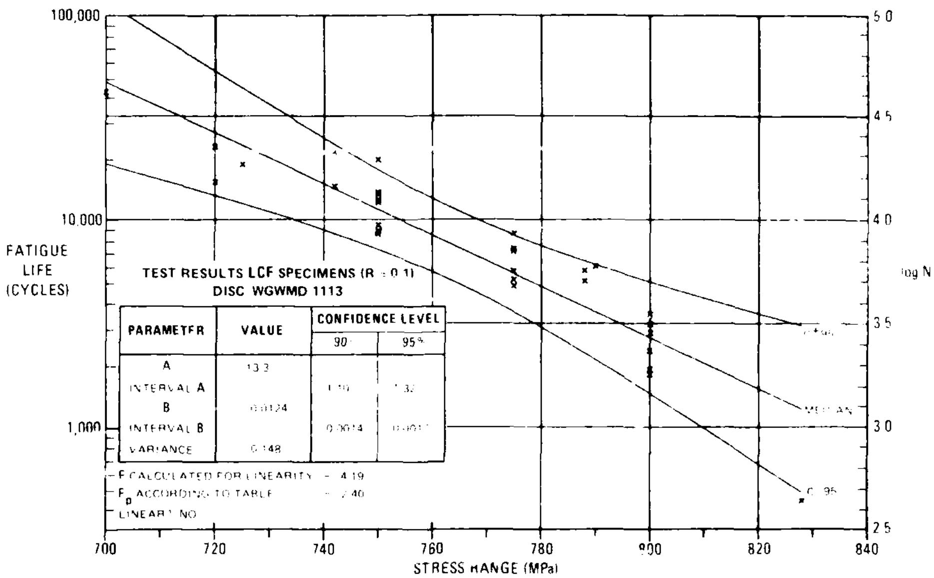

Fig. 17 Fitted relationship between fatigue life and stress range for the WGWMD 1113 disc data

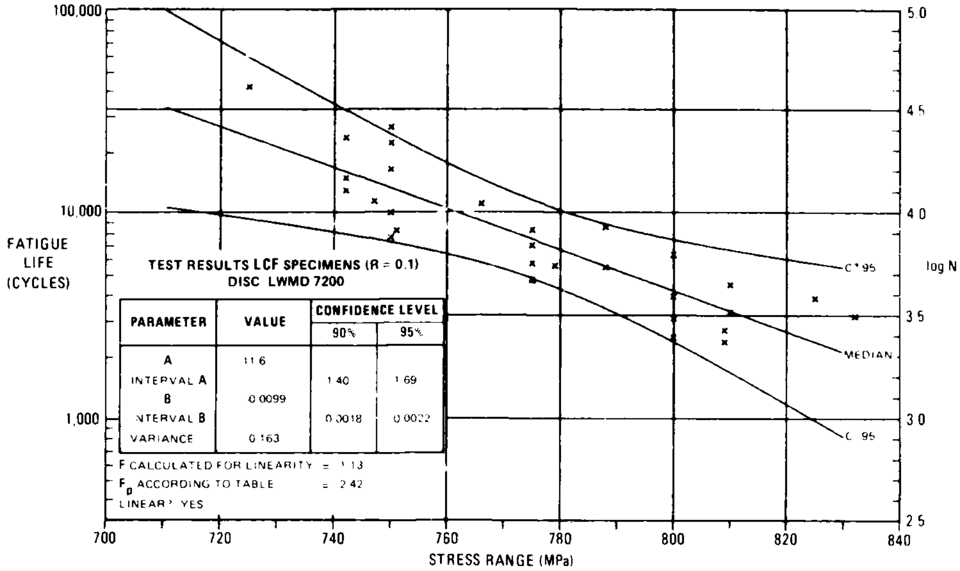

Fig. 18 Fitted relationship between fatigue life and stress range for the LWMD 7200 disc data

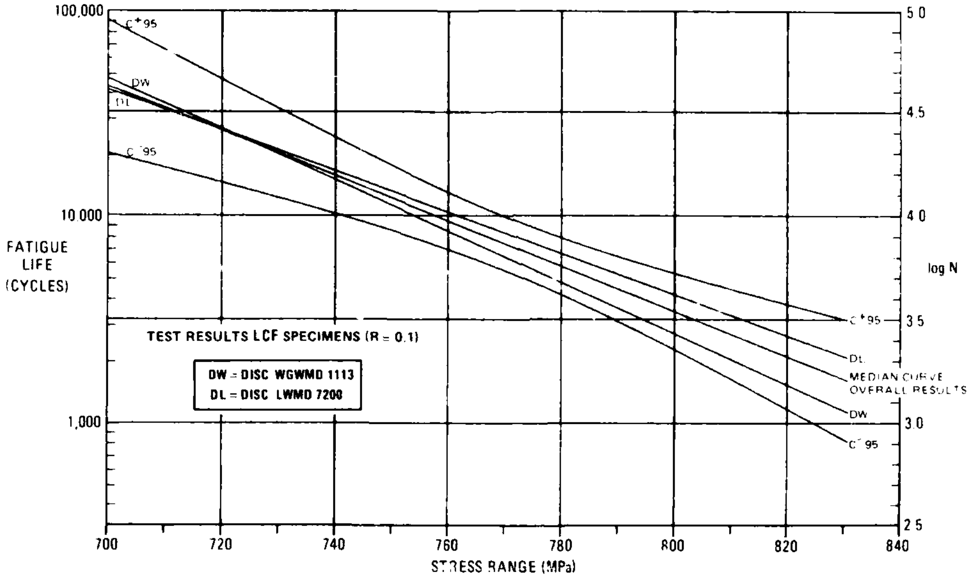

Fig. 19 Comparison of the fitted linear relationships for the individual discs with the overall fitted curve. The 95% confidence interval is for the overall curve

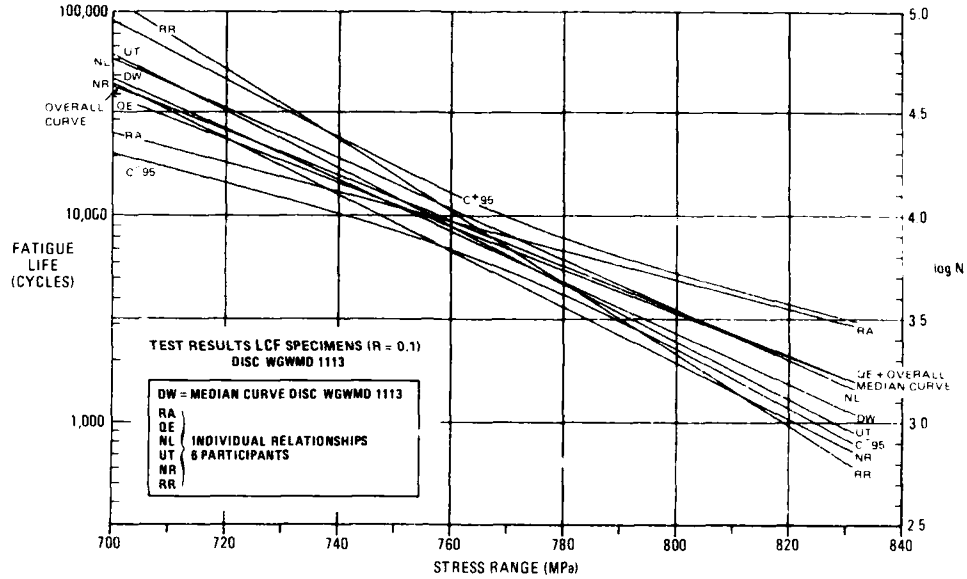

Fig. 20 Comparison between the overall median curve for both discs, the median curve for disc WGWMD 1113 and the fitted curves for the 6 associated individual laboratories. The 95% confidence interval relates to the overall curve

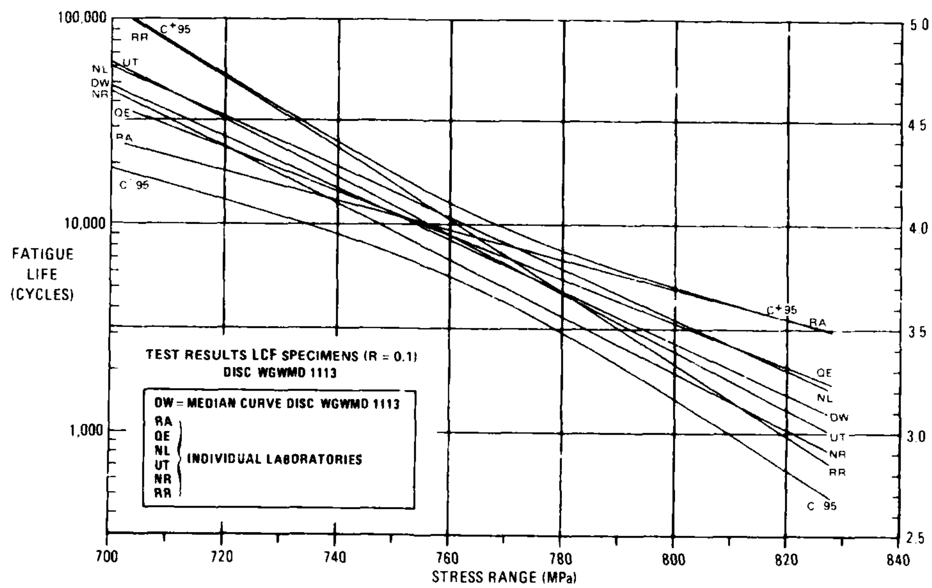

Fig. 21 Comparison between the median curve (and associated 95% confidence interval) for disc WGWMD 1113 and the individual laboratories

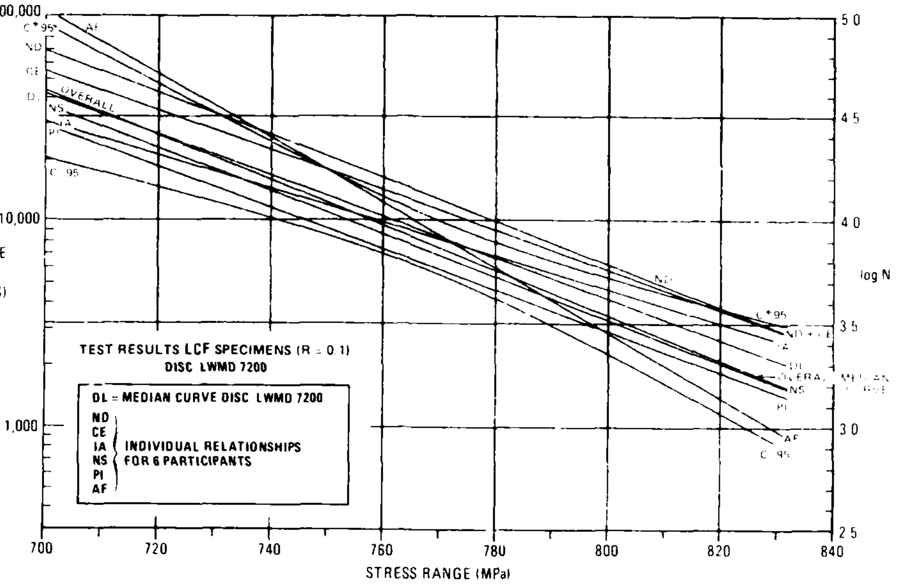

Fig. 22 Comparison between the median curve for both discs, the median curve for disc LWMD 7200 and the fitted curves for the 6 associated laboratories.
The 95% confidence interval relates to the overall curve

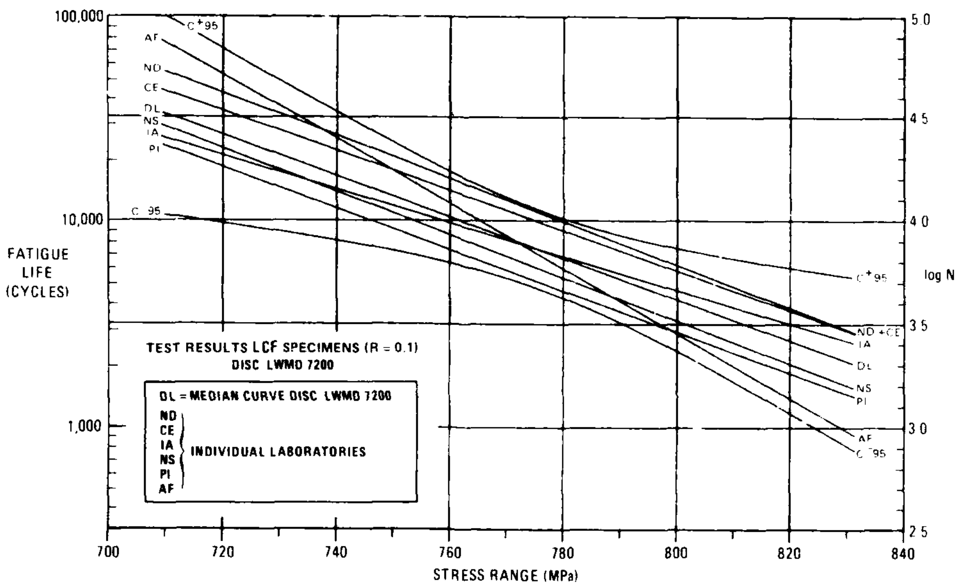

Fig. 23 Comparison between the median curve (and associated 95% confidence interval) for disc LWMD 7200 and the individual laboratories

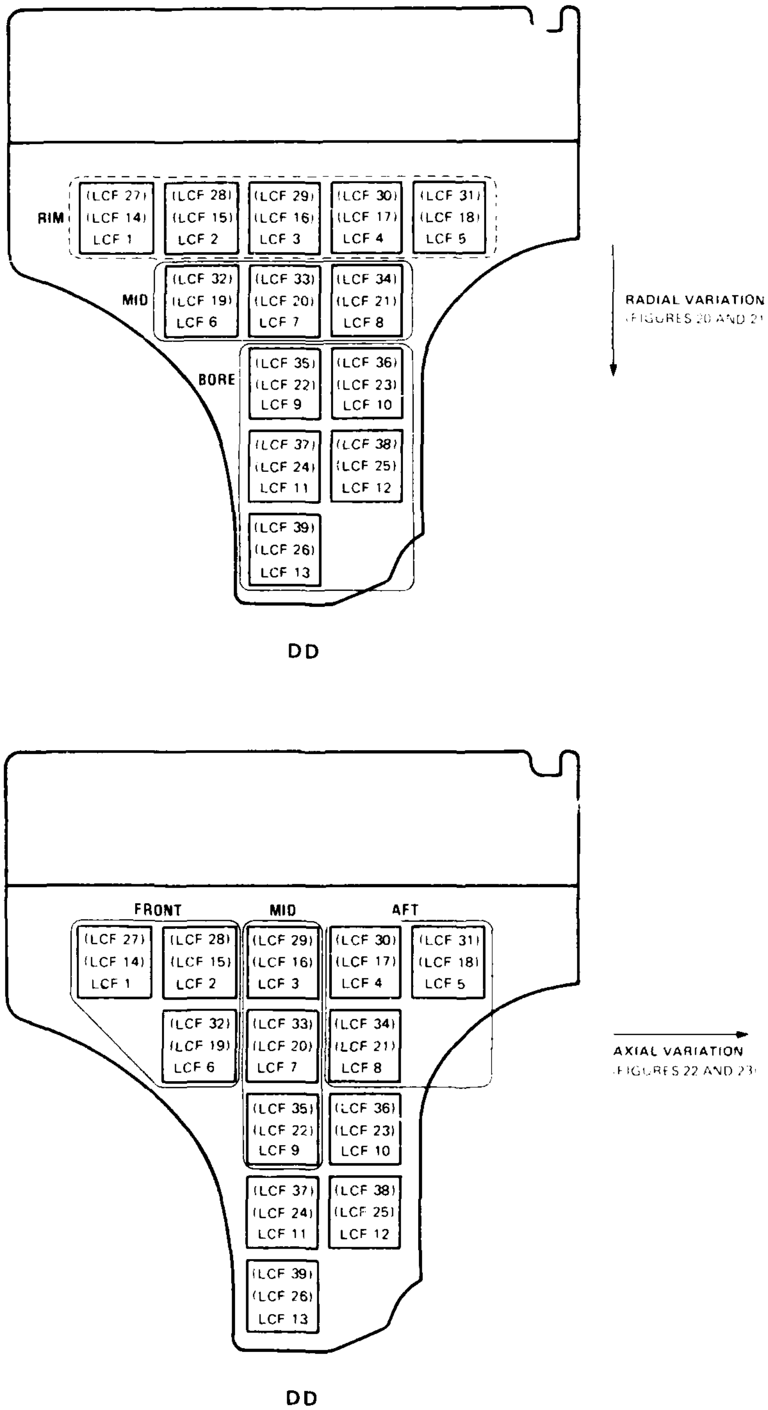

Fig 24 Selection of specimens for control of material property variations in radial and axial directions

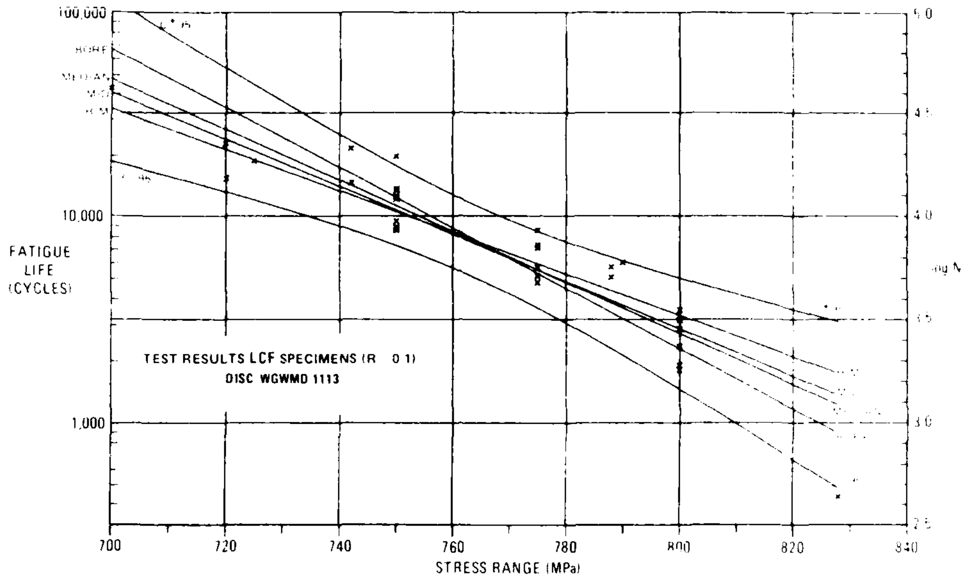

Fig. 25 Comparison between various radial locations in the disc with the disc median curve and its associated 95% confidence interval

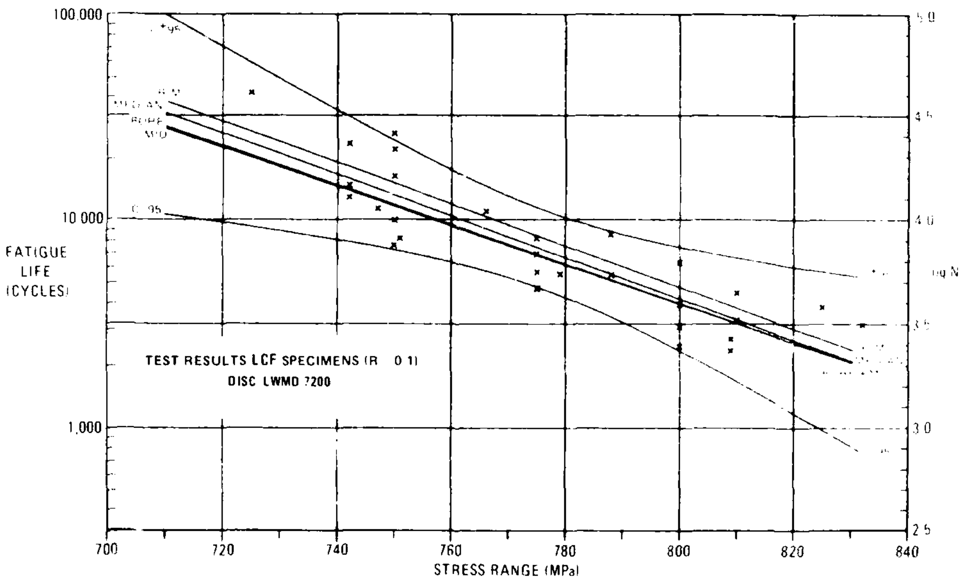

Fig. 26 Comparison between various radial locations in the disc with the disc median curve and its associated 95% confidence interval

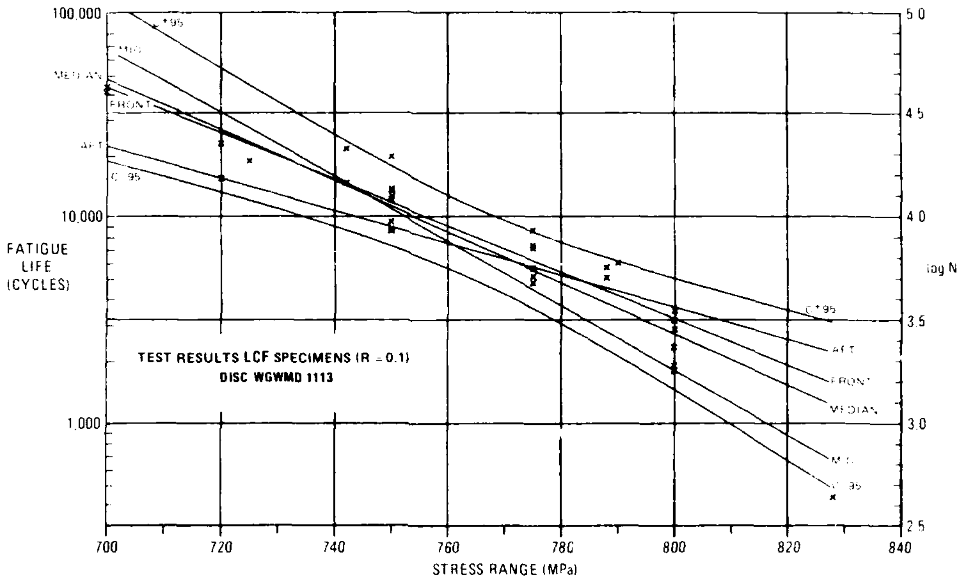

Fig. 27 Comparison between various axial locations in the disc with the disc median curve and its associated 95% confidence interval

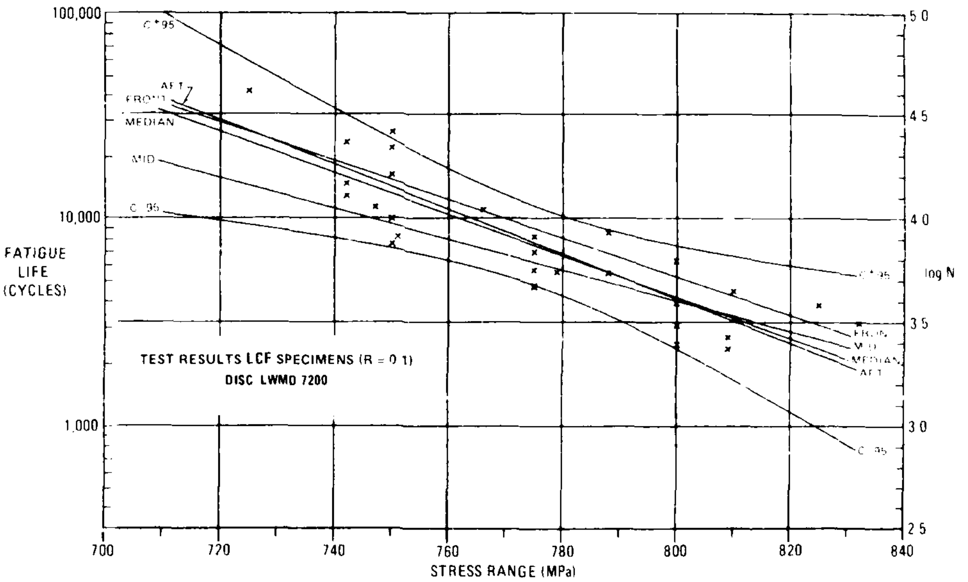

Fig. 28 Comparison between various axial locations in the disc with the disc median curve and its associated 95% confidence interval

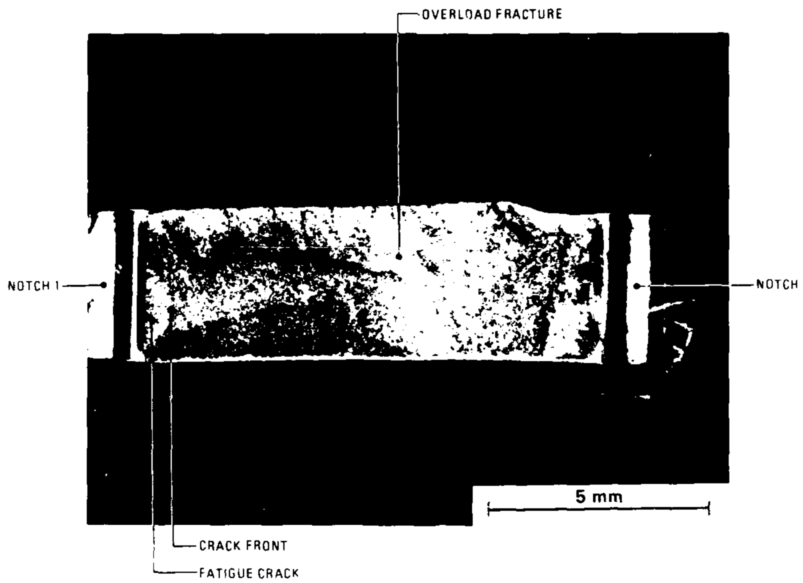

Fig. 29 Size of the fatigue crack at a 1% increase in PD-level for the K_t 2.2 specimen

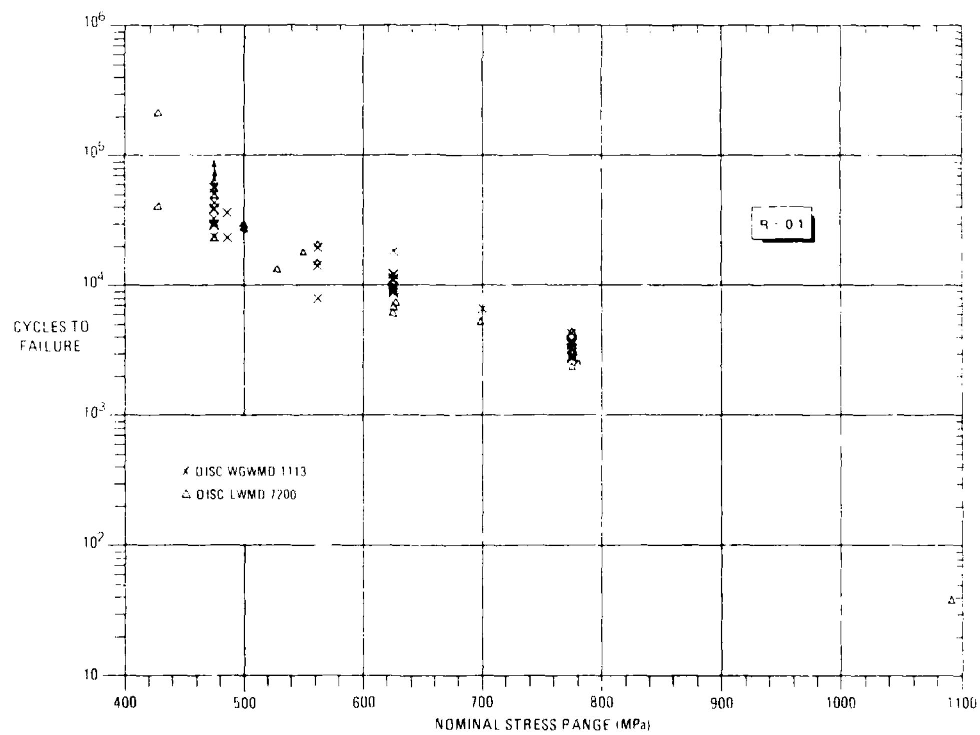

Fig. 30 Test results K_t 2.2 specimens; life to failure

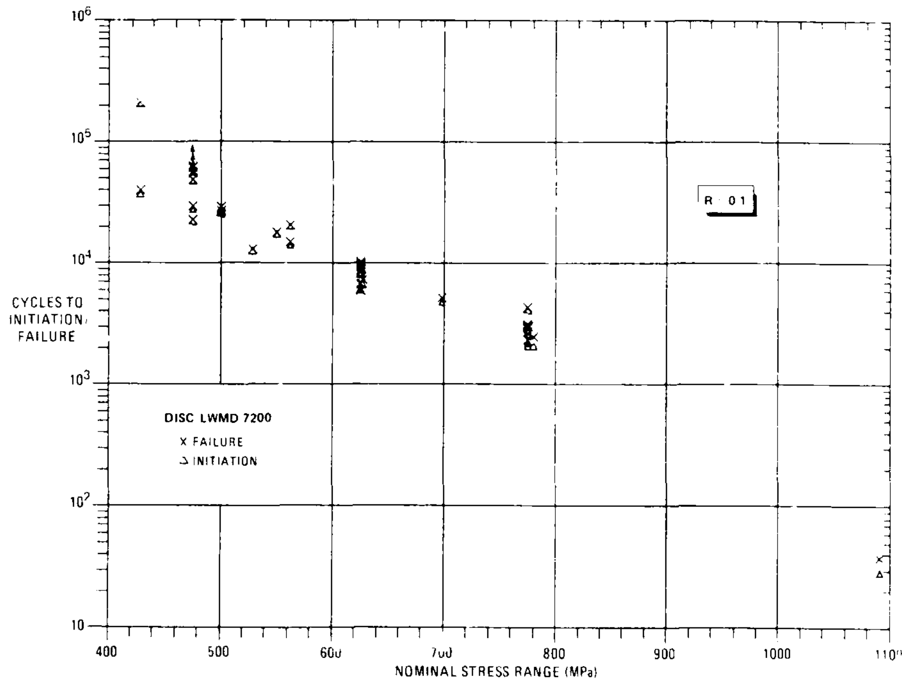

Fig. 31 Test results K_t 2.2 specimens, disc LWMD 7200 only.
Both initiation life and life to failure are indicated

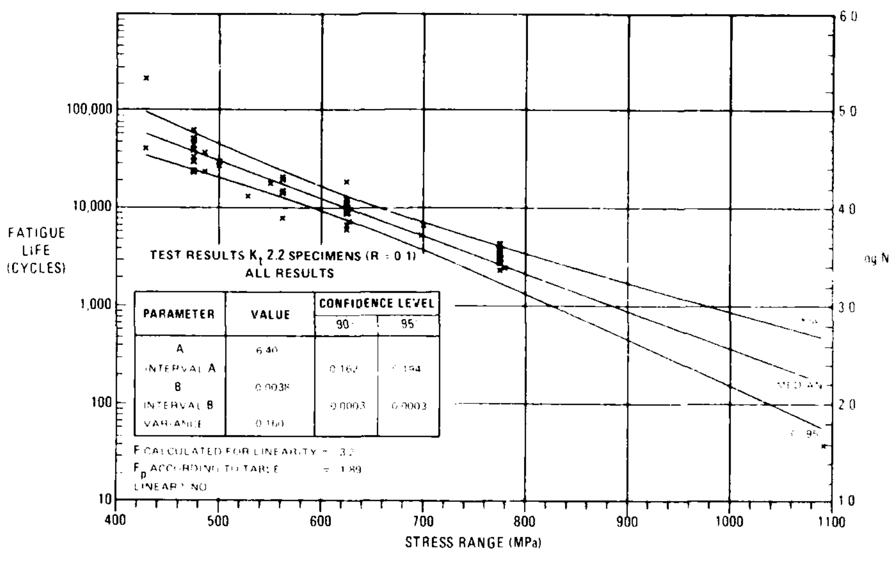

Fig. 32 Fitted relationship between fatigue life and stress range for all K_t 2.2 data.
The 95% confidence interval has also been indicated

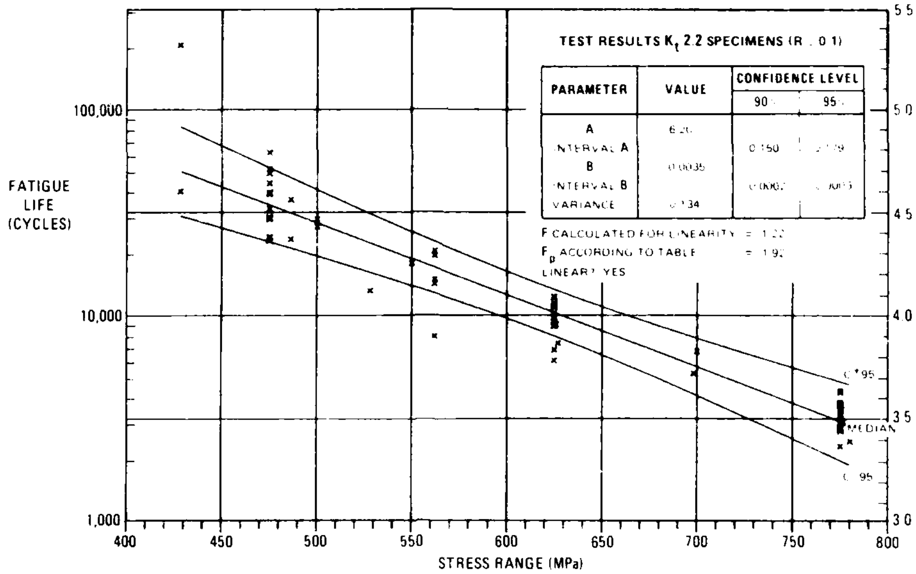

Fig. 33 Fitted relationship between fatigue life and stress range for all K_t 2.2 data in the appropriate life regime; the 95% confidence interval for the median curve is also indicated

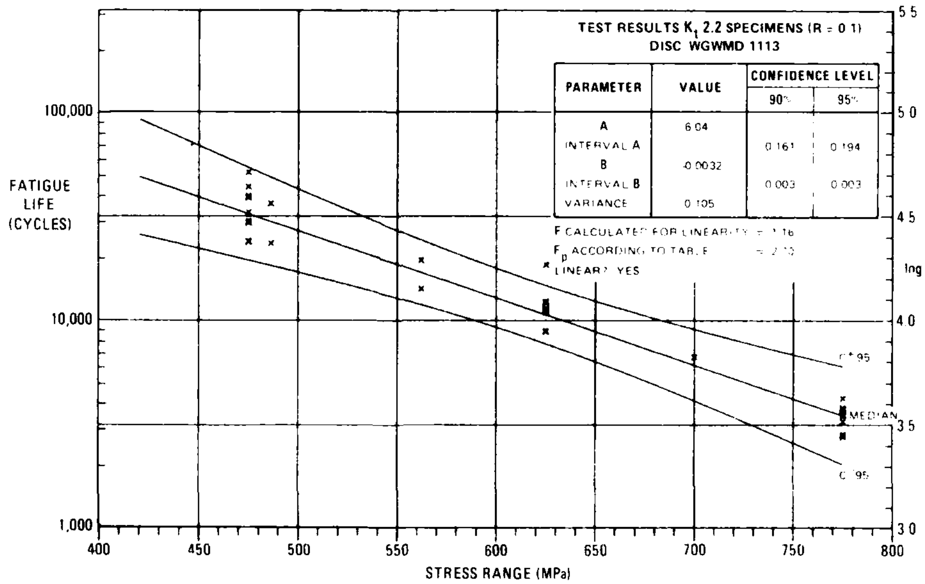

Fig. 34 Fitted relationship between fatigue life and stress range for the WGWMD 1113 disc data

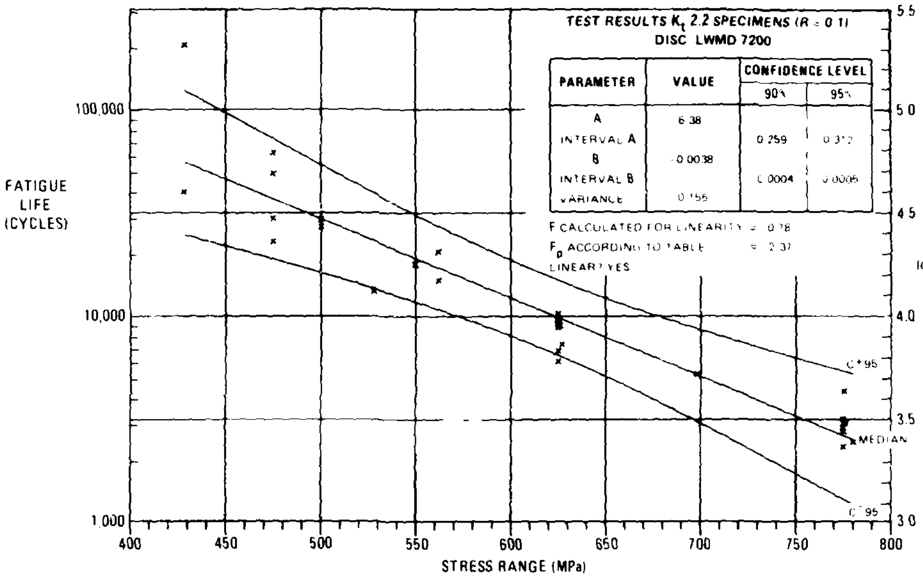

Fig. 35 Fitted relationship between fatigue life and stress range for the LWMD 7200 disc data

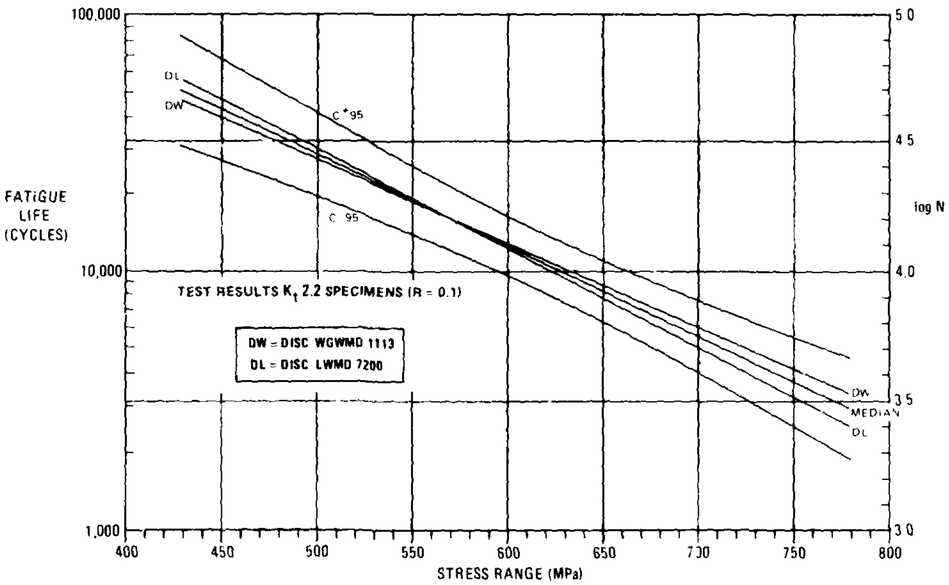

Fig. 36 Comparison of the fitted median curves for the individual discs with the overall median curve. The 95% confidence interval relates to the overall curve

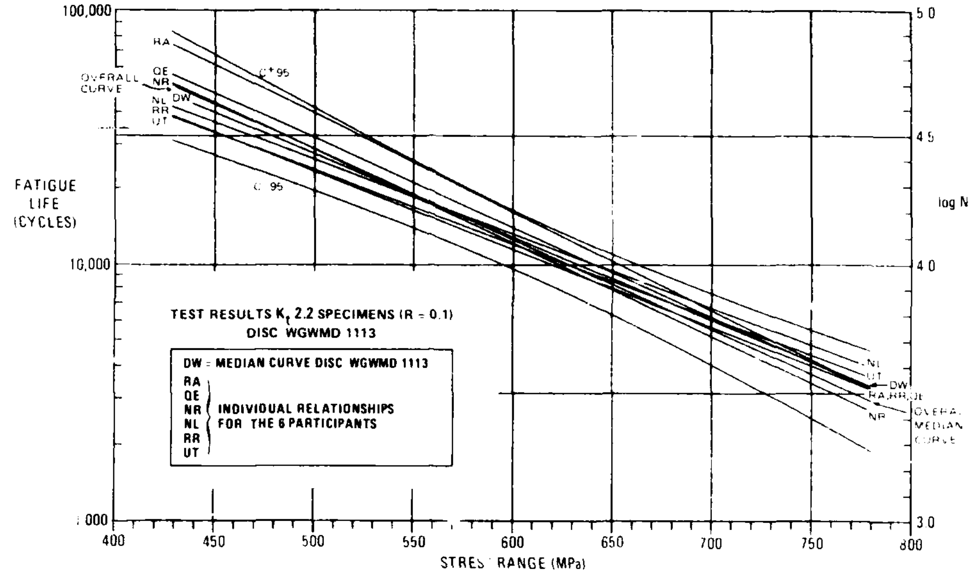

Fig. 37 Comparison between the overall median curve for both discs, the median curve of disc WGWMD 1113 and the fitted curves for the 6 associated individual laboratories. The 95% confidence interval relates to the overall curve

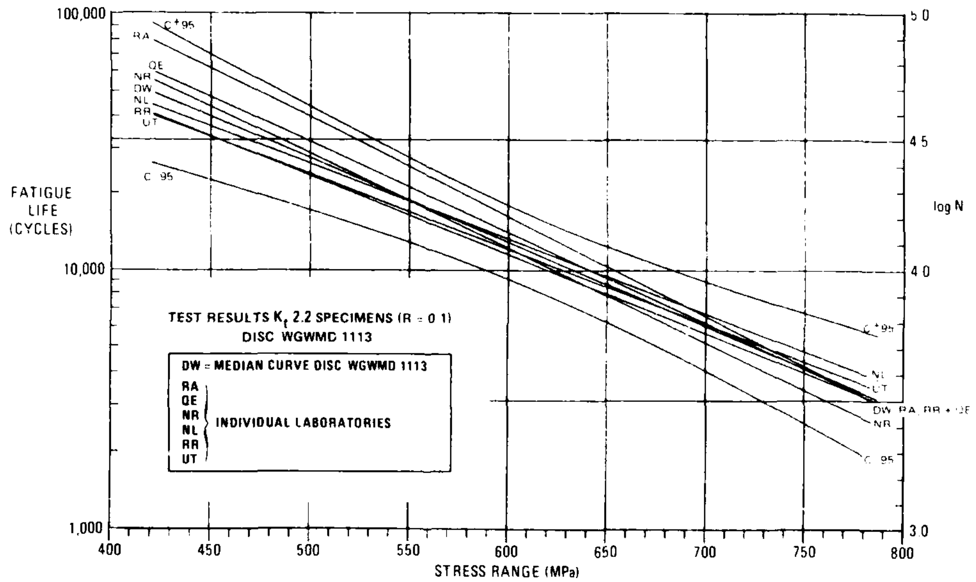

Fig. 38 Comparison between the median curve (and associated 95% confidence interval) of disc WGWMD 1113 and the curves for the individual laboratories

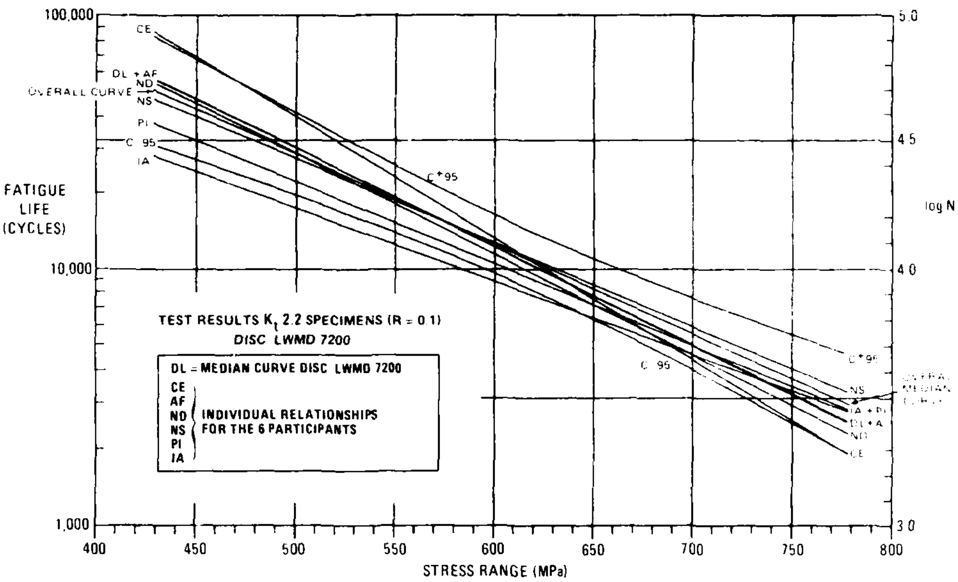

Fig. 39 Comparison between the overall median curve for both discs, the median curve of disc LWMD 7200 and the fitted curves for the 6 associated individual laboratories.
The 95% confidence interval relates to the overall curve

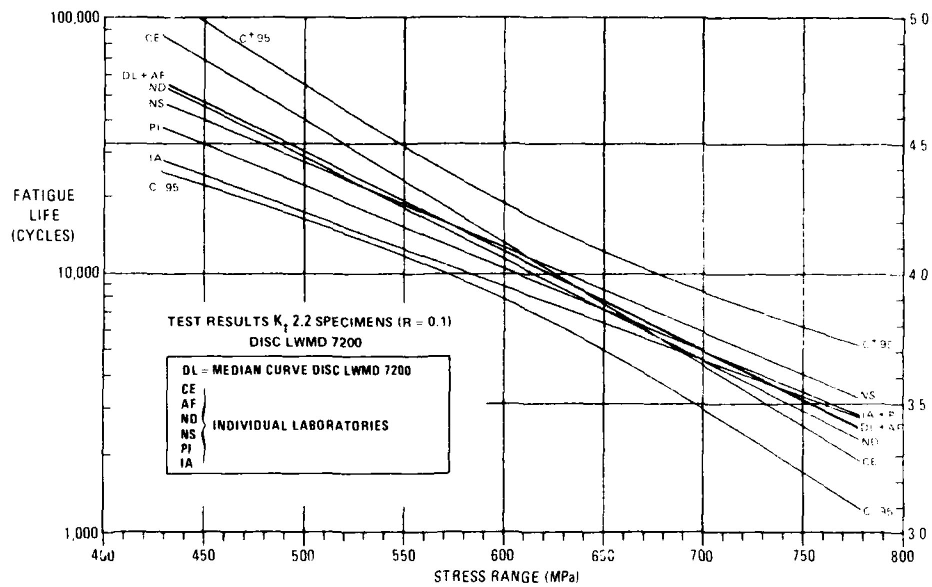

Fig. 40 Comparison between the median curve (and associated 95% confidence interval) of disc LWMD 7200 and the curves for the individual laboratories

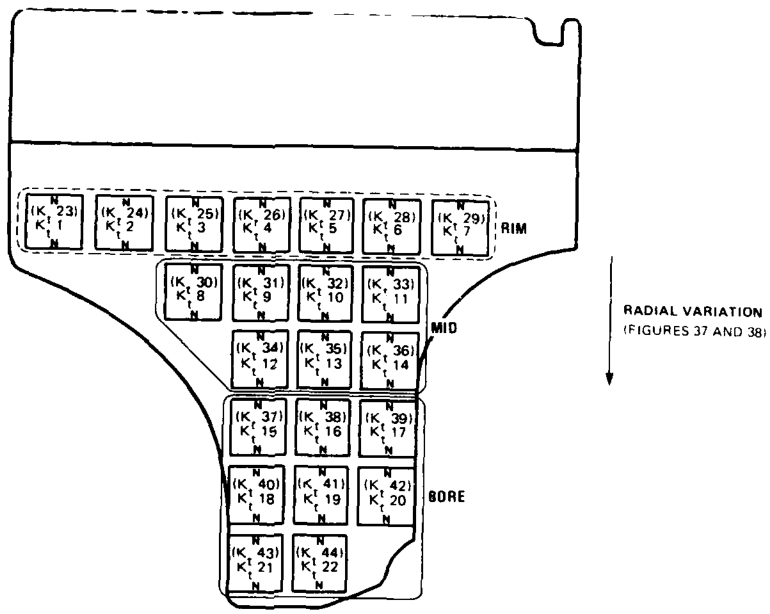

CC

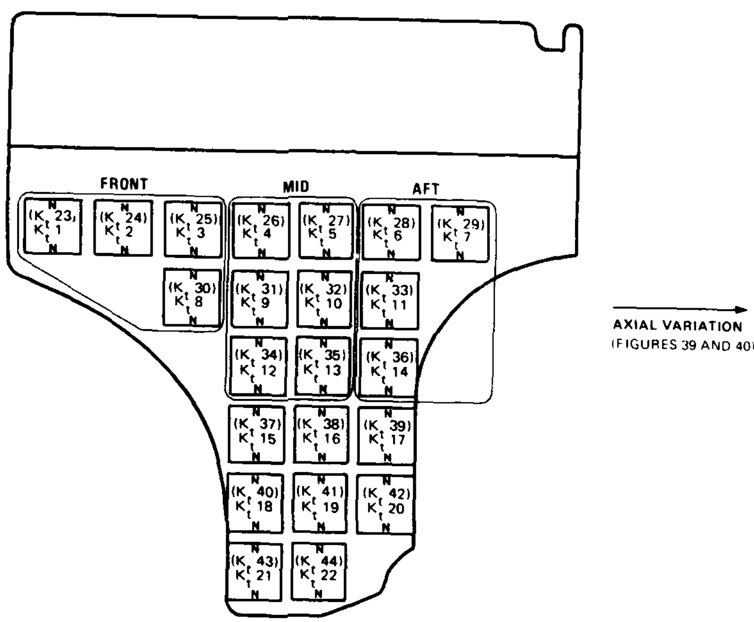

CC

Fig. 41 Selection of specimens for control of material property variation in radial and axial directions

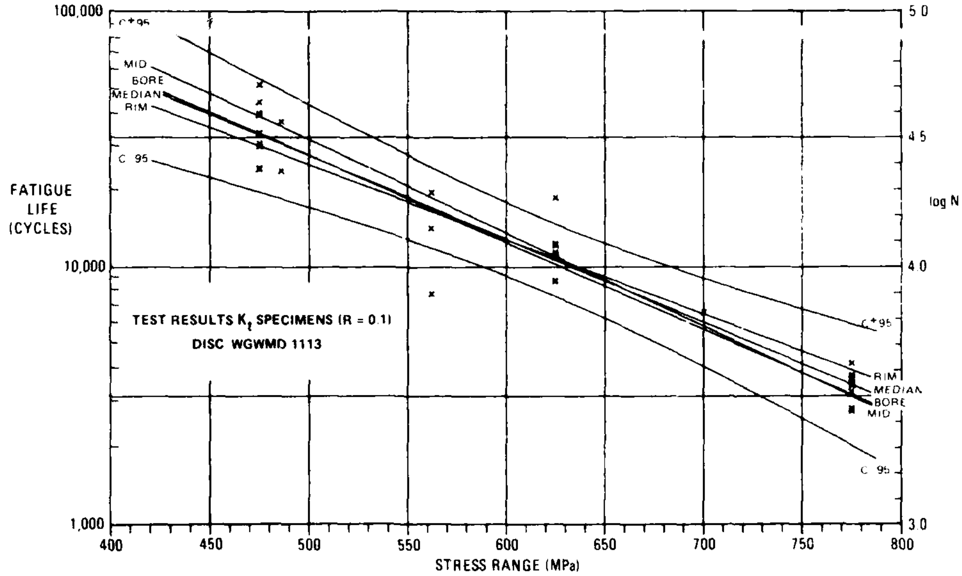

Fig. 42 Comparison between various radial locations in the disc with the disc median curve and its associated 95% confidence interval

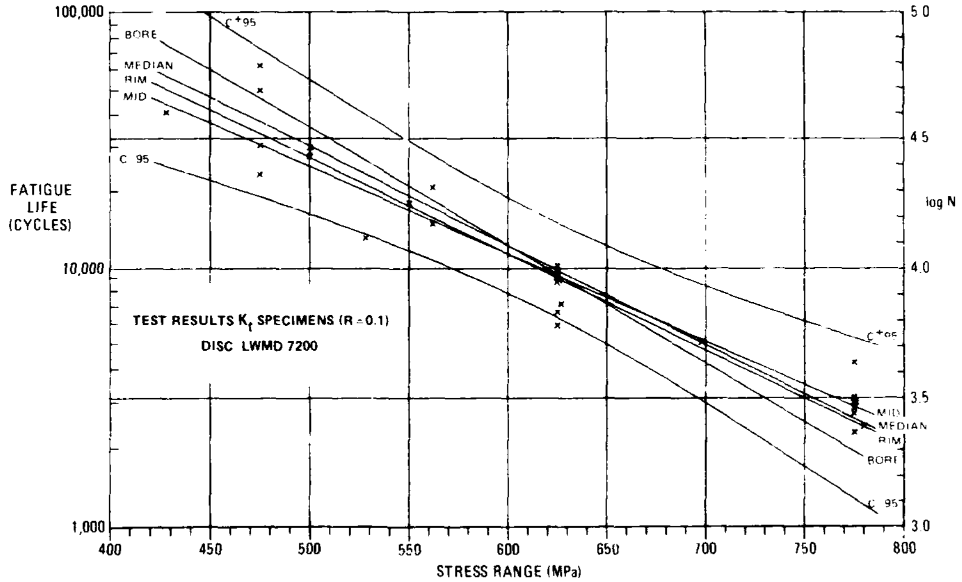

Fig. 43 Comparison between various radial locations in the disc with the disc median curve and its associated 95% confidence interval

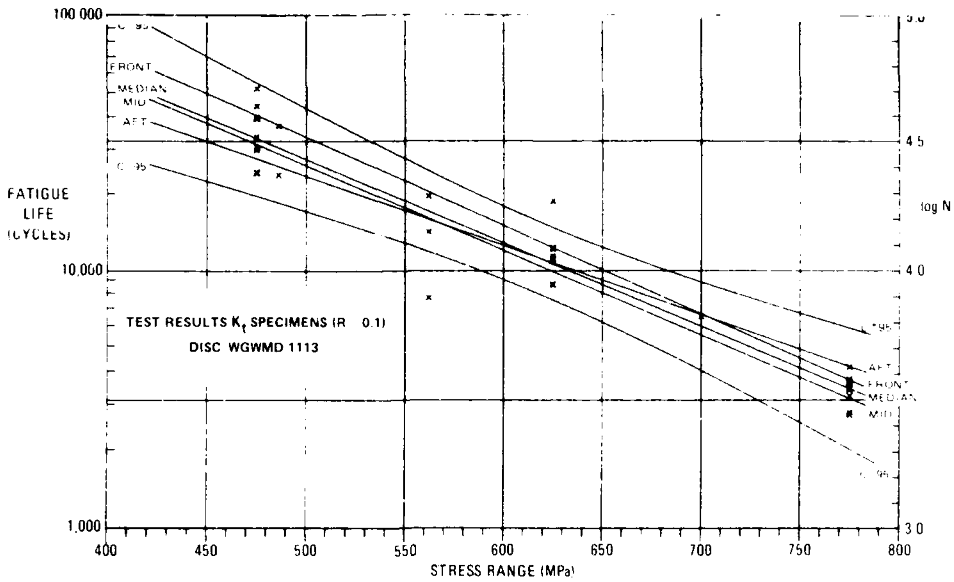

Fig. 44 Comparison between various axial locations in the disc with the disc median curve and its associated 95% confidence interval

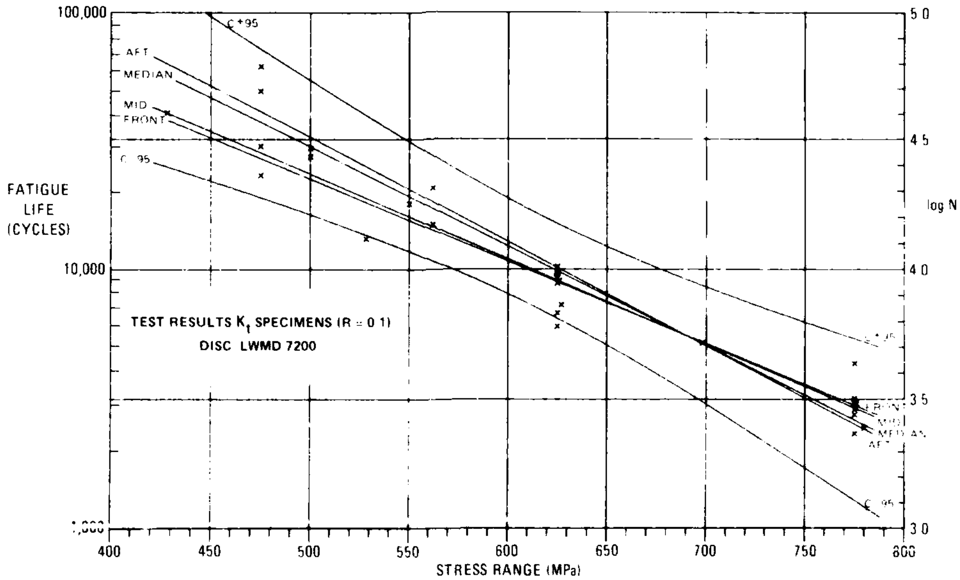

Fig 45 Comparison between various axial locations in the disc with the disc median curve and its associated 95% confidence interval

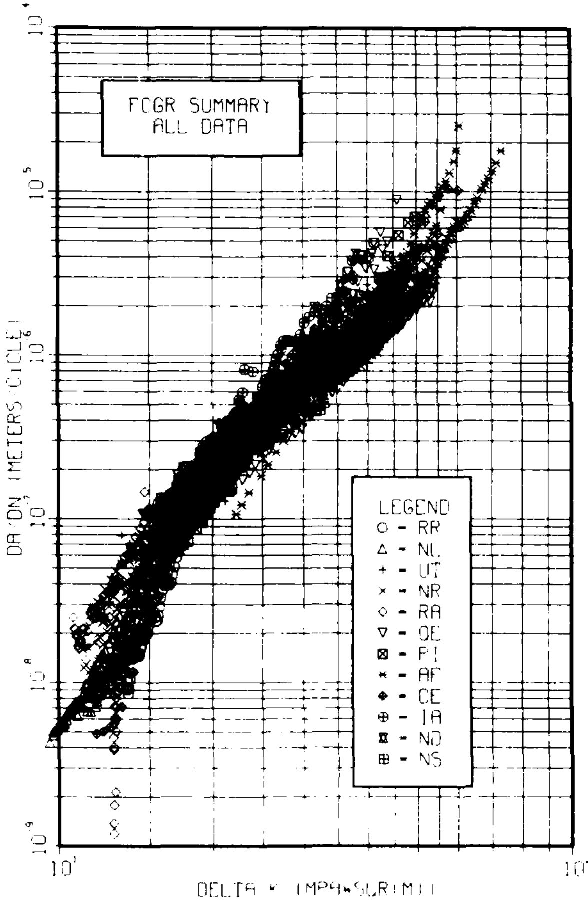

Fig. 46 Fatigue crack growth rate (FCGR) summary; all data

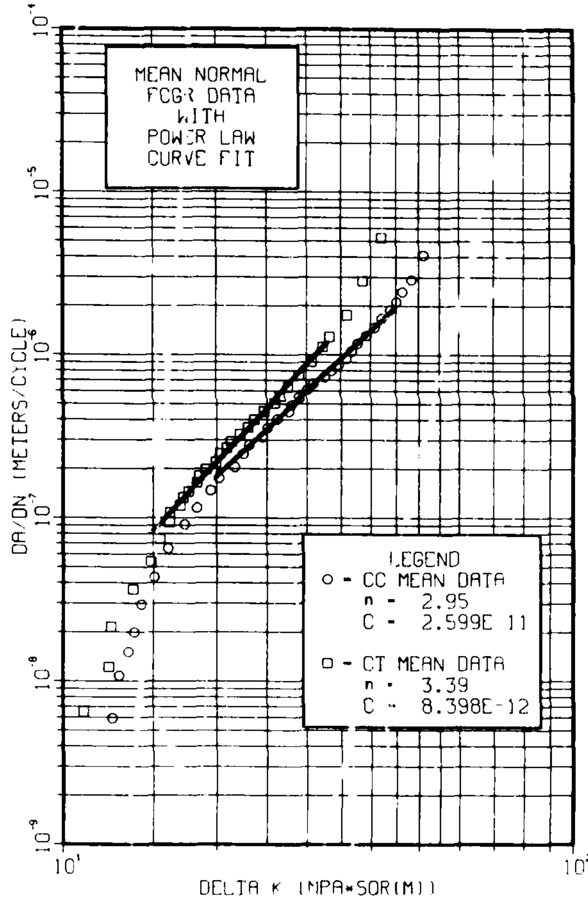

Fig. 47 Mean normal FCGR-data with power law curve fit

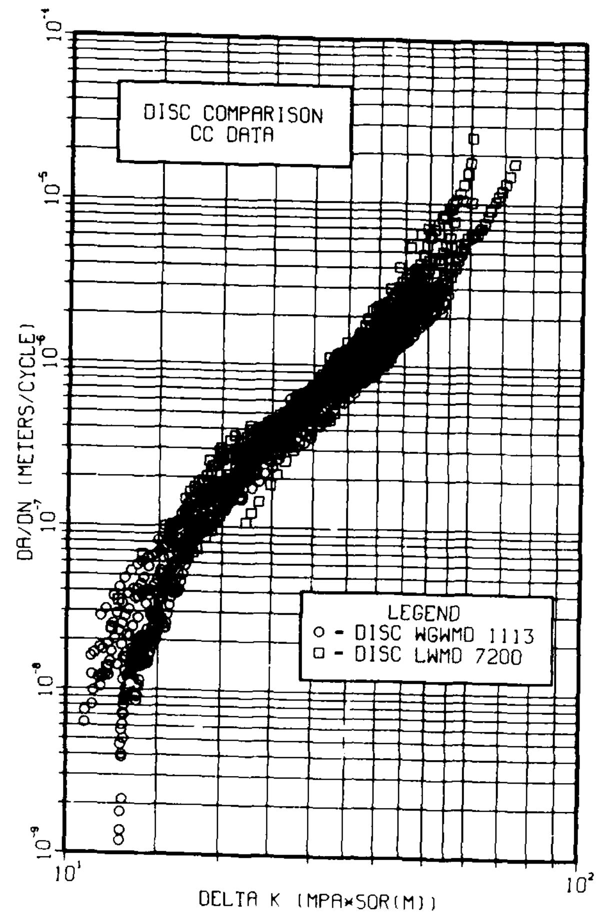

Fig. 48 Disc comparison, CC-data

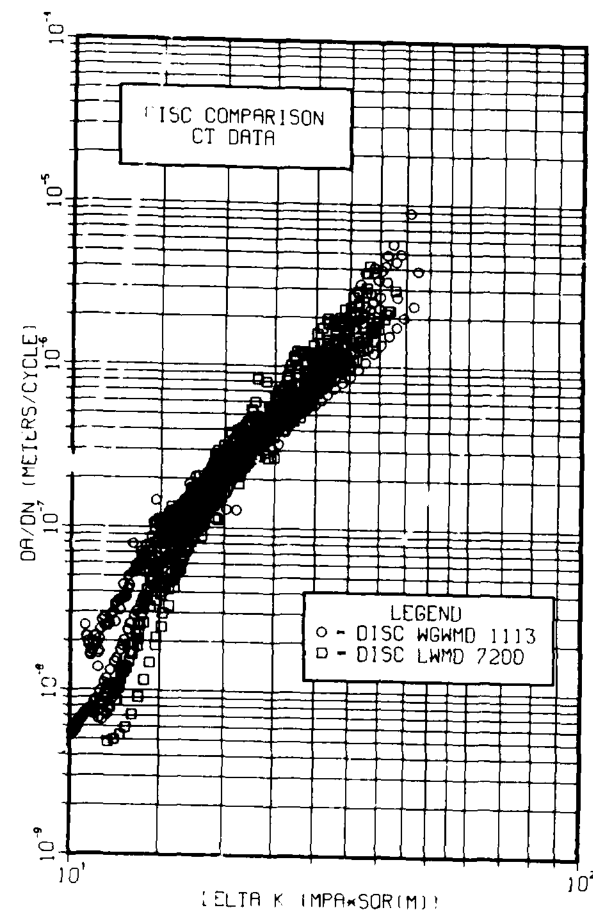

Fig. 49 Disc comparison, CT-data

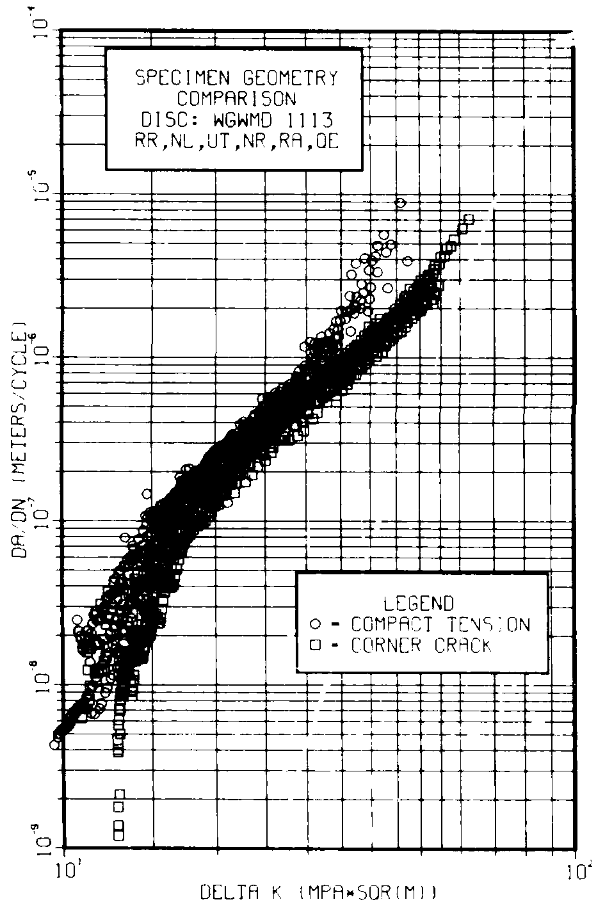

Fig. 50 Specimen geometry comparison; disc WGWMD 1113, RR, NL, UT, NR, RA, OE

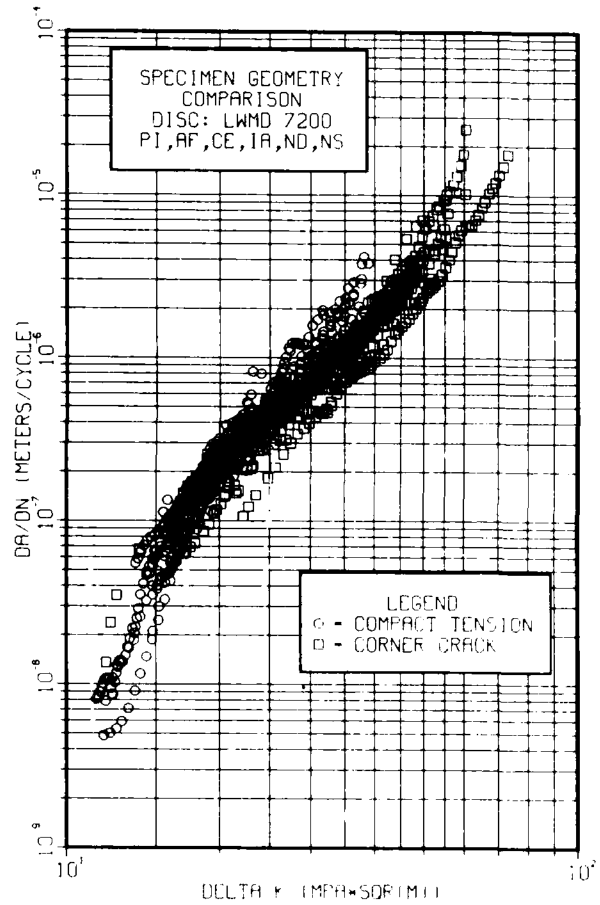

Fig. 51 Specimen geometry comparison, disc LWMD 7200, PI, AF, CE, IA, ND, NS

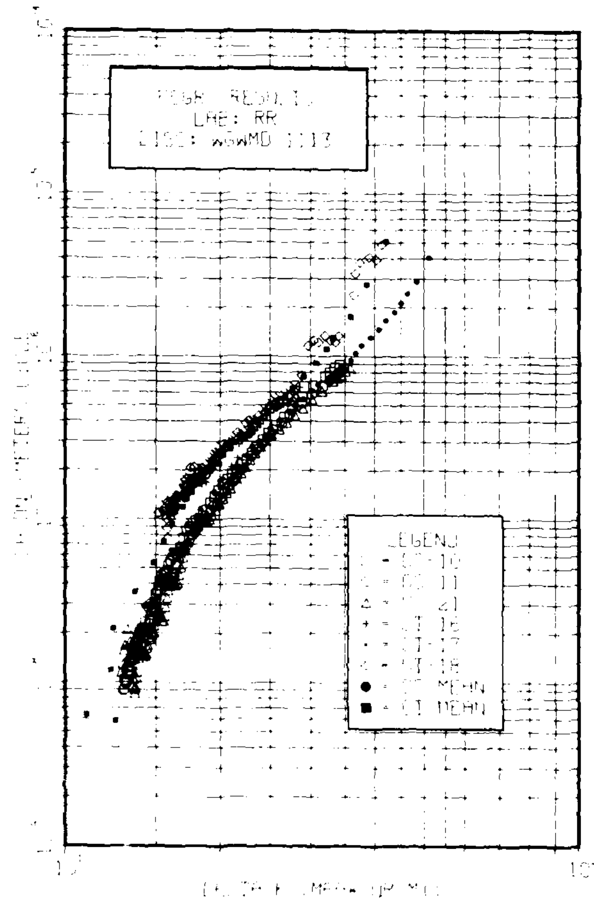

Fig. 52 Fatigue crack growth results, disc WGWMD 1113, laboratory RR

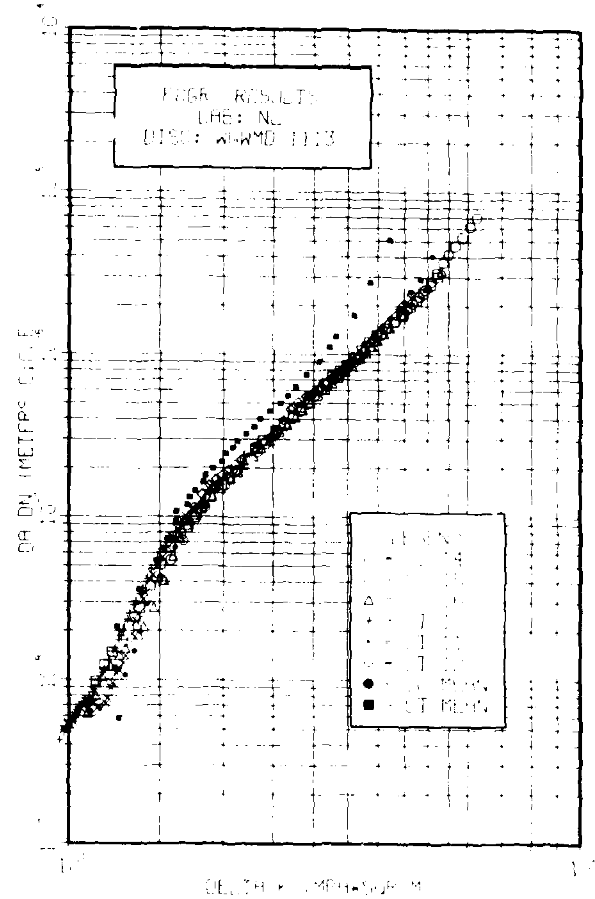

Fig. 53 Fatigue crack growth results, disc WGWMD 1113, laboratory NL

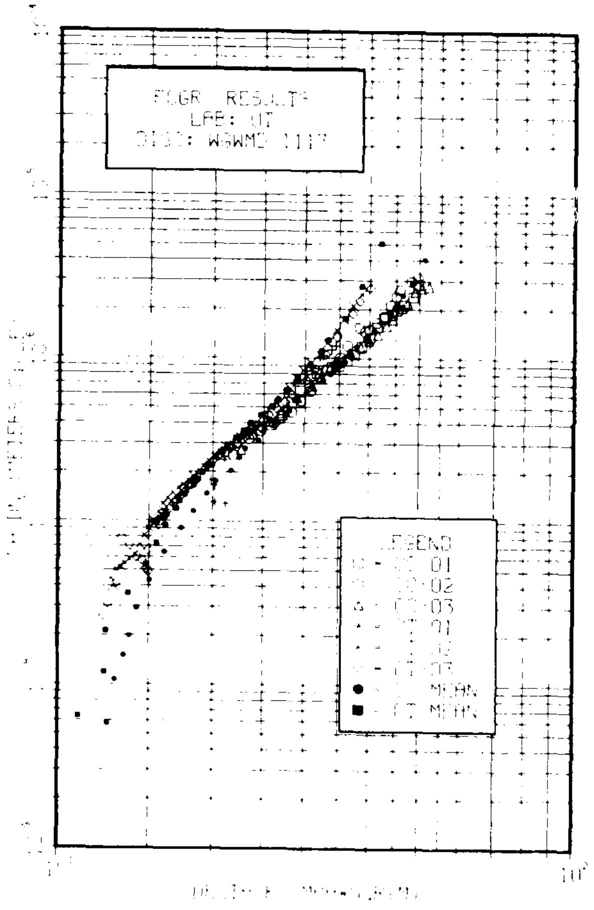

Fig. 54 Fatigue crack growth results, disc WGWMD 1113, Laboratory UT

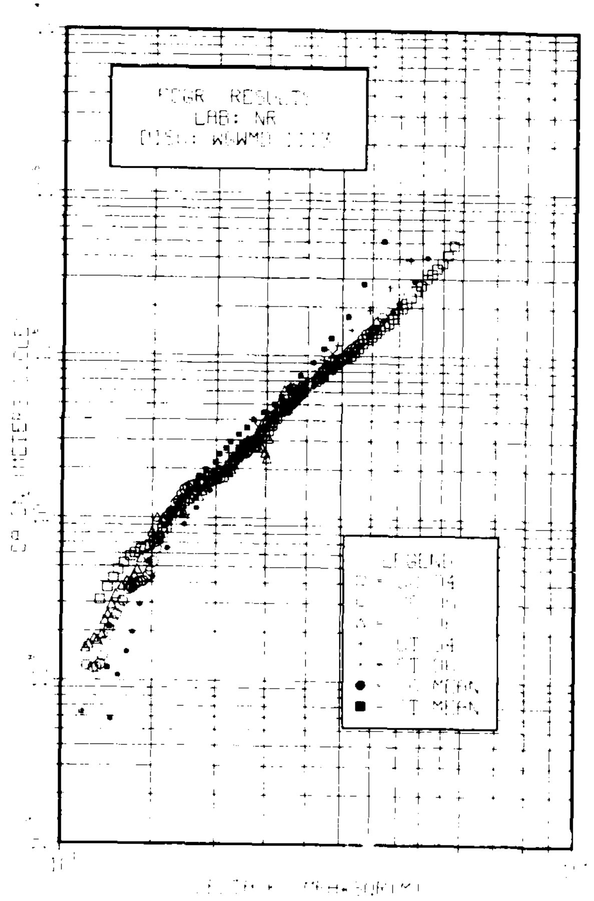

Fig. 55 Fatigue crack growth results, disc WGWMD 1113, Laboratory NR

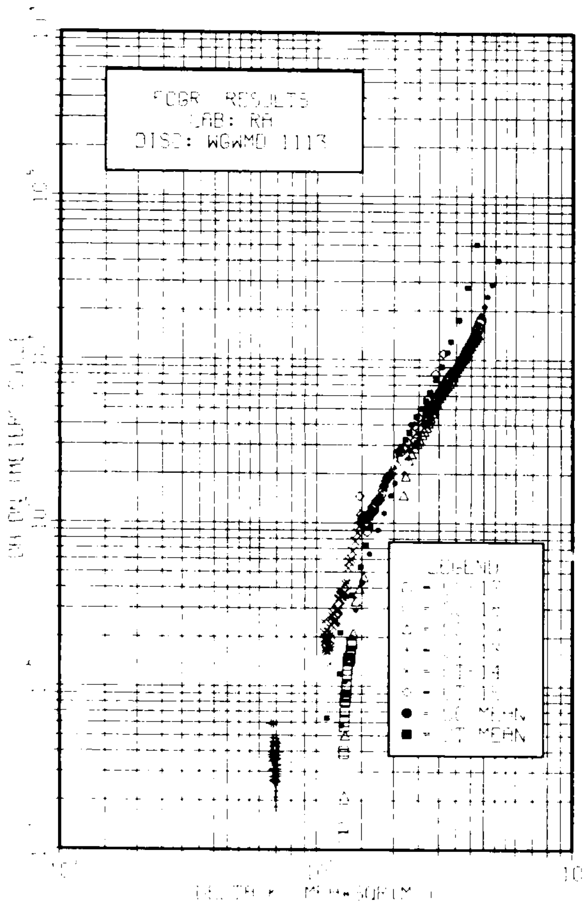

Fig. 56 Fatigue crack growth results; disc WGWMD 1113, laboratory RA

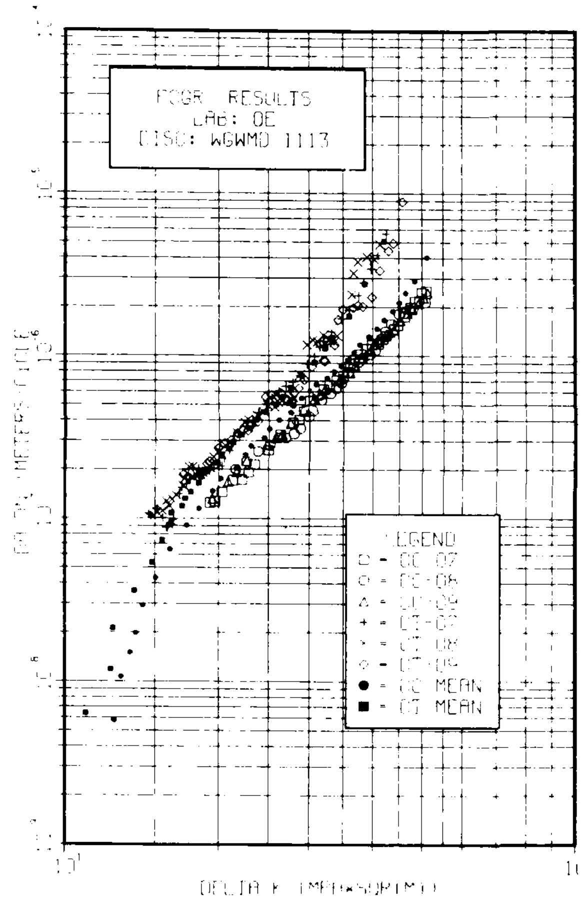

Fig. 57 Fatigue crack growth results, disc WGWMD 1113, laboratory QE

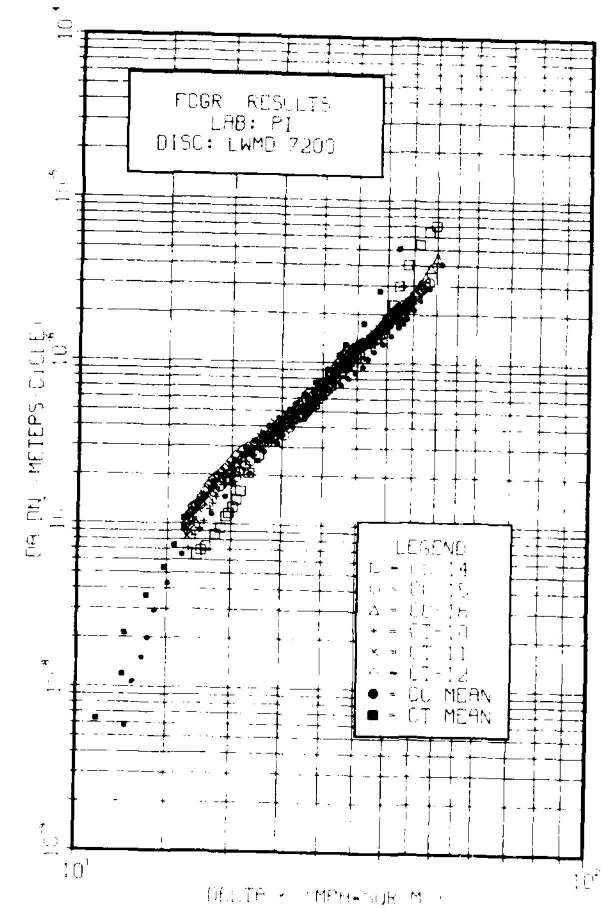

Fig. 58 Fatigue crack growth results, disc LWMD 7200, laboratory PI

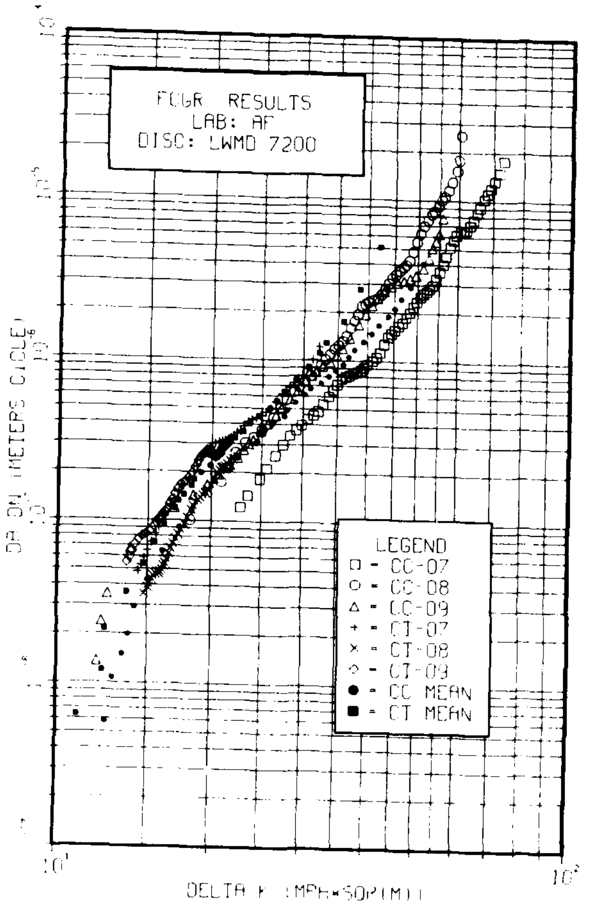

Fig. 59 Fatigue crack growth results, disc LWMD 7200; laboratory AF

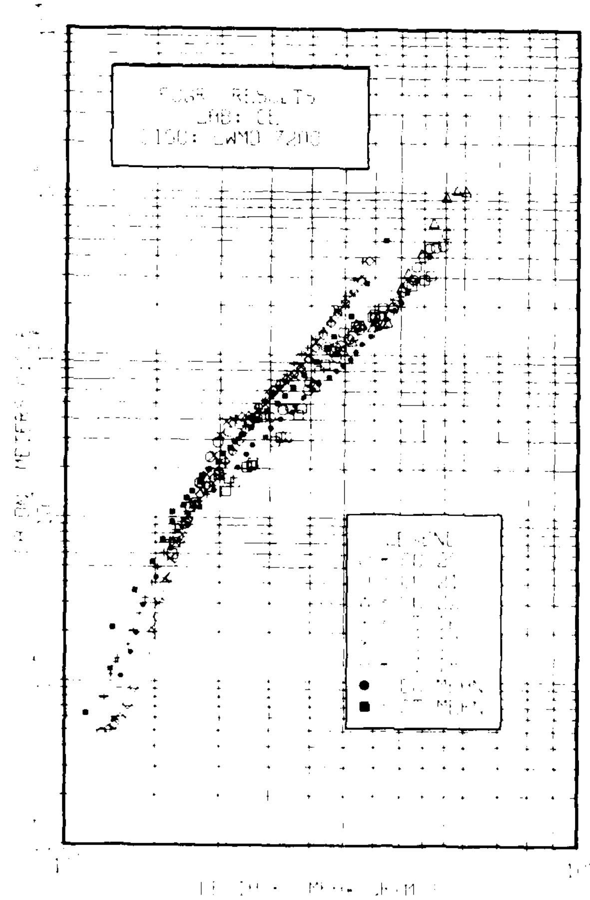

Fig. 60 Fatigue crack growth results; disc LWMD 7200, laboratory CE

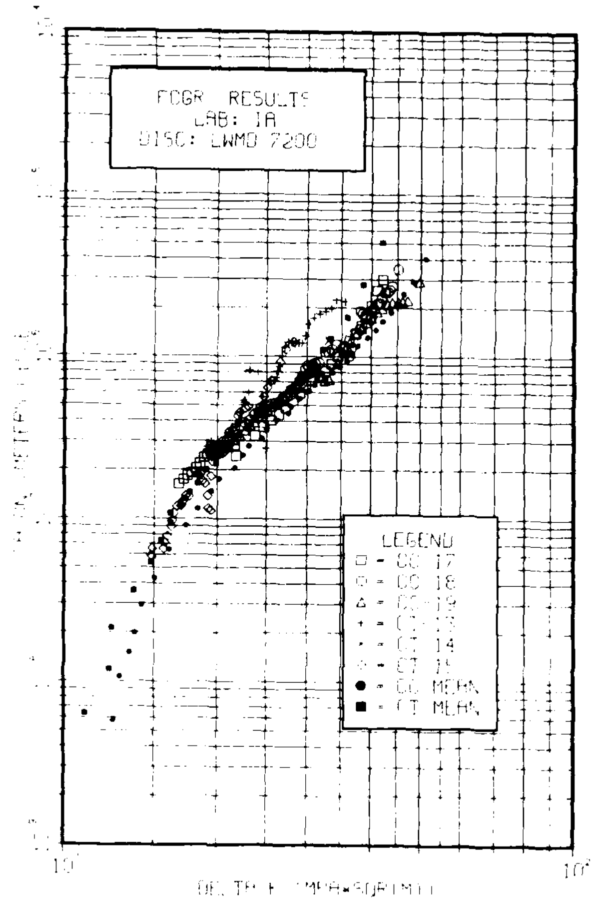

Fig. 61 Fatigue crack growth results; disc LWMD 7200, laboratory IA

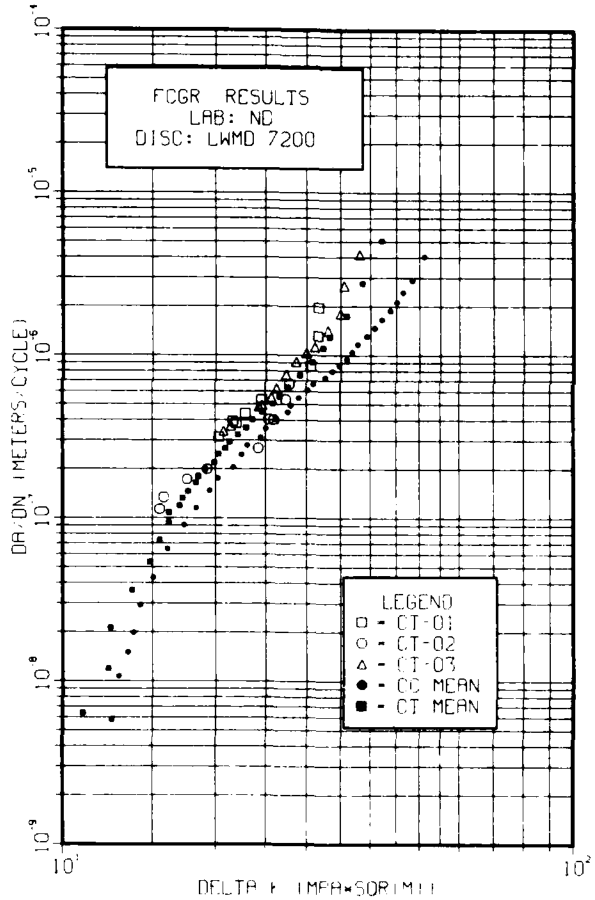

Fig. 62 Fatigue crack growth results, disc LWMD 7200, laboratory ND

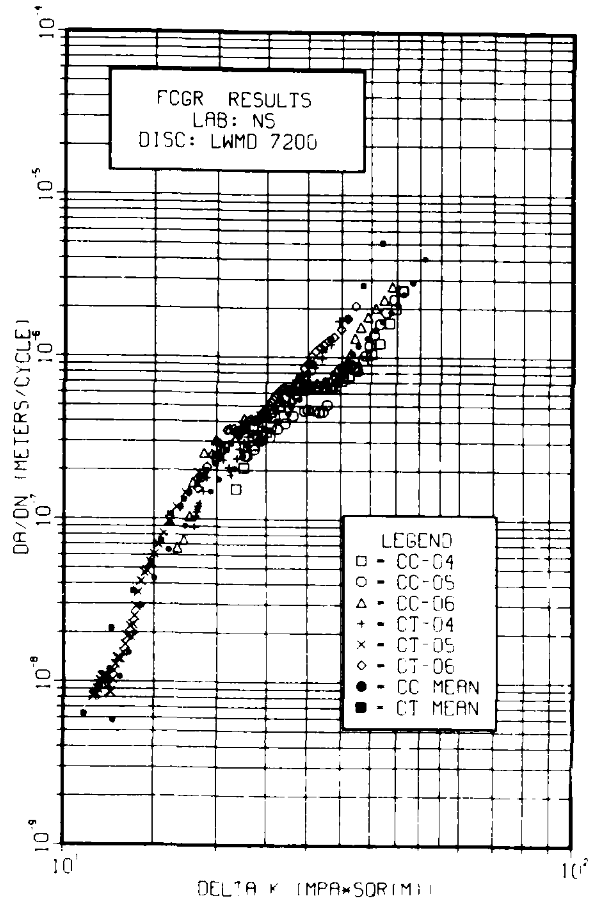

Fig. 63 Fatigue crack growth results, disc LWMD 7200, laboratory NS

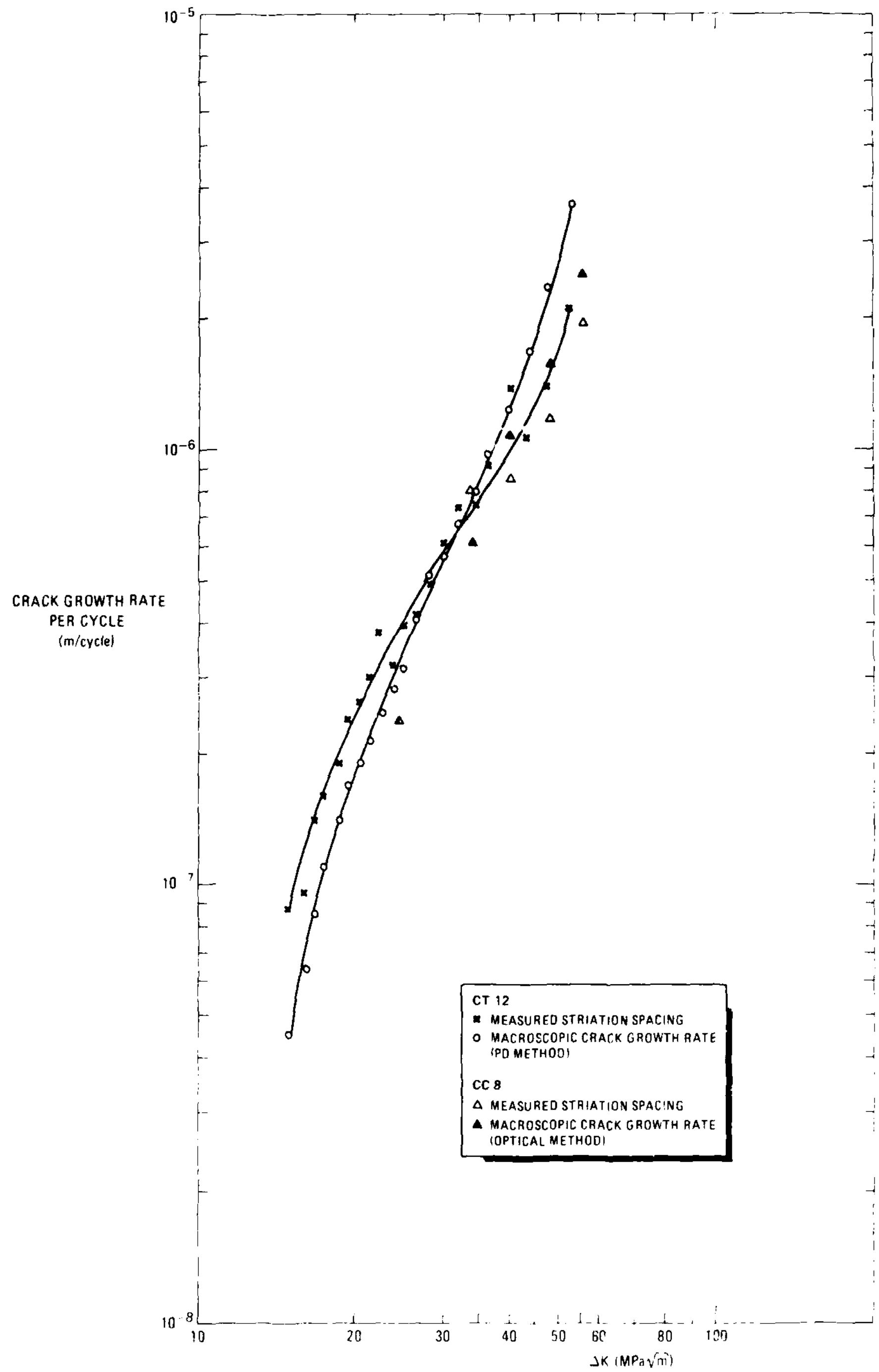

Fig. 64 Comparison between measured striation spacing and macroscopic crack growth rates for specimens CT 12 and CC 8 (disc WGWMD 1113)

(a)

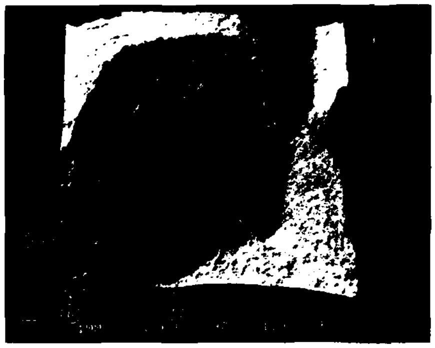

(b)

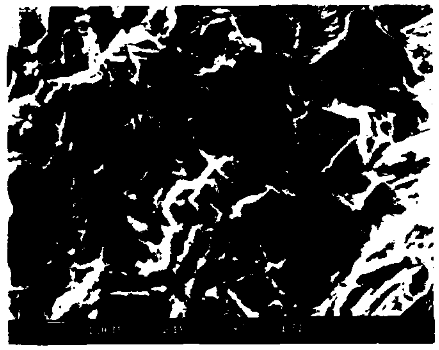

RIGHT SIDE OF CRACK SURFACE AT a = 0.6 mm
(ΔK = 17.3 MPa$\sqrt{m}$)

(c)

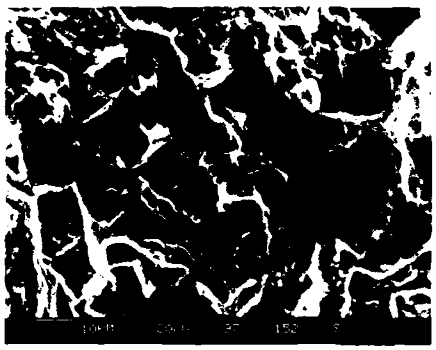

LEFT SIDE OF CRACK SURFACE AT a = 2.14 mm
(ΔK = 33.2 MPa$\sqrt{m}$)

(d)

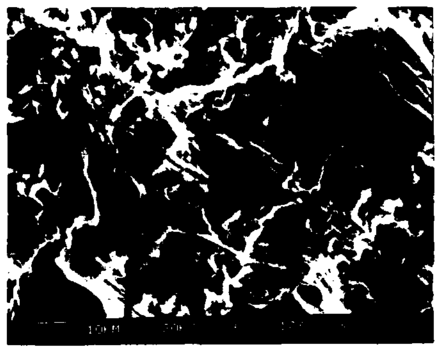

45° LINE AT a = 2.78 mm
(ΔK = 36.7 MPa$\sqrt{m}$)

(e)

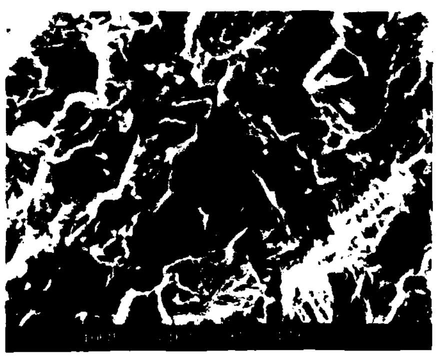

45° LINE AT a = 4.23 mm
(ΔK = 51.4 MPa$\sqrt{m}$)

(f)

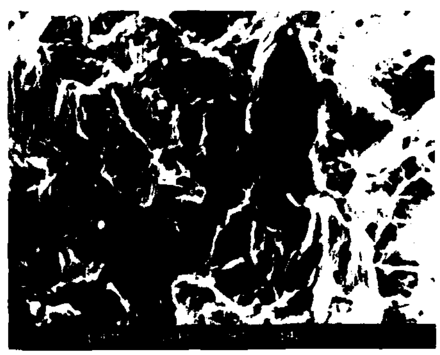

RIGHT SIDE OF CRACK SURFACE AT a = 4.23 mm
(ΔK = 55.6 MPa$\sqrt{m}$)

Fig. 65 Fractographic appearance of specimen CC 8

APPENDIX A

NLR TR 86019 L

REVISED WORKING DOCUMENT FOR THE AGARD
COOPERATIVE TEST PROGRAMME ON TITANIUM ALLOY
ENGINE DISC MATERIAL

by
A.J.A. Mom

SUMMARY

This revised working document provides a detailed lay-out for the tests to be performed in the AGARD cooperative test programme on titanium alloy engine disc material.

CONTENTS

1. INTRODUCTION

This report provides a working document for the actual test procedures of the AGARD Engine Disc Material Testing programme. Apart from the specimen design and testing procedure, the report includes a detailed description of the potential drop (PD) measurement system. The standard test procedure as described herein is the basis for the collaborative testing as performed in the AGARD CORE programme, for which the objectives and goals have already been presented [1].

Table A1 shows the testing matrix of the CORE programme.

2. SPECIMENS

Four standard test specimens have been selected, two for LCF testing and two for crack propagation testing:
- smooth cylindrical specimen, $K_t = 1$, LCF-life, see Figure A1-a;
- flat double edge notched specimen, $K_t = 2.2$, LCF-life, see Figure A1-b;
- *ASTM CT (compact type)-specimen, crack propagation, see Figure A1-c;*
- Corner crack (CC)-specimen, crack propagation, see Figure A1-d.

All specimens for the CORE programme have been machined at one location from Ti-6Al-4V material, which was obtained from disc forgings, delivered by Rolls Royce, Derby. The orientation of the specimens was selected in such a way that the envisioned crack plane corresponded to the crack plane to be expected in service i.e. radial and perpendicular to the disc plane.

APPENDIX A

3. TEST PROCEDURES

3.1 Smooth cylindrical specimen (Figure A1-a)

3.1.1 General
Simple LCF life tests will be performed on this specimen. Check firstly the loading axiality of the test bench/specimen combination by the measurement of axial strains on opposite sides of the specimen test section under elastic loading conditions. The loading axiality is considered acceptable if the maximum difference in these strains is below 5 %.

3.1.2 Test conditions

1. Laboratory air, room temperature.

2. Trapezoidal loading waveform; R = 0.1, f = 0.25 Hz; see Figure A2.

3. Selection of stress levels:
Based on available Ti-6Al-4V LCF-life data (see Figure A3) it is estimated that for anticipated lives of 2000, 7000 and 25000 cycles the following stress levels should be chosen. (Note: selected stress levels refer to the low end of the scatterband because actual testing is to be performed at R = 0.1, while the data in Figure A3 are for R = 0.1.):

N (cycles)	stress range (MN/m^2)
2000	850
7000	800
25000	750

Tests should start at the 750 MN/m^2 stress level. Select additional stress levels (based on the initial test result) to obtain data for the total 2000 - 25,000 cycles range. Note: test preferably two specimens at each stress level!

4. The σ-ϵ hysteresis loop should be identified (recorded) for each specimen at each stress level. The σ-ϵ loop changes especially during the very early portion of the fatigue life (perhaps only the first few cycles). Thereafter a steady state condition is reached. Try to record a number of σ-ϵ loops until steady state conditions exist. The results may later be used for deriving various life relations. The storage of the hysteresis data may be done in a plotted format or digitised for follow-on computer analysis.

3.2 Flat double edge notched specimen (Figure A1-b)

3.2.1 General
Simple LCF tests will be performed on this specimen; however, apart from the number of cycles to failure the number of cycles to "initiate" a certain crack will also be measured. Crack initiation is determined by using the potential drop (PD) measurement technique which is able to register small cracks.

3.2.2 Loading axiality
Check the loading axiality of the test frame/specimen combination by the measurement of axial strains on the opposite surfaces under elastic loading conditions. The loading axiality is considered acceptable if the maximum difference in strains is 5 %.

3.2.3 Procedure for PD instrumentation and measurement (Figure A4)

1. Attach at each notch one set of potential probes diagonally at opposite corners. Use Ti-wire (for reasons of convenience Pt-wire might also be used) with a diameter of ca. 0.3 - 0.5 mm.
Weld the wire exactly at the corner so that the contact area is not greater than 0.5 x 0.5 mm (Figure A4)
Welding equipment which may be used is e.g.:
- from Hughes Aircraft Systems (Weybridge Surrey, UK): MCW 550 MC power supply + VTA-90 weld head, or:
- from Unitek, California: type 125 power supply + type 32F weld head.

2. The Ti-wires will probably be connected to (Cu) potential cables which are connected to the voltmeter. Ensure that the two dissimilar metal joints (Ti/Cu) for each set are at the same temperature in order to avoid thermally induced voltages.

3. Apart from the two notch voltages a reference voltage should also be measured. Attach the Ti-wire reference leads to the reference block as indicated in Figure A4. The reference block is made out of the same material as the specimen (in this case Ti-6Al-4V). Mount the reference block to the machine frame close to the specimen.
Note: It may be difficult, because of limited equipment capabilities, to measure 3 voltages (2 notch voltages and the reference voltage). In that case one of the notch voltages (the one which does not crack initially) can be used as the reference.

4. Design a system which is suitable to realise a uniform current distribution through the specimen. Individual laboratories may choose their own approach tailored to their equipment capabilities. Figure A4 shows one of the possibilities for a current input system.

5. Check for good insulation between specimen and machine frame.

APPENDIX A

6. Measure the notch and reference PD values during the test at both current on and current off conditions (Figure A5). Correct the "current on" values with the "current off" values.

7. Plot the normalized notch voltages (V_{notch}/V_{ref}) versus cycles and determine the crack formation life value, for this purpose defined as the number of cycles at which the normalized notch voltage is 1 % above the initial value. Note that fluctuations in V_{ref} (e.g. due to noise) may obscure the 1 % level (this is especially the case if V_{ref} is relatively small compared to V_{notch}). In that case it would be appropriate to neglect V_{ref}, provided that the fluctuations are not the result of temperature or current variations.

8. Assure that during the fatigue test enough voltage readings are made to enable an accurate cyclic life determination at the 1 % increase level of the normalized potential.

9. Preliminary tests showed that a 1 % increase in PD value corresponded with a crack of 0.6 mm depth and 1.75 mm surface length.

3.2.4 Test conditions

1. Laboratory air, room temperature.

2. Trapezoidal loading waveform; R = 0.1; f = 0.25 Hz, see Figure A2.

3. Selection of stress levels.

Based on available Ti-6Al-4V notched LCF life data (see Figure A6 for K_t = 2.5) the following nominal stress levels are chosen for anticipated total lives of respectively 2000, 7000 and 25000 cycles:

N	nominal stress range (MPa)
2000	775
7000	625
25000	[illegible]

Note that the data indicated in Figure A6 refer to a specimen with a K_t of 2.5 whereas the flat double edge notched specimen contains two notches with a K_t of 2.2. Adjust the applied stress ranges if test results show this to be necessary. Test two specimens at each stress level; begin with the 625 MPa level.

3.3 Compact type (CT) specimen (Figure A1-c)

3.3.1 General

Crack propagation tests will be performed on this specimen using the same trapezoidal waveform as already mentioned before. Crack length measurement is carried out by using the PD technique, making use of a calibration formula.

3.3.2 Procedure for PD instrumentation and measurement (see also Figure A7)

1. Drill and tap holes (M3) and attach current input and output studs at the locations indicated in Figure A7. The stud location must be checked and should be within 0.2 mm.

2. Attach current leads also to the reference block. The reference block must be of the same material as the specimen.

3. Check for good insulation between specimen and machine frame (infinite resistance). The specimen may be insulated by insulation of the loading pins within the clevis or by insulation of the clevis to the machine, e.g. by attaching the (threaded end of the) clevis to the swivel as e.g. shown in Figure A4.

4. Weld PD wires to the edge of the notch at diagonally opposite corners. Use Ti-wire with a diameter of about 0.3 - 0.5 mm. Ensure that the contact area of the weld is not greater than 0.5 x 0.5 mm. For reasons of convenience Pt-wire may also be used instead of Ti-wire. Ti-wire, however, diminishes thermal voltages.

5. Attach the Ti PD wires to the potential cables which are connected to the voltmeter. Ensure that the two dissimilar metal joints are at the same temperature to avoid thermally induced voltages.

6. Measure the notch voltage and adjust current to give an initial voltage in the range 1.6 - 1.9 mV. This should correspond to a current of approximately 7.5 A.

7. Attach the reference wires (also Ti) to the reference block such that the measured PD is approximately equal to the notch voltage.

8. Attach the reference wires to potential cables leading to the voltmeter. Ensure the same temperature at the two dissimilar metal joints.

9. Support all PD wires such that no weld failures will occur during the test.

10. Allow the PD signals to stabilise before the start of the test.

11. Record at the onset of the test the notch and reference PD values and the corresponding crack length for calibration purposes.

12. Record during the test, at appropriate intervals, the notch and reference PD values. Data sampling should be done such that at least 100 but no more than 500 data prints are recorded.

13. Record the final notch and reference PD values at the end of the test. Determine the final average crack length (see also point 14) on the fracture surface. The results are to be used for calibration purposes.

14. The final average crack length is easily determined by heat tinting (~ 30 min. at 500 °C; lower temperatures may also be applied) and a subsequent tensile test resulting in specimen failure. If heat tinting is to be avoided, because e.g. the fracture surface will be used for detailed fractographic investigation, the final crack length can also be measured either in the scanning electron microscope or directly by optical means dependent on the visibility of the transition between the fatigue and overload area.

15. The final average crack length is determined by averaging 5 measurements taken at 0, 25, 50, 75 and 100 % of the specimen width.

16. Calculate the crack length for all data points, making use of the well known final crack length, out of the calibration curve (Figure A8 [2]) or the calibration formula:

$$\frac{V/V_o}{V_{ref}/V_{ref_o}} = A + A_1\left(\frac{a}{W}\right) + A_2\left(\frac{a}{W}\right)^2 + A_3\left(\frac{a}{W}\right)^3 \qquad (1)$$

in which V = notch voltage

V_o = notch voltage at the start of the test (crack size 0)

V_{ref} = reference voltage

V_{ref_o} = reference voltage at the start of the test

with A = 0.5766
A_1 = 1.9169
A_2 = -1.0712
A_3 = 1.6898

or (in reversed notation):

$$\frac{a}{W} = B + B_1\,\frac{V/V_o}{V_{ref}/V_{ref_o}} + B_2\left[\frac{V/V_o}{V_{ref}/V_{ref_o}}\right]^2 + B_3\left[\frac{V/V_o}{V_{ref}/V_{ref_o}}\right]^3 \qquad (2)$$

with B = -0.5051
B_1 = 0.8857
B_2 = -0.1398
B_3 = $2.398.10^{-4}$

For example: with $\left(\frac{a}{W}\right)_{final}$ the value of $\frac{V_{final}/V_o}{V_{ref_{final}}/V_{ref_o}}$ can be calculated. Making use of the final, measured notch voltage (V_{final}), the final reference voltage ($V_{ref_{final}}$) and the initial reference voltage V_{ref_o} the value of the initial notch voltage V_o (according to the calibration curve) can be calculated. This value may not correspond to the actually measured initial notch voltage, which may be due to an inaccuracy in final crack length measurement (or averaging method) or to the effect of plastic zone formation (see also point 18). Making use of this calculated initial notch voltage the crack length at every data point (V versus N) can now be calculated with equation (2).

17. The use of V_{ref} may obscure the results if the noise level is high and if V_{ref} is small compared to V_{notch}. In that case V_{ref} may be neglected provided that the fluctuations in V_{ref} are not the result of current or temperature variation.

18. During the initial part of the test on the CT-specimens the notch voltage will firstly increase and afterwards stabilize, see Figure A9. This is one of the reasons not to use the measured initial notch voltage for crack length calculation but instead the calculated initial notch voltage (see also point 16).

3.3.3 Test conditions

1. Laboratory air, room temperature.

2. Trapezoidal loading waveform (NB: see also point 6); $R = 0.1$; $f = 0.25$ Hz, see Figure A2.

3. For Ti-disc materials we are especially interested in crack growth rates between approximately 5.10^{-5} and 10^{-3} mm/cycle. This refers to crack growth rates normally encountered in service. Therefore, and also based on Figure A10 [3], the ΔK-values mentioned further on have been selected for the tests.

4. Precrack the first specimen at $\Delta K = 13.5$ MN/m$^{3/2}$ ($\Delta P = 5.87$ kN) and continue the test with the same load. Stop the test at $\Delta K = 55$ MN/m$^{3/2}$ ($K_{max} = 60$ MN/m$^{3/2}$); this corresponds with a crack length of about 11.5 mm.
Caution: because of the crack front curvature at the specimen surface the surface crack length underestimates the average crack length. Therefore, build in some additional safety.
For the calculation of the stress intensity factor the following formula is used (valid for a/W between 0.2 and 1):

$$K_I = \frac{P}{B\sqrt{W}} . f(a/W) \text{ where}$$

$$f(\tfrac{a}{W}) = \frac{2 + a/W}{(1-a/W)^{3/2}} \{0.886+4.64a/W-13.32(a/W)^2+14.72(a/W)^3-5.6(a/W)^4\}$$

To facilitate the calculation of K_I, values of f(a/W) are tabulated in Table A2 for specific values of a/W.

5. With the first specimen, starting at $\Delta K = 13.5$ MN/m$^{3/2}$, the crack growth curve is determined for growth rate values above 10^{-4} mm/ cycle. Extrapolate the crack growth curve to 10^{-5} mm/cycle and determine the corresponding ΔK value. Start the test with the second specimen at this value and continue (with the same load applied) the test until a/W = 0.65. The third specimen may be used to check the data already obtained with the two previous tests.

6. Precracking and load shedding may be applied to prevent very long initiation times. If load shedding is performed then this should be done according to ASTM E 647 (latest revision).
Precracking is carried out using sinusoidal loading. During the actual test trapezoidal loading should be applied; however, in the case of low crack growth rates, which seriously retard the test duration, sinusoidal loading (5 Hz) is also allowed. In that case the test should be stopped at high load and at regular intervals if so required for the PD measurements, see Figure A11. Ensure that both current on and current off measurements are carried out when the current, and hence the signal, is sufficiently stabilised.
Compare the crack growth rates for the high and low frequency waveforms.

3.4 Corner crack (CC) specimen (Figure A1-d)

3.4.1 General
Crack propagation tests in the "physically" short crack regime will be performed on this specimen using the same trapezoidal waveform as already mentioned before. Crack length measurement is carried out by using the PD technique, making use of a calibration formula.

3.4.2 Loading axiality
Check the loading axiality of the test bench/specimen combination by the measurement of axial strains (under elastic loading conditions) on opposite surfaces. The loading axiality is considered acceptable if the maximum difference in strains is 5 %.

3.4.3 Procedure for PD instrumentation and measurement (see also Figure A12)
The procedure outlined below is based on a detailed Rolls Royce PD measurement procedure. Where necessary some minor deviations from this procedure have been made.
Note: The PD technique is optional for this specimen! Crack growth should also be measured optically (see further on, point 13).

1. Spot weld a 50 μm Ø titanium probe wire* to each support wire, see Figure A12. Heat input should be preferably lower than 0.5 Watt-second.

2. Assemble the 4 PD lead support wires* in a ceramic holder using refractory cement. If desired the support wires may also be eliminated; twist in this case the two fine 50 μm wires from the notch to the measurement points.

* Whenever possible the support wires and the PD probes should be of the same base material as the test piece; for this programme pure Ti-wires are recommended; however, Pt wires may also be used.

3. Cement the ceramic block to one of the faces of the test piece not containing the notch and spot weld a probe wire on either side of the notch as shown in Figure A12. It is critical for the probe wire to be located right on the edge of the notch because the PD calibration is strongly dependent on z, the separation of the probes (see Figure A13 [2]).

APPENDIX A

4. Spot weld the remaining wires to the test piece away from the notch as shown in Figure A12. These will be used to monitor a reference potential. The reference wires may also be welded on one of the 3 edges not containing the notch.

5. Check each wire for good electrical connection.

6. Check that the specimen grips are fully insulated from the machine and that they are correctly aligned (see above).

7. Mount the specimen into the machine, being careful not to disturb the welds.

8. Attach current leads to the test specimen, or to another (e.g. the specimen grips) location assuring good current uniformity (see also remarks about the flat double edge notched specimen).

9. Secure 2 thermocouples to test piece as shown in Figure A12 (only optional, not necessary for CORE-programme).

10. Make the necessary connections (PD, thermocouple etc.) to the measurement system.

11. Switch current on: 15A. (If equipment capabilities do not allow this current then choose your own value.) At this current the PD value over the crack will increase from about 100 μV to over 2000 μV.

12. Allow the PD signals to stabilise.

13. Surface crack length measurements should in principle be carried out by optical means, e.g. by a travelling microscope arrangement. Don't use replicas because this may affect crack growth behaviour. The PD measurement system may be used solely if it turns out that the accuracy gained by the PD method is at least equal to the optical measurement accuracy. The resolution of the optical crack length measurement should be better than 0.05 mm.
Try to avoid stopping the machine for crack length measurement; dwell effects at load can alter fatigue crack growth behaviour. Take photographs if this will help in crack growth measurement.

14. Start the test using a constant load amplitude and grow the crack to a/W = 0.5 maximum. Clearly this will be determined by the fracture toughness of the material.

15. Record at appropriate crack lengths the corresponding notch and reference PD values for current on and off conditions (Figure A5).

16. Avoid breaking the specimen during the fatigue test. Stop the test at a/W = 0.5 maximum (this depends on K_{max}, see further) and measure the final notch voltage. This is necessary for obtaining the final notch voltage/crack length pair for calibration purposes. To prevent static crack growth during the final measurement it is recommended to stop the test at $\Delta K = 55\ MN/m^{3/2}$ (or $K_{max} = 60\ MN/m^{3/2}$).

17. Measure the final average crack length on the fracture surface (and the initial crack length used in the calibration where possible).
The optical measurement of the final crack length can easily be performed after heat tinting the specimen at the end of the test (e.g. 30 minutes at 500 °C although a temperature as low as 350 °C may also be used) and by a subsequent tensile test to failure.
Heat tinting may negatively affect the recognition of detailed features on the fracture surface of the specimen. If individual laboratories would like to perform a fracture surface investigation it is therefore recommended not to heat tint but to measure the final crack length in the scanning electron microscope, or by optical means if the distinction between fatigue and overload area can be easily recognised.

18. The final average crack length is obtained by averaging 5 radial measurements taken at 0°, 22.5°, 45°, 67.5° and 90° starting from the crack corner.

19. The calibration procedure of notch voltage to crack length for the CC-specimen is as follows:
   - determine the final, average crack length and the corresponding notch voltage;
   - draw a straight line from this data point to the origin (this may be performed if a/W << 0.05, see Figure A13);
   - compare the slope of this line to the slope of the calibration curve (Figure A13).

3.4.4 Test conditions

1. Laboratory air; room temperature.

2. Trapezoidal loading waveform (N.B. see also point 5); R = 0.1; f = 0.25 Hz, see Figure A2.

3. For Ti-disc materials in the "short" crack regime we are interested in crack growth rates between approximately 5.10^{-5} and 10^{-3} mm/cycle. This refers to crack growth rates normally encountered in service. Therefore select a ΔK-value of about 15 MPa$\sqrt{m}$ to start with at a = 0.5 mm (see also point 6).

APPENDIX A

4. The stress intensity actor at the specimen <u>surface</u> can be calculated using the formula:

$$K_{I_{surface}} = 1.16 \ \frac{2}{\pi} \sigma\sqrt{\pi a}, \text{ approximately valid for } \frac{a}{W} < 0.2$$

For higher values of $\frac{a}{W}$ the formula has the following form:

$$K_{I_{surface}} = \left\{1.12-0.13 \frac{a}{W} +1.84 \left(\frac{a}{W}\right)^2 +0.11\left(\frac{a}{W}\right)^3 +0.8\left(\frac{a}{W}\right)^4 \right\} \frac{2}{\pi} \sigma\sqrt{\pi a}$$

A graphical representation is given in Figure A14 [4].
It is clear from this figure that the stress intensity factor at an angle of 45° is different from $K_{surface}$. At a/W = 0.5 $K_{45°}$ is more than 10 % lower than $K_{surface}$. Because the PD technique provides information on the <u>mean</u> crack size it is therefore logical to use also a mean K-value for the calculation of crack propagation data. The K_{mean} is easily derived from $K_{surface}$ as shown below.
Based on the data given in a paper of Pickard [5] the ratio between $K_{surface}$ and $K_{45°}$ has been plotted in Figure A15. Assuming a quadratic curve through the data points (only for a/W > 0.5 is there some deviation) the value of $K_{45°}$ can be expressed in terms of $K_{surface}$:

$$K_{45°} = \{0.94-0.18 \ (a/W)^2\}K_{surface}$$

The K_{mean}, for this purpose simply defined as $\frac{K_{45°} + K_{surface}}{2}$, is now easily derived:

$$K_{mean} = \frac{K_{45°} + K_{surface}}{2}$$
$$= \{0.97-0.09 \ (a/W)^2\}K_{surface}.$$

For the final calculation of the test results the two above given equations for $K_{surface}$ (for a/W < 0.2 and a/W > 0.2) should therefore simply be multiplied with the factor $\{0.97-0.09 \ (a/W)^2\}$ to derive a K_{mean}. In the following, for reasons of simplicity and also because the actual difference *is only small*, only the $K_{surface}$ values will be given for describing the test conditions.

5. Initiate a fatigue crack from the notch using an alternating stress of 540 MN/m^2 (Maximum stress = 600 MN/m^2; R = 0.1). This corresponds to an alternating stress intensity at the side surfaces of the specimen of $\Delta K = 11.2 \ MN/m^{3/2}$ (a = 0.25 mm).
At an alternating stress intensity $\Delta K = 11.2 \ MN/m^{3/2}$ the crack growth rate is estimated to be 2.10^{-5} mm/cycle (see Figure A10 [3]). This means that if the normal test frequency were to be used (15 cycles/minute) every 0.1 mm of crack growth would take about 5 hours. Therefore initially a test frequency of 5 Hz is recommended. A crack size increment of 0.1 mm (5000 cycles) will then occur within ~ 1000 seconds (~ 15-20 minutes). Return to a frequency of 15 cycles/minute when a = 0.5 mm. If the load is held constant during the test this will give the following ΔK levels at the corresponding surface crack lengths:

a (mm)	$\Delta K (MN/m^{3/2})$
0.25	11.2
0.5	15.8
1.0	22.4
2.0	31.6
6.0	88

If the above stress intensities are used the appropriate and realistic crack growth rate values (between 10^{-4} and 10^{-3} mm/cycle) occur in the physically short crack regime.
If the crack growth rates encountered do not agree with the above indicated values then the applied stress levels should be corrected so that appropriate crack growth rates are obtained. Consult the coordinators. In coordination with the first laboratory doing the test they will decide which adjustments should be made and communicate the new stress levels to all other laboratories.

6. If the stress intensity used for crack initiation is too low then a higher (e.g. 20 % higher) stress intensity may be chosen. If the crack initiates at the higher stress intensity a subsequent load reduction may be carried out (if necessary) to obtain appropriate crack growth rates (between 10^{-4} and 10^{-3} mm/cycle) between a = 0.5 → 2 mm.
This procedure will be illustrated by the following simple example:

a = 0.25 mm, assume at $\Delta K = 11.2 \ MN/m^{3/2}$ ($\Delta\sigma = 540 \ MN/m^2$; σ : 60 → 600 MN/m^2) no crack initiation; then increase stress level 20 %;

a = 0.25 mm, $\Delta K = 13.4 \ MN/m^{3/2}$ ($\Delta\sigma = 650 \ MN/m^2$; σ : 72 → 722 MN/m^2).

APPENDIX A

If the load is held constant then this will result in:

a(mm)	ΔK(at Δσ = 650 MN/m^2)		ΔK(at Δσ = 540 MN/m^2)
0.25	13.4		
0.30	14.7		
0.35	15.8	reduce load to original level →	13.2
0.40	16.9		14.1
0.50	18.9		15.8

continue testing at this load level

7. Test the 3 specimens such that a reliable determination of the total crack growth curve is obtained.

4. FORMAT FOR THE DELIVERY OF TEST RESULTS

All CORE programme results should be sent in to the coordinators according to the following format:

Smooth cylindrical specimen

1. Specimen number
2. Stress level (Δσ); MN/m^2
3. Cycles to failure N_f
4. Additional comments, if necessary.

Flat double edge notched specimen

1. Specimen number
2. Stress level (Δσ); MN/m^2
3. Cycles to crack formation (1 %), N_i
4. Cycles to failure N_f
5. Additional comments, if necessary.

Compact type specimen

1. Specimen number
2. da/dN - ΔK curve on supplied graphical paper
3. 50 data sets (a_i versus N_i) representing the total a versus N curve. The data delivered by the various laboratories will all be handled similarly, using a secant procedure, to obtain representative da/dN- ΔK curves
4. Additional comments, if necessary.

Corner crack specimen

1. Specimen number
2. da/dN - ΔK curve on supplied graphical paper
3. 50 data sets (a_i versus N_i) representing the total a versus N curve. The data delivered by the various laboratories will all be handled similarly, using a secant procedure, to obtain representative da/dN- ΔK curves
4. Additional comments, if necessary.

5. REFERENCES

1. Mom, A.J.A. — Proposal for an AGARD coordinated international test programme on damage tolerance in titanium alloy engine discs; presented at AGARD SMP meeting in Vimeiro, Portugal, 1983

2. Hicks, M.A., Pickard, A.C. — A comparison of theoretical and experimental methods of calibrating the electrical potential drop technique for crack length determination; Int. Journ. of Fracture, 20, 1982, pp. 91-101

3. Powell, B.E., Duggan, T.V., Jeal, R. — The influence of minor cycles on low cycle fatigue crack propagation, Int. Journal of Fatigue, January 1982, pp. 4-14

4. Pickard, A.C., Brown, C.W., Hicks, M.A. — The development of advanced specimen testing and analysis techniques applied to fracture mechanics lifing of gas turbine components, in: ASME International Conference on Advances in Life Prediction Methods; Ed. by D.A. Woodford and J.R. Whitehead, published by ASME, New York, 1983

5. Pickard, A.C. — Stress intensity factors for cracks with circular and elliptic crack fronts, determined by 3D finite element methods, Numerical Methods in Fracture Mechanics; Pineridge Press, pp. 599-614 (1980), Swansea, UK

APPENDIX A

TABLE A1

Overview of CORE programme; number of specimens indicated for each individual laboratory. All tests at room temperature

Type of test		LCF-life / crack formation		crack propagation	
Test specimen		smooth cylindrical	flat notched K_t ~ 2.2	corner crack	ASTM CT
Number of specimens		6	6	3	3
Crack detection	potential drop		+	$+^{*)}$	+
	optical			+	
goal			only initial crack formation	"short" crack range	total da/dN - ΔK curve

*) = optional

TABLE A2

$$K = \frac{P}{B\cdot W}\cdot f\left(\frac{a}{W}\right)$$

$$f\left(\frac{a}{W}\right) = \frac{2 + a/W}{(1-a/W)^{3/2}}\,(0.886 + 4.64\,a/W - 13.32(a/W)^2 + 14.72(a/W)^3 - 5.6(a/W)^4)$$

a'	a/W	f(a/W)	a'	a/W	f(a/W)
0	0.244	4.848	3.5	0.379	6.886
0.1	0.248	4.899	4.0	0.398	7.242
0.2	0.252	4.950	4.5	[illegible]	7.623
0.3	0.256	5.002	5.0	0.437	8.033
0.4	0.260	5.054	5.5	0.456	8.477
0.5	0.263	5.107	6.0	[illegible]	8.966
0.6	0.267	5.159	6.5	[illegible]	[illegible]
0.7	0.271	[illegible]	7.0	[illegible]	[illegible]
0.8	0.275	[illegible]	7.5	[illegible]	[illegible]
0.9	[illegible]	[illegible]	8.0	0.552	[illegible]
1.0	0.283	[illegible]	8.5	0.571	[illegible]
1.1	[illegible]	5.427	9.0	[illegible]	[illegible]
1.2	0.290	5.482	9.5	[illegible]	[illegible]
1.3	0.294	5.537	10.0	[illegible]	[illegible]
1.4	0.298	5.593	10.5	0.648	[illegible]
1.5	[illegible]	5.649	11.0	[illegible]	[illegible]
1.6	0.306	[illegible]	11.5	0.687	[illegible]
1.7	0.310	[illegible]	12.0	0.706	[illegible]
1.8	[illegible]	[illegible]	12.5	0.725	[illegible]
1.9	[illegible]	5.878			
2.0	[illegible]	5.936			
2.5	[illegible]	6.236			
3.0	0.360	[illegible]			

Calculation of f(a/W) for ASTM [illegible] specimen with W = 26 mm.
a' = real crack length starting from notch root
a = defined distance from crack tip to centerline of the loading holes
(a = a' + 6.35 mm for this specimen)

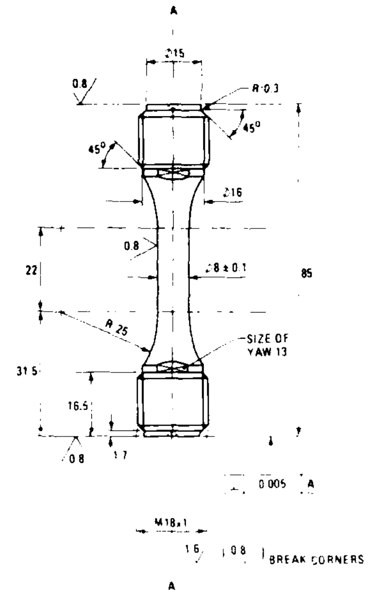

A1–a CYLINDRICAL UNNOTCHED LCF SPECIMEN

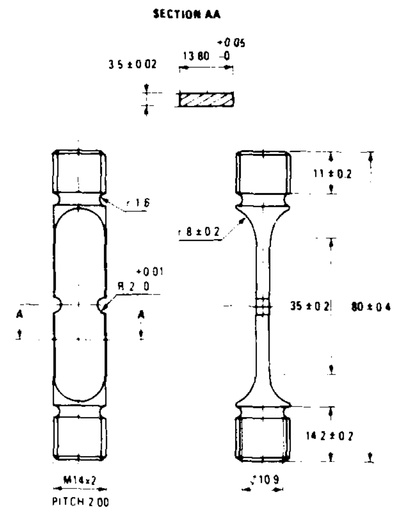

A1–b FLAT DOUBLE EDGE NOTCHED SPECIMEN ($K_t \approx 2.2$)

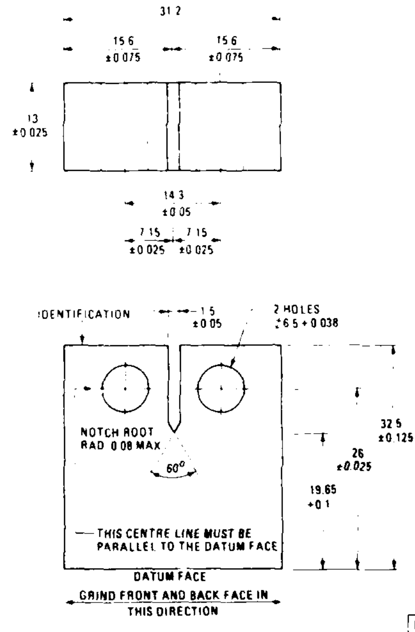

A1–c CT-SPECIMEN

DIMENSIONS IN mm

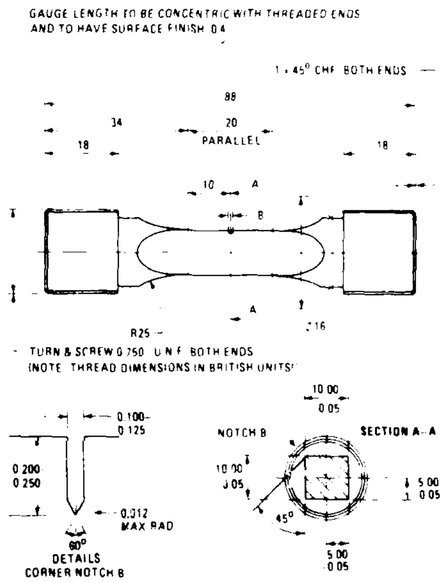

A1–d CORNER CRACK SPECIMEN

Fig. A1 Specimens used in the AGARD programme

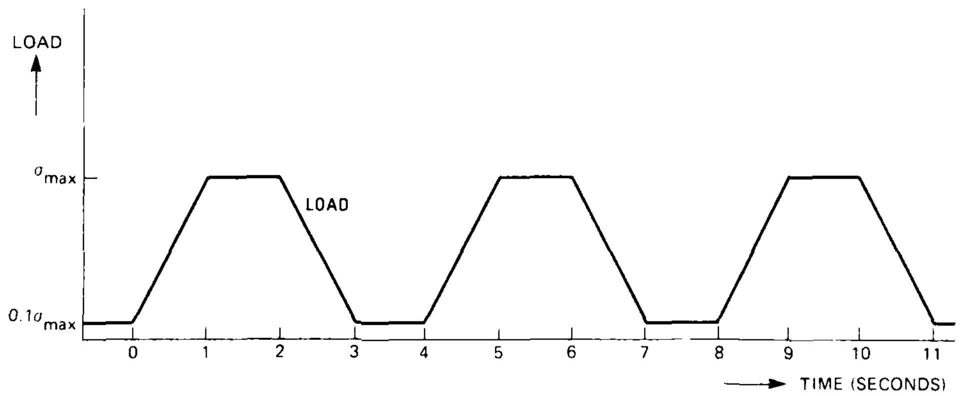

Fig. A2 Load waveform used in CORE programme

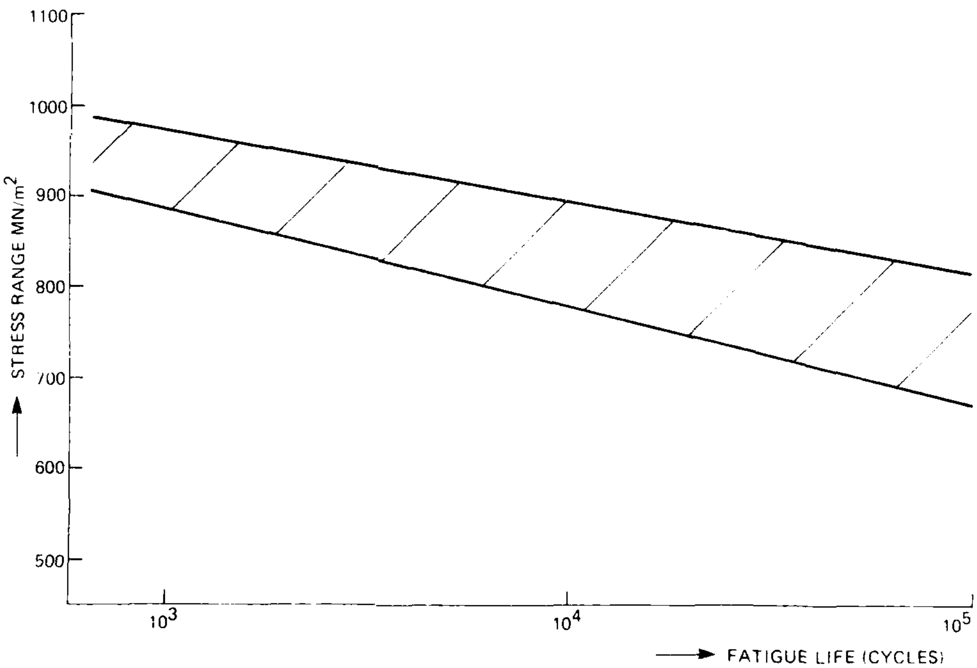

Fig. A3 Ti-6Al-4V plain specimen fatigue life scatterband (based on various data, R = 0)

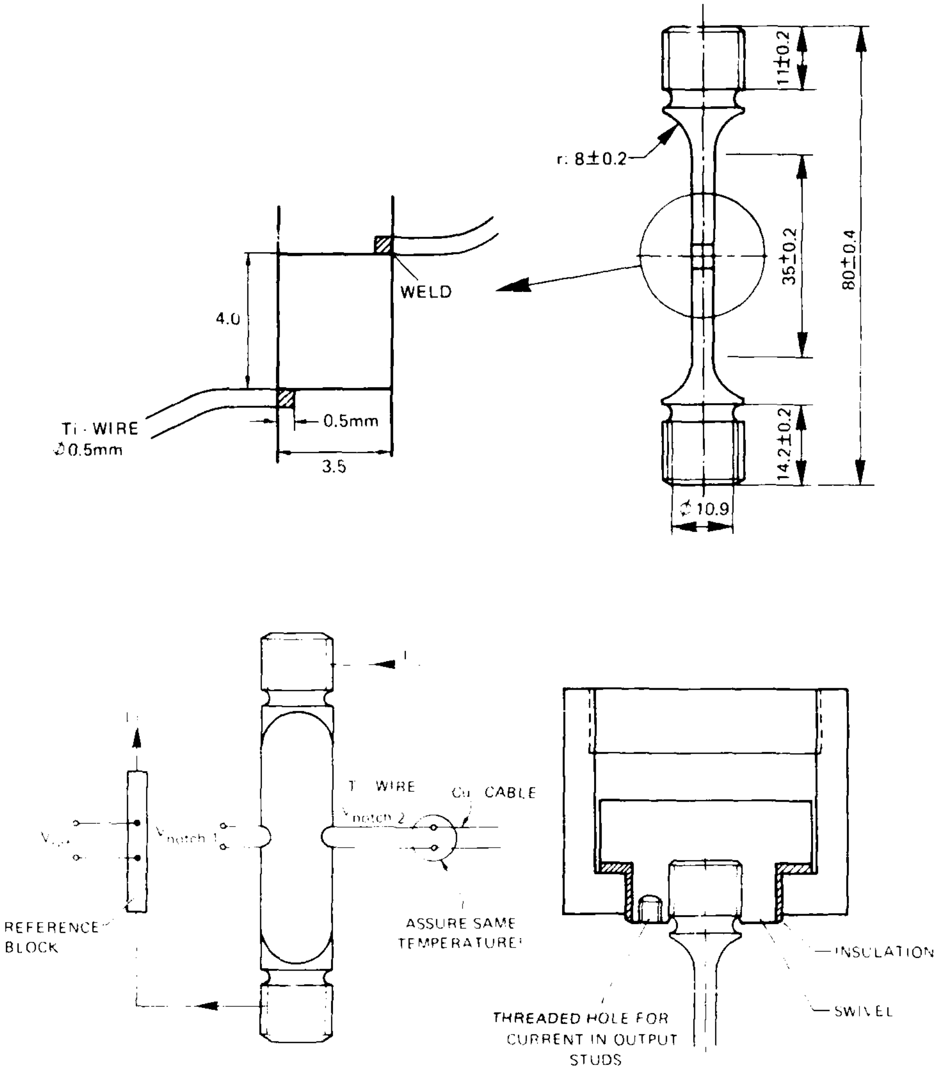

Fig. A1 Set-up of current and voltage wiring for PD-measurement

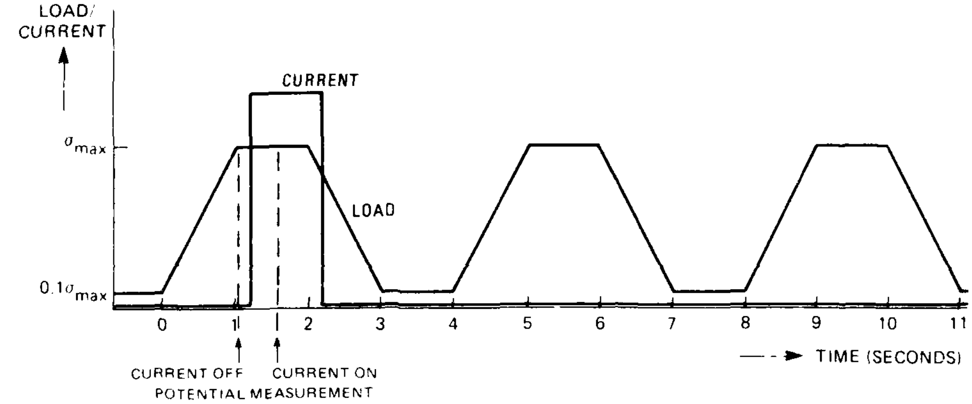

Fig. A5 PD-measurement at current off and current on conditions

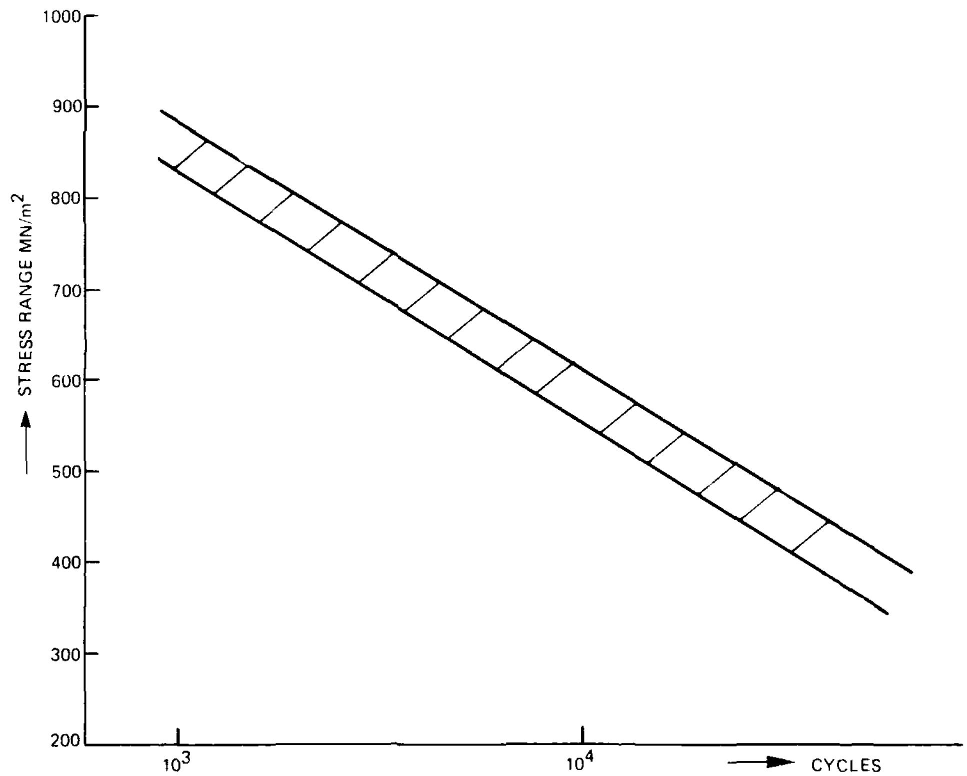

Fig. A6 Fatigue life scatterband for notched Ti-6Al-4V specimens (K_t = 2.5)

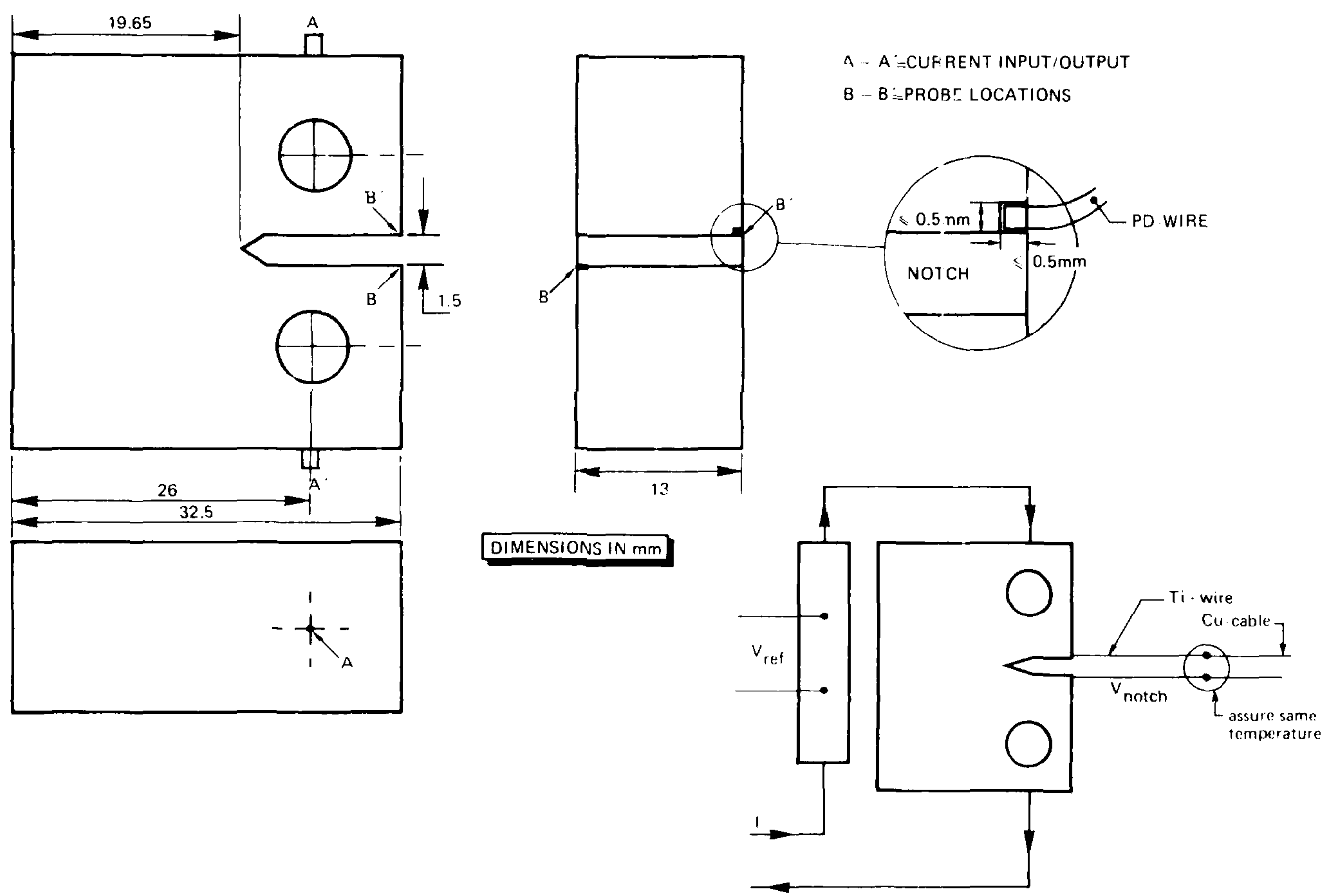

Fig. A7 Set-up of PD measurement system for CT specimen

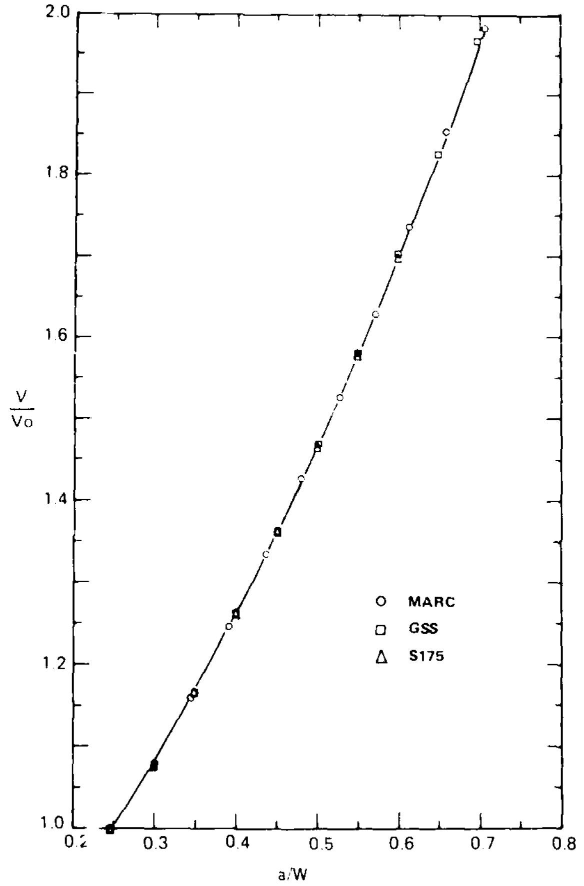

Fig. A8 Finite element PD-analysis for CT-specimen normalised to $V/V_0 = 1$ at $a/W = 0.244$ [2]

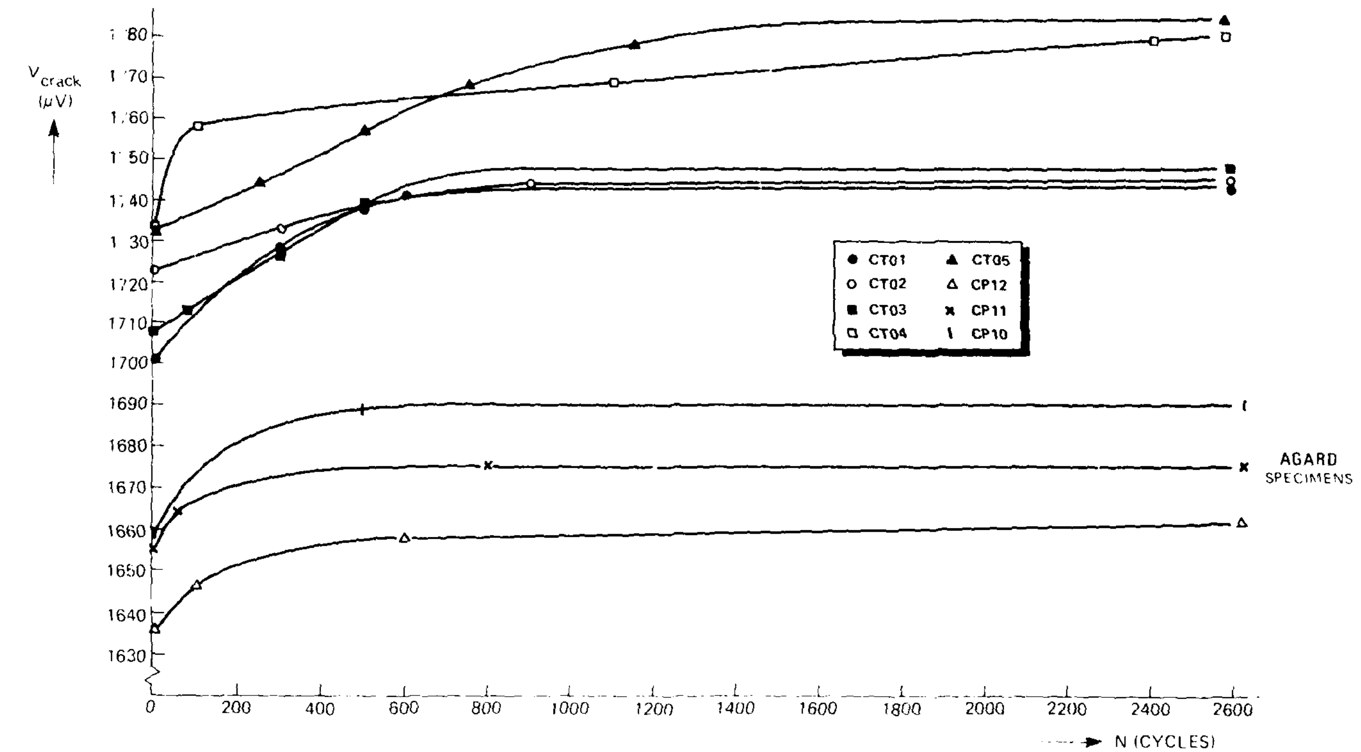

Fig. A9 PD-signal shows start up effect during testing of CT specimens

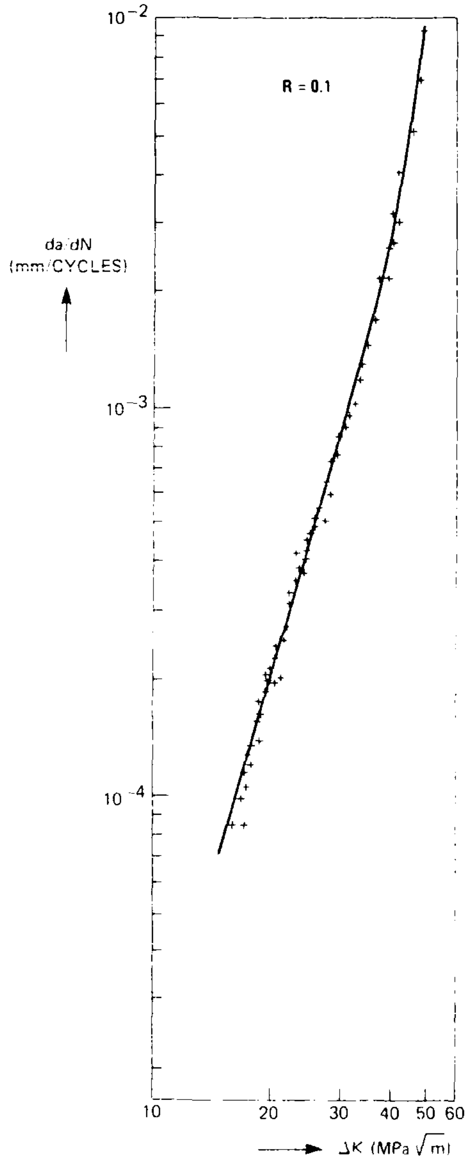

Fig. A10 Crack growth data for Ti-6Al-4V CT-specimens [3]

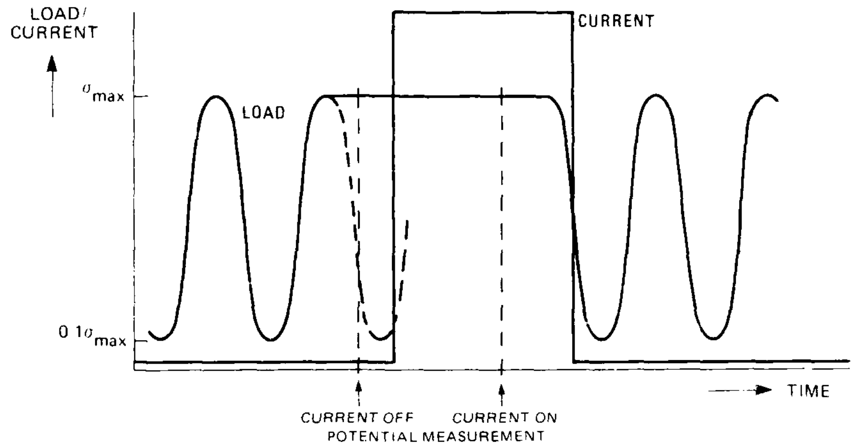

Fig. A11 Potential drop data sampling at high frequency CT-specimen testing

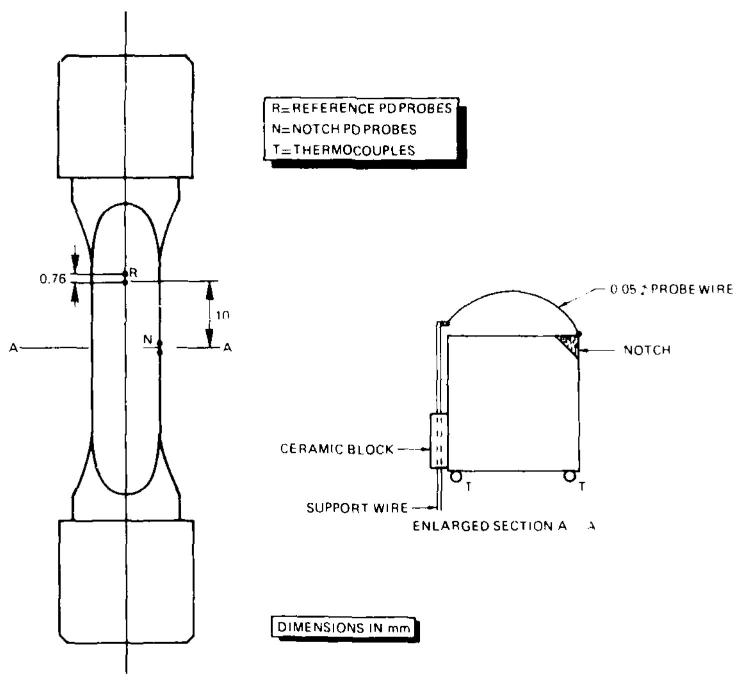

Fig. A12 PD-instrumentation of corner crack specimen.
Note: the exact distance between reference leads is not important; this only results in a reference voltage which is about the same as the initial notch voltage

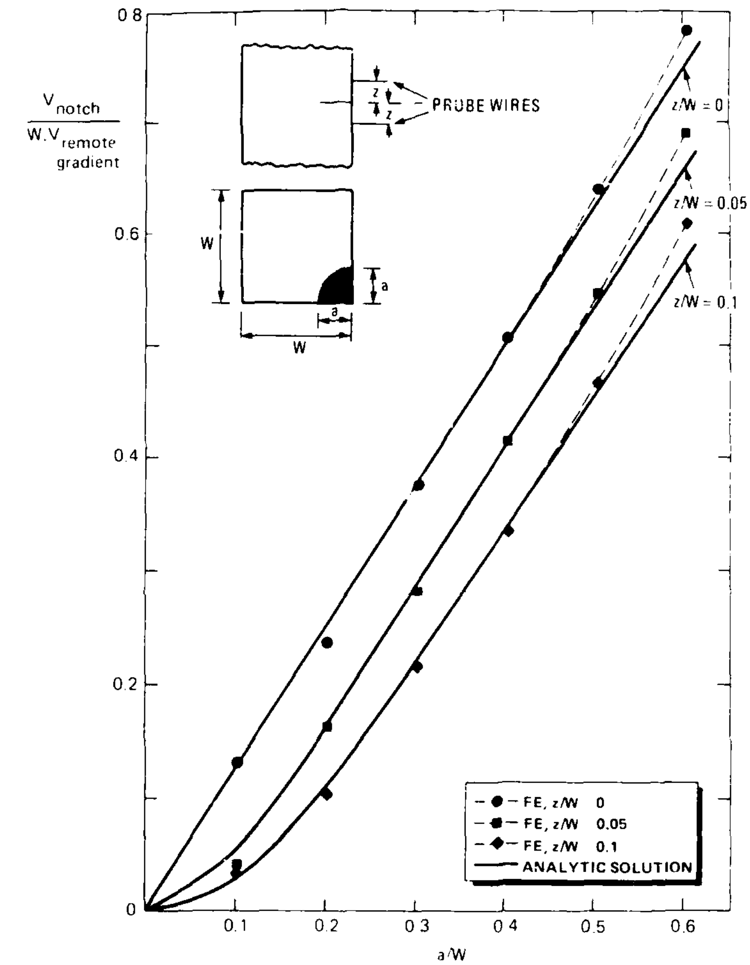

Fig. A13 Comparison of analytic and finite element solutions for various probe locations on the corner crack specimen [2].
Note: a quarter circular crack has been assumed with surface crack length = average crack length = a

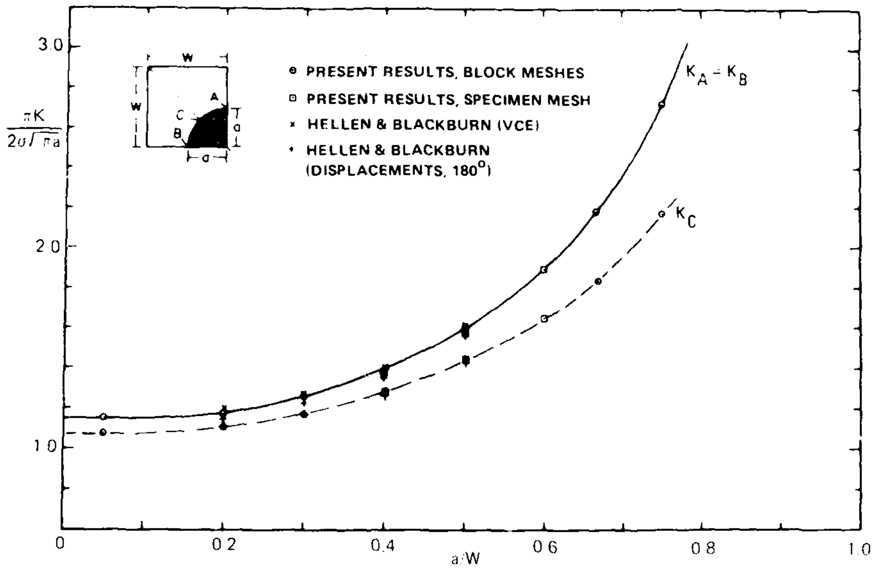

Fig. A14 Variation of normalised stress intensity with crack length for the corner crack geometry [4]

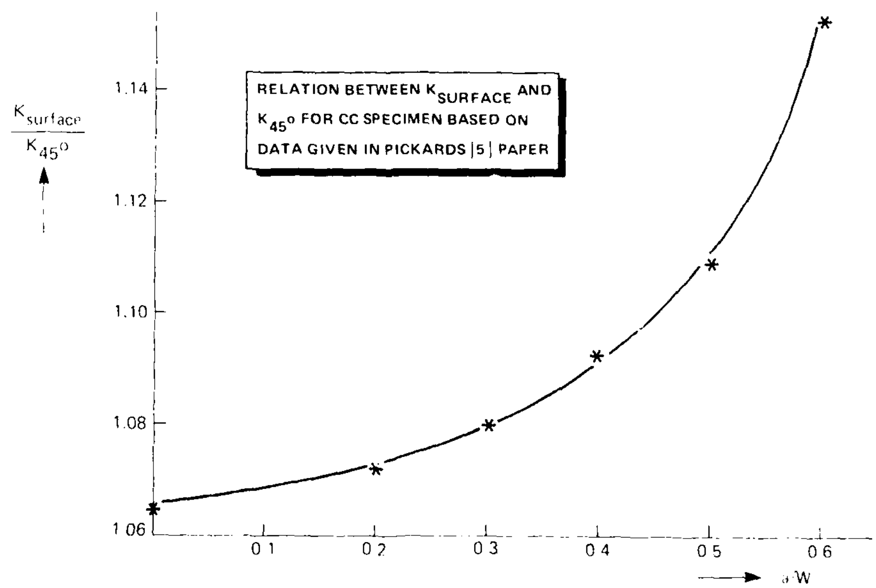

Fig. A15 Relation between $K_{surface}$ and K_{45^o} for CC-specimen

APPENDIX B

The statistical analysis of the [illegible] and K_t 2.2 data is based on the procedures described in ASTM E739 "Standard practice for statistical analysis of linear or linearized stress-life (S-N) and strain-life (ε-N) fatigue data".
A short summary of the procedure applied in the current AGARD programme is presented below.

Line equation

The statistical analysis is based on the assumption that the S-N relationship can be approximated by a straight line for a specific interval of stress. The following line equation was used:

$$Y = A + BX$$

in which $\quad Y = \log N$

$\qquad\qquad X = \Delta\sigma$

The coefficients A and B of this linear model can be calculated according:

$$\hat{A} = \bar{Y} - \hat{B}\bar{X}$$

$$\hat{B} = \frac{\sum_{i=1}^{k} (X_i - \bar{X})(Y_i - \bar{Y})}{\sum_{i=1}^{k} (X_i - \bar{X})^2}$$

$$\bar{X} = \frac{\sum_{i=1}^{k} X_i}{k} \qquad \text{(average } X_i \text{ value)}$$

$$\bar{Y} = \frac{\sum_{i=1}^{k} Y_i}{k} \qquad \text{(average } Y_i \text{ value)}$$

k = total number of test specimens.

$\hat{A}$ and $\hat{B}$ are called the *maximum likelihood estimators* of A and B.
(The symbol "caret" (^) denotes estimate; the symbol "overbar" (‾) denotes average).

Variance

To estimate the variance of the normal distribution for log N the following expression is recommended:

$$\hat{\sigma}^2 = \frac{\sum_{i=1}^{k} (Y_i - \hat{Y}_i)^2}{k - 2}$$

in which: $\hat{Y}_i = \hat{A}_i + \hat{B}X_i$

The term k-2 is used instead of k to make $\hat{\sigma}^2$ an unbiased estimator of the normal population variance σ^2.

Confidence intervals for A and B

The confidence intervals for A and B are given by:

$$\hat{A} \pm t_p \hat{\sigma} \left[\frac{1}{k} + \frac{\bar{X}^2}{\sum_{i=1}^{k} (X_i - \bar{X})^2} \right]^{\frac{1}{2}}$$

$$\hat{B} \pm t_p \hat{\sigma} \left[\sum_{i=1}^{k} (X_i - \bar{X})^2 \right]^{-\frac{1}{2}}$$

The value of t_p is read from the t-distribution using the desired value [illegible] the confidence level [illegible], associated with the confidence interval (see Table B1). The entry parameter n (the degrees [illegible] freedom of t) equals k - 2 for the two above equations.

APPENDIX B

Confidence band for the entire median S - N curve

The confidence band for the entire log N - $\Delta\varepsilon$ curve is calculated using the following equation:

$$Y = \hat{A} + \hat{B}X \pm \sqrt{2F_p \hat{\sigma}} \left[\frac{1}{k} + \frac{(X - \bar{X})^2}{\sum_{i=1}^{k} (X_i - \bar{X})^2} \right]^{\frac{1}{2}}$$

in which F_p is given in Table B2. This table contains two entry parameters n_1 and n_2, which are the statistical degrees of freedom for F. For the above equation $n_1 = 2$ and $n_2 = k-2$.

Testing of the applicability of the linear model

The linearity control test can only be performed if the programme was planned such that tests were performed at at least three different X_i levels ($\Delta\varepsilon$ - levels) and that at least one of the tests was duplicated.
The procedure is as follows:
Assume 1) the log life of the j-th replicate specimen tested at the i-th level of X is given the value Y_{ij}

2) fatigue tests were conducted at ℓ different values of X

3) m_i replicate values of Y are observed at each X_i

then the hypothesis of linearity is rejected when the computed value of

$$\frac{\sum_{i=1}^{\ell} m_i \, (\hat{Y}_i - \bar{Y}_i)^2 / (\ell - 2)}{\sum_{i=1}^{\ell} \sum_{j=1}^{m_i} (Y_{ij} - \bar{Y}_i)^2 / (k - \ell)}$$

exceeds F_p, where the value of F_p is read from Table B2 for the chosen significance level of 95 %. This table has two entry parameters n_1 and n_2; for this case $n_1 = \ell - 2$ and $n_2 = k - \ell$.
Note that the total number of specimens tested is given by

$$k = \sum_{i=1}^{\ell} m_i$$

REPORT DOCUMENTATION PAGE

1. Recipient's Reference	2. Originator's Reference	3. Further Reference	4. Security Classification of Document
	AGARD-R-766	ISBN 92-835-0475-5	UNCLASSIFIED

5. Originator Advisory Group for Aerospace Research and Development
North Atlantic Treaty Organization
7 rue Ancelle, 92200 Neuilly sur Seine, France

6. Title

AGARD ENGINE DISC COOPERATIVE TEST PROGRAMME

7. Presented at

8. Author(s)/Editor(s)

A.J.A.Mom
M.D.Raizenne

9. Date

August 1988

10. Author's/Editor's Address

Various

11. Pages

86

12. Distribution Statement This document is distributed in accordance with AGARD policies and regulations, which are outlined on the Outside Back Covers of all AGARD publications.

13. Keywords/Descriptors

Fatigue tests	Crack initiation
Fatigue (materials)	Crack propagation
Cracking (fracturing)	Aircraft engines

14. Abstract

This report describes the initial results of an AGARD test programme on fatigue behaviour of engine disc materials. The first phase of this programme, the Core Programme, was aimed at test procedure and specimen standardisation and calibration of the various laboratories. A detailed working document has been prepared and is included in this report. It describes the testing fundamentals and procedures and includes the analysis procedures used for handling the test data.

Fatigue crack initiation and propagation testing was performed on Ti-6Al-4V material under room temperature and constant amplitude loading conditions using four different specimen designs. All results were statistically analysed for possible significant differences in material behaviour due to disc processing variables, specimen location in the disc or testing laboratory.

This publication was sponsored by the Structures and Materials Panel of AGARD.

AGARD Report No.766	AGARD-R-766
Advisory Group for Aerospace Research and Development, NATO AGARD ENGINE DISC COOPERATIVE TEST PROGRAMME by A.J.A.Mom and M.D.Raizenne Published August 1988 86 pages This report describes the initial results of an AGARD test programme on fatigue behaviour of engine disc materials. The first phase of this programme, the Core Programme, was aimed at test procedure and specimen standardisation and calibration of the various laboratories. A detailed working document has been prepared and is included in this report. It describes the testing fundamentals and P.T.O.	Fatigue tests Fatigue (materials) Cracking (fracturing) Crack initiation Crack propagation Aircraft engines

AGARD Report No.766	AGARD-R-766
Advisory Group for Aerospace Research and Development, NATO AGARD ENGINE DISC COOPERATIVE TEST PROGRAMME by A.J.A.Mom and M.D.Raizenne Published August 1988 86 pages This report describes the initial results of an AGARD test programme on fatigue behaviour of engine disc materials. The first phase of this programme, the Core Programme, was aimed at test procedure and specimen standardisation and calibration of the various laboratories. A detailed working document has been prepared and is included in this report. It describes the testing fundamentals and P.T.O.	Fatigue tests Fatigue (materials) Cracking (fracturing) Crack initiation Crack propagation Aircraft engines

AGARD Report No.766	AGARD-R-766
Advisory Group for Aerospace Research and Development, NATO AGARD ENGINE DISC COOPERATIVE TEST PROGRAMME by A.J.A.Mom and M.D.Raizenne Published August 1988 86 pages This report describes the initial results of an AGARD test programme on fatigue behaviour of engine disc materials. The first phase of this programme, the Core Programme, was aimed at test procedure and specimen standardisation and calibration of the various laboratories. A detailed working document has been prepared and is included in this report. It describes the testing fundamentals and P.T.O.	Fatigue tests Fatigue (materials) Cracking (fracturing) Crack initiation Crack propagation Aircraft engines

AGARD Report No.766	AGARD-R-766
Advisory Group for Aerospace Research and Development, NATO AGARD ENGINE DISC COOPERATIVE TEST PROGRAMME by A.J.A.Mom and M.D.Raizenne Published August 1988 86 pages This report describes the initial results of an AGARD test programme on fatigue behaviour of engine disc materials. The first phase of this programme, the Core Programme, was aimed at test procedure and specimen standardisation and calibration of the various laboratories. A detailed working document has been prepared and is included in this report. It describes the testing fundamentals and P.T.O.	Fatigue tests Fatigue (materials) Cracking (fracturing) Crack initiation Crack propagation Aircraft engines

procedures and includes the analysis procedures used for handling the test data.

Fatigue crack initiation and propagation testing was performed on Ti-6Al-4V material under room temperature and constant amplitude loading conditions using four different specimen designs. All results were statistically analysed for possible significant differences in material behaviour due to disc processing variables, specimen location in the disc or testing laboratory.

This publication was sponsored by the Structures and Materials Panel of AGARD.

ISBN 92-835-0475-5

procedures and includes the analysis procedures used for handling the test data.

Fatigue crack initiation and propagation testing was performed on Ti-6Al-4V material under room temperature and constant amplitude loading conditions using four different specimen designs. All results were statistically analysed for possible significant differences in material behaviour due to disc processing variables, specimen location in the disc or testing laboratory.

This publication was sponsored by the Structures and Materials Panel of AGARD.

ISBN 92-835-0475-5

procedures and includes the analysis procedures used for handling the test data.

Fatigue crack initiation and propagation testing was performed on Ti-6Al-4V material under room temperature and constant amplitude loading conditions using four different specimen designs. All results were statistically analysed for possible significant differences in material behaviour due to disc processing variables, specimen location in the disc or testing laboratory.

This publication was sponsored by the Structures and Materials Panel of AGARD.

ISBN 92-835-0475-5

procedures and includes the analysis procedures used for handling the test data.

Fatigue crack initiation and propagation testing was performed on Ti-6Al-4V material under room temperature and constant amplitude loading conditions using four different specimen designs. All results were statistically analysed for possible significant differences in material behaviour due to disc processing variables, specimen location in the disc or testing laboratory.

This publication was sponsored by the Structures and Materials Panel of AGARD.

ISBN 92-835-0475-5

AGARD

NATO OTAN

7 rue Ancelle · 92200 NEUILLY-SUR-SEINE

FRANCE

Telephone (1)47.38.57.00 · Telex 610 176

DISTRIBUTION OF UNCLASSIFIED AGARD PUBLICATIONS

AGARD does NOT hold stocks of AGARD publications at the above address for general distribution. Initial distribution of AGARD publications is made to AGARD Member Nations through the following National Distribution Centres.Further copies are sometimes available from these Centres, but if not may be purchased in Microfiche or Photocopy form from the Purchase Agencies listed below.

NATIONAL DISTRIBUTION CENTRES

BELGIUM
Coordonnateur AGARD — VSL
Etat-Major de la Force Aérienne
Quartier Reine Elisabeth
Rue d'Evere, 1140 Bruxelles

CANADA
Director Scientific Information S‹ ›vices
Dept of National Defence
Ottawa, O ›ario K1A 0K2

DENMARK
Danish De ›search Board
Ved Idræ
2100 Co

FRANCE
O.N.E.R.
29 Avenu
92320 Ch

GERMANY
Fachin
Phy
Ka
D-

GREEC
He
Aircr
Departn
Holargos, .

ICELAND
Director of Aviation
c/o Flugrad
Reyjavik

ITALY
Aeronautica Militare
Ufficio del Delegato Nazionale all'AGARD
3 Piazzale Adenauer
00144 Roma/EUR

LUXEMBOURG
See Belgium

NETHERLANDS
Netherlands Delegation to AGARD
National Aerospace Labo›tory, NLR
P.O. Box 126
2600 AC D

NORWAY
Nor
A

GAR

MSB)
(AR)

ITED KINGDOM
Defence Research Information Centre
Kentigern House
65 Brown Street
Glasgow G2 8EX

UNITED STATES
National Aeronautics and Space Administration (NASA)
Langley Research Center
M/S 180
Hampton, Virginia 23665

THE UNITED STATES NATIONAL DISTRIBUTION CENTRE (NASA) DOES NOT HOLD STOCKS OF AGARD PUBLICATIONS, AND APPLICATIONS FOR COPIES SHOULD BE MADE DIRECT TO THE NATIONAL TECHNICAL INFORMATION SERVICE (NTIS) AT THE ADDRESS BELOW.

PURCHASE AGENCIES

National Technical
Information Service (NTIS)
5285 Port Royal Road
Springfield
Virginia 22161, USA

ESA/Information Retrieval Service
European Space Agency
10, rue Mario Nikis
75015 Paris, France

The British Library
Document Supply Division
Boston Spa, Wetherby
West Yorkshire LS23 7BQ
England

Requests for microfiche or photocopies of AGARD documents should include the AGARD serial number, title, author or editor, and publication date. Requests to NTIS should include the NASA accession report number. Full bibliographical references and abstracts of AGARD publications are given in the following journals:

Scientific and Technical Aerospace Reports (STAR)
published by NASA Scientific and Technical
Information Branch
NASA Headquarters (NIT-40)
Washington D.C. 20546, USA

Government Reports Announcements (GRA)
published by the National Technical
Information Services, Springfield
Virginia 22161, USA

SPS

Printed by Specialised Printing Services Limited
40 Chigwell Lane, Loughton, Essex IG10 3TZ

ISBN 92-835-0475-5

END

DATE

FILMED

12-88

DTIC